USAAVRADCOM-TR-80-D-32

WIND TUNNEL EVALUATION OF AEROELASTICALLY CONFORMABLE ROTORS

R. H. Blackwell, K. C. Frederickson
SIKORSKY AIRCRAFT DIVISION
United Technologies Corporation
Stratford, Conn. 06602

January 1981

Approved for public release;
distribution unlimited.

Prepared for

APPLIED TECHNOLOGY LABORATORY
U. S. ARMY RESEARCH AND TECHNOLOGY LABORATORIES (AVRADCOM)
Fort Eustis, Va. 23604

BLANK PAGES
IN THIS
DOCUMENT
WERE NOT
FILMED

APPLIED TECHNOLOGY LABORATORY POSITION STATEMENT

This report presents the results of a wind tunnel evaluation of an Aeroelastically Conformable Rotor (ACR). The ACR is a rotor system in which aeroelastic properties are explicitly selected to produce blade elastic response which results in reduced rotor systems loads. As part of the program an analytical effort was conducted to select a set of parameters for experimental evaluation. The parameters selected from this study included blade torsional stiffness, tip sweep, and camber. Two 9-foot model rotors were fabricated and tested in the Langley Research Center Transonic Dynamics Wind Tunnel to investigate the effect of these parameters on rotor loads, vibration, and performance. The results of this wind tunnel test demonstrated that blades can be designed to produce dynamic twist which causes them to experience significantly lower forward flight blade loads than a conventional design without adverse effects on performance.

Paul H. Mirick of the Aeronautical Technology Division served as project engineer for this effort.

Unclassified

SECURITY CLASSIFICATION OF THIS PAGE (When Data Entered)

REPORT DOCUMENTATION PAGE

READ INSTRUCTIONS BEFORE COMPLETING FORM

1. REPORT NUMBER: USAAVRADCOM TR-80-D-32	2. GOVT ACCESSION NO.: AD-A096429
3. RECIPIENT'S CATALOG NUMBER:	
4. TITLE (and Subtitle): WIND TUNNEL EVALUATION OF AEROELASTICALLY CONFORMABLE ROTORS	5. TYPE OF REPORT & PERIOD COVERED: Final Report
	6. PERFORMING ORG. REPORT NUMBER: SER-510039
7. AUTHOR(s): R. H. Blackwell, Jr. K. C. Frederickson	8. CONTRACT OR GRANT NUMBER(s): DAAJ02-77-C-0047
9. PERFORMING ORGANIZATION NAME AND ADDRESS: Sikorsky Aircraft Division United Technologies Corporation Stratford, Connecticut 06602	10. PROGRAM ELEMENT, PROJECT, TASK AREA & WORK UNIT NUMBERS: 62209A 1L262209AH76 00 208 EK
11. CONTROLLING OFFICE NAME AND ADDRESS: Applied Technology Laboratory, US Army Research and Technology Laboratories (AVRADCOM) Fort Eustis, Virginia 23604	12. REPORT DATE: Jan 1981 13. NUMBER OF PAGES: 113
14. MONITORING AGENCY NAME & ADDRESS (if different from Controlling Office)	15. SECURITY CLASS. (of this report): Unclassified 15a. DECLASSIFICATION/DOWNGRADING SCHEDULE

16. DISTRIBUTION STATEMENT (of this Report)

Approved for public release; distribution unlimited.

17. DISTRIBUTION STATEMENT (of the abstract entered in Block 20, if different from Report)

18. SUPPLEMENTARY NOTES

19. KEY WORDS (Continue on reverse side if necessary and identify by block number)

Helicopter Rotor
Torsional Flexibility
Dynamic Twist
Tip Sweep

20. ABSTRACT (Continue on reverse side if necessary and identify by block number)

The concept of controlling blade dynamic twist to reduce rotor system loads and to improve aerodynamic efficiency was investigated through wind tunnel testing and analysis. Blade design features which promote favorable dynamic twist were selected based on aeroelastic analysis. Two four-bladed 9-ft diameter 1/6 scale model rotors which permitted parametric investigation of blade torsional stiffness, tip sweep, and camber were fabricated and subjected

DD FORM 1 JAN 73 1473 EDITION OF 1 NOV 65 IS OBSOLETE

Unclassified

SECURITY CLASSIFICATION OF THIS PAGE (When Data Entered)

323 800

20. Continued

to forward flight testing in the Langley Research Center Transonic Dynamics Wind Tunnel. The azimuthal variation of dynamic twist was determined based on measured twisting moments. Results showed that relative to a conventional stiffness blade, 20 to 40 percent reductions in vibratory flatwise and torsional moments and 10-percent reductions in power were achieved at an advance ratio of 0.3 by configurations which produced noseup elastic twist on the advancing blade. Four/rev hub vibration was also reduced by blades which reduced advancing blade total twist. The important trends shown by the test results were adequately predicted by a blade aeroelastic response analysis although magnitudes of blade loads were generally underpredicted.

PREFACE

The work reported herein was performed by the Sikorsky Aircraft Division of United Technologies Corporation under Contract DAAJ02-77-C-0047 for the Applied Technology Laboratory of the U. S. Army Research and Technology Laboratories (AVRADCOM). Funding for the fabrication of the baseline model rotor blades was provided jointly by the Applied Technology Laboratory, the Structures Laboratory and Sikorsky. The test program was conducted in the Langley Research Center Transonic Dynamics Tunnel.

Mr. W. E. Nettles and Mr. P. H. Mirick served as the Contracting Officer's Technical Representative for the Applied Technology Laboratory. Mr. W. T. Yeager, Jr. of the Structures Laboratory managed the wind tunnel test program under the supervision of Dr. C. E. Hammond. Mr. R. H. Blackwell, Jr. was the Task Manager for Sikorsky activities. The model blades were designed and built by Mr. R. J. Murrill, Mr. L. B. Kaplan, Mr. A. Sacculo and Mr. T. Lesnick under the supervision of Mr. E. F. Kiely.

TABLE OF CONTENTS

LIST OF ILLUSTRATIONS

LIST OF ILLUSTRATIONS - (cont'd)

LIST OF ILLUSTRATIONS - (cont'd)

LIST OF ILLUSTRATIONS - (cont'd)

LIST OF ILLUSTRATIONS - (cont'd)

INTRODUCTION

Increasingly stringent helicopter mission requirements compel the rotor designer to examine all possible methods of improving system performance, reducing loads, and reducing cost. The technology associated with advanced airfoils, twist distributions, planform variations, and advanced materials is finding its way into current and near-term future designs. Efficient development of these new systems obviously relies on careful integration of aerodynamic and structural design. If, for example, changes made to improve aerodynamic performance expand the performance-defined flight envelope but produce higher blade loads than considered in the structural design the gains may be lost. On the other hand, structural design if it leads to significant dynamic response may alter the rotor disc angle-of-attack pattern to one that is different from that considered by the aerodynamicist. The result might be a poor match of airfoil, twist and planform with the aerodynamic environment. Of particular concern is the dynamic twisting response of the blades. On current designs, blade elastic twist can contribute several degrees to angle of attack at selected positions on the rotor disc. Recent years have seen an acknowledgement of this situation and first step attempts to explore how dynamic twist might be impacting blade behavior and whether or not it can be used to advantage.

Historically, blade torsional properties (to the degree that they were selected at all) were largely based on scaling of past successful designs. As long as the blades were stiff in torsion, such as they would be in a conventional metal blade design and as long as increases in camber, twist or tip sweep were not being considered, this design process was satisfactory. However, when use of composite materials, advanced airfoils, increased twist, and/or tip sweep are considered, the risk of choosing inappropriate torsional properties by extrapolating from past experience is more significant. Now, a clear statement of the relation between blade design properties and dynamic twist and the relation among dynamic twist and rotor loads, performance, vibration, and handling qualities is mandatory. When it is thoroughly understood, controlled dynamic twist will become a commonplace design variable to be considered in the evolution of any new blade configuration. Dynamic twist clearly has a potential role in changing twist with flight condition. The desire to have high twist in hover for peak efficiency and low advancing blade twist in forward flight for low blade loads is well known. The compromises imposed by a fixed twist design are unavoidable.

In recent years theoretical and experimental research into the concept of the conformable rotor has been performed. (The acronym ACR is used in this report to refer to an Aeroelastically Conformable Rotor). Tests of low torsional stiffness, soft inplane hingeless model rotor blades described in Reference 1 demonstrated useful effects of tip sweep and noseup camber on blade bending moments. The analytic work described in Reference 2 examined the potential for improving rotor capability through control of blade dynamic twist. Results suggested that with respect to a conventional design, forward flight blade and control system loads could be reduced and hover and forward flight performance improved by blades incorporating reduced torsional stiffness, tip sweep and reflex camber. Results, especially in the area of forward flight performance, were shown to be sensitive to the details of the aerodynamic model. It was concluded that testing would be required to determine performance effects with confidence.

The general objective of the program described in this document was to further the understanding of blade torsional response and its role in the blade design process. The specific objectives were:

1. To select blade parameters which have a controlling influence of torsional response.

2. To define, through analysis, a set of design parameters which result in elastic response having beneficial effects on rotor behavior.

3. To substantiate the predicted effects of parameter changes on dynamic response and rotor behavior.

4. To provide a data base for use in blade design.

---

1. Doman, G. S., et al., Investigation of Aeroelastically Adaptive Rotors, Boeing Vertol Company; USAAMRDL TR 77-3, Eustis Directorate, U.S. Army Air Mobility Research and Development Laboratory, Fort Eustis, Virginia, May 1977, AD A042083.

2. Blackwell, R. H., Investigation of the Compliant Rotor Concept, Sikorsky Aircraft Division, United Technologies Corporation, USAAMRDL TR 77-7, Eustis Directorate, U.S. Army Air Mobility Research and Development Laboratory, Fort Eustis, Virginia, June 1977, AD A042338.

5. To provide data for blades showing significant aeroelastic response so that the adequacy of current aeroelastic modelling techniques can be assessed.

The approach adopted to achieve these objective was as follows:

1. Perform a literature survey to identify evidence of blade dynamic response impacting rotor capability.

2. Extend previous analytic design efforts to select a limited set of parameter changes and rotor attributes (performance, blade loads, etc.) for experimental evaluation.

3. Design, fabricate and test model rotor blades which permit direct examination of the blade parameters and rotor attributes selected based on the analysis. Make a special attempt to quantify the blade torsional response produced by the various designs for a wide range of operating conditions.

4. Compare measured rotor behavior and that predicted by the Sikorsky blade aeroelastic analysis (Y200 Program).

This approach attempts to make effective use of past results, analysis and test. The analysis is a cost-effective means of identifying attractive configurations even if absolute magnitudes of benefits are not predicted. Test evaluation of significant designs quantifies benefits. The post-test correlation study serves to evaluate the analysis and also helps to explain any phenomena measured during the test.

REVIEW OF PREVIOUS RESEARCH

In order to guide the selection of blade design configurations for analysis, fabrication and testing under this program, results of past analyses, and test efforts were reviewed. The objective was to identify significant effects of blade design parameters on elastic response and the effects of that response on rotor behavior. The following paragraphs summarize the findings of the review.

TORSIONAL STIFFNESS

Analytic results reported in Reference 2 showed that for steady and low frequency (1/rev and 2/rev) forcing, the amplitude of blade torsional response is inversely proportional to torsional stiffness. The Reference 2 results showed that in order to achieve levels of elastic twist required to improve forward flight performance or significantly reduce blade loads with forcing mechanisms (camber, tip sweep or chordwise offset of blade aerodynamic and structural axes) of realistic magnitudes, reduced blade torsional stiffness is required. Stiffness reductions on the order of four or five to one were considered. Analysis described in Reference 1 showed that adjusting the radial distribution of blade torsional stiffness and the control system stiffness was effective in controlling the radial distribution of elastic twist. In order to cause a redistribution of airloads, the stifffness reduction should be placed on the outer portion of the blade. Reducing control system stiffness or inboard blade stiffness will only increase rigid body motion of the blades and require a compensating amount of control input. The net effect on blade twist and radial distribution of airloads will be small. The model test program described in Reference 3 compared blades of scale stiffness and blades of 3x scale stiffness. Results from the Reference 3 work, which are discussed further in Reference 2, showed the anticipated three-to-one increase in blade steady and one/rev elastic twist for the softer blade. The one/rev twist was phased to twist the advancing blade nosedown. Performance data taken at an advance ratio of 0.3 showed a a 15-percent increase in power required at a given thrust for the more responsive blade. The model test program described in Reference 1 showed that

---

3. Niebanck, C. F., Model Rotor Test Data for Verification of Blade Response and Rotor Performance Calculations, Sikorsky Aircraft Division, United Technologies Corporation; USAAMRDL Technical Report 74-29, Eustis Directorate, U. S. Army Air Mobility Research and Development Laboratory, Fort Eustis, Virginia, May 1974, AD 786562.

reductions in torsional stiffness in conjunction with tip sweep or camber can significantly increase the collective and longitudinal cyclic pitch required for trimmed flight at high speeds.

References 4 and 5 showed that vibratory control loads are strongly influenced by torsional stiffness. Analysis presented in Reference 4 shows a reduction in retreating blade oscillatory torsional moments with decreased torsional stiffness. The reductions were predicted to be functions of blade stiffness and were not affected by independent torsional inertia or blade frequency changes.

CAMBER

Results from References 1, 2, 3, 5 and 6 describe the effects of airfoil camber on blade response and rotor system loads. In each case noseup pitching moment produced a twisting response, which decreased advancing blade twist and reduced vibratory blade loads. For the configurations examined, the effects on performance were generally small or adverse. Reference 1 indicates that positive c_{mo} (noseup pitching moment) has a favorable effect on flying qualities but decreases absolute propulsive force capability. Reference 6 and additional in-house Sikorsky studies on high c_{lmax} airfoils incorporating large negative c_{mo} indicate that unless a blade design can be established which avoids the large advancing blade nosedown twist, the aerodynamic benefits of delayed stall are accompanied by large penalties in control system and blade weight. The Controllable Twist

---

4. Blackwell, R. H., Investigation of the Effects of Blade Structural Design Parameters on Helicopter Stall Boundaries, Sikorsky Aircraft Division, United Technologies Corporation, USAAMRDL TR 74-25, Eustis Directorate, USAAMRDL, Fort Eustis, Virginia, May 1974 AD 784594.

5. Gabel, R., and Tarzanin, R. F., Blade Torsional Tuning to Manage Rotor Stall Flutter, AIAA Paper No 72-958, American Institute of Aeronautics and Astronautics, September 1974.

6. Paglino, V. M., The Potential Benefits of Advanced Airfoils for Helicopter Applications, NAVAIR Report prepared under Contract N00019-73-C-0225, March 1974.

Rotor (Reference 7) which can achieve 1P variations in twist similar to those produced by camber, showed that depending upon steady twist, noseup or nosedown advancing blade twist (camber) could be used to improve performance.

TIP SWEEP

Effects of tip sweep on dynamic response, rotor loads and performance are described in References 1, 2 and 8. The consensus is that blade flatwise bending moments are reduced by tip sweep. Depending upon rotor configuration (amount of sweep, built-in twist, airfoil and torsional stiffness), tip sweep may improve forward flight efficiency. According to Reference 2, sweep, like camber, improves speed stability and reduces propulsive force capability. Reference 6 data indicate that high-frequency control loads (usually attributed to stall flutter) are alleviated by tip sweep. Tip sweep and negative c_{mo} increase twist in hover. On blades of sufficiently reduced torsional stiffness, this effect can be used to improve hover performance.

BUILT-IN TWIST

Large amounts of built-in twist produce tip-down bending of the advancing blade and subsequent nosedown twisting. Results presented in Reference 8 for -6 degree and -16 degree twist blades illustrate the increase in flatwise and torsional moments which result from increased twist. The Compliant Rotor Study, Reference 2, showed the need to select built-in twist so that the combination of built-in and steady elastic twist is appropriate for the intended flight spectrum. Analysis in Reference 2 showed that at a $C_T/\sigma = 0.10$, peak hover efficiency occurs at -22 to -26 degrees of blade twist.

4
B

7. Lemnios, A. Z., et al., Full Scale Wind Tunnel Tests of a Controllable Twist Rotor, American Helicopter Society, 32nd Annual National Forum, May 1976.

8. Prillwitz, R., Structural Evaluation of High Performance Rotor Blade Swept Tips, Engineering Report SER-651073, Sikorsky Aircraft Division, United Technologies Corporation, October 1972.

FLATWISE AND EDGEWISE STIFFNESS DISTRIBUTION

Radial distributions of flatwise and edgewise stiffness affect the proximity of blade mode frequencies to multiples of rotor speed and to each other. As such they affect aircraft vibration and blade loads. On hingeless rotor blades which have the pitch bearing in the hub system, the action of lift and drag forces acting on the deformed blade contributes to significant blade torsion deflections. In this case the radial distributions of bending stiffness may significantly affect the resulting torsional response. On articulated blades and blades which have the pitch bearing outboard of the principal root flexibility, this effect is less significant.

DISTRIBUTION OF AERODYNAMIC-CENTER AND CENTER-OF-GRAVITY AXES

Offset of the blade section aerodynamic center from the center of gravity has a powerful effect on aeroelastic response. The radial distribution of the chordwise offset can be varied, according to Reference 1, to control the amplitude and phase of low-frequency torsional response. Offset of the c.g. introduces coupling between flatwise and torsional response and as the c.g. is moved aft it tends to aggravate stability problems.

FLATWISE-TORSIONAL COUPLING

Coupling of blade flatwise and torsional response produced either by offset of blade axes or through tailoring of composite fiber orientation may be useful in producing an elastic twist which improves the distribution of rotor disc airloads. To the degree that an ACR blade tends to produce flap-torsion coupling, the proper pitch-flap coupling at the root might need to be reconsidered in order to maintain or enhance flying qualities or blade loads.

TIP ANHEDRAL

Wind tunnel tests conducted jointly by NASA and Sikorsky and reported in Reference 9 explored the effects on blade loads and performance of adding an anhedral tip to a conventional stiffness blade. Anhedral has been proposed as a means of improving hover performance. Examination of the forward flight torsional moment data suggests that both the drag acting on the drooped portion of the blade and the inertial effects of the out-of-plane mass contribute to significant changes in dynamic twist.

9. Weller, W., Experimental Investigation of Effects of Blade Tip Geometry on Loads and Performance for an Articulated Rotor System, NASA-TP-1303; AVRADCOM-TR-78-53, Structures Laboratory, U.S. Army Research and Technology Laboratories (AVRADCOM), Langley Research Center, Hampton, Virginia, January 1979.

SELECTION OF ROTOR CONFIGURATIONS FOR FABRICATION AND TESTING

Based on the review outlined in the previous section, it was decided that a systematic evaluation of the effects of three parameters - torsional stiffness, tip sweep, and camber - on rotor performance, blade and control system loads, and vibratory hub loads would provide a much needed data base on which later work might build. Obtaining data for parametric variations in tip sweep and camber for blades of two torsional stiffnesses was adopted as the plan. These parameters were selected because (1) they have significant effects on blade response and offer significant latitude for improvement of rotor attributes, (2) they are being incorporated to some extent on advanced rotor designs and might be more effectively applied if the implications of the resulting dynamic response were better understood, and (3) they are adequately modelled by the Sikorsky blade aeroelastic analysis (Y200 Program). The magnitudes of the various parameters were chosen to demonstrate trends of dynamic response and hopefully sizeable improvements in rotor behavior. No attempt was made, however, to select any optimal configurations. The rationale for the selection of built-in twist, torsional stiffness, tip sweep and camber values is discussed in the Blade Design Analysis section.

In addition to torsional stiffness, tip sweep and camber, evaluation of an anhedral tip was added to the program. In view of the potentially powerful effect which anhedral tips could have on dynamic twist, it was decided to test them under this program. Modelling of anhedral tips is not possible with the current version of the Y200 program. The geometry of the anhedral tip was scaled from that of full scale anhedral tip blades which have been fabricated for test on the UH-60A aircraft.

BLADE DESIGN ANALYSIS

As pointed out earlier, the objective of the program was more to obtain parametric data than to define optimal configurations. The approach adopted to maximize the amount of ACR data obtained was to build one set of low torsion stiffness blades having bendable trailing edge tabs to vary camber and capable of accepting several tips. As a result, the values of such parameters as torsional stiffness and built-in twist chosen for the ACR blades must represent a compromise between those that might be selected for specific combinations of sweep and camber. Design analysis was conducted with the Sikorsky blade aeroelastic analysis to assist in the selection of stiffness and twist for the demonstrator rotors. The analysis was then exercised for variations in tip sweep and camber to predict blade windup, to give estimates of the control ranges required on the model, and to quantify the anticipated improvements in rotor loads and performance for different segments of the flight envelope.

The blade aeroelastic analysis (Y200 Program) with variable inflow was used to explore the effects of built-in twist on performance and blade loads in forward flight. The Y200 Program is documented in Reference 10 and the United Technologies Research Center Prescribed Wake Inflow Analysis is documented in Reference 11. A sample of the results is shown in Figure 1. For a blade having conventional torsional stiffness inboard and a four-to-one reduction in stiffness outboard of the 50-percent radius and a 20-degree swept tip at the 93.5-percent radius position, peak L/D_E occurs at about -12 degrees of built-in twist for the cruise condition shown. Predicted flatwise and torsional moments increase with built-in twist as expected. The four-to-one reduction in outboard blade torsional stiffness was selected based on consideration of the steady and one/rev windup which would be produced by 5- to 10-percent span swept tips

10. Arcidiacono, P. J., Prediction of Rotor Instability at High Forward Speeds, Volume I, Steady Flight Differential Equations of Motion for a Flexible Helicoper Blade with Chordwise Mass Unbalance, Sikorsky Aircraft Division, United Technologies Corporation; USAAVLABS 68-18A, U. S. Army Aviation Material Laboratories, Fort Eustis, Virginia, February 1969, AD 685860.

11. Landgrebe, A. J., An Analytical Method for Predicting Rotor Wake Geometry, Journal of the American Helicopter Society, Volume 14, No. 4, October 1969, pp. 20 - 32.

and variations in section pitching moment coefficient from 0 to +0.06. The swept tips were assumed to be balanced around the quarter chord of the unswept section by adding appropriate leading edge weight inboard of the sweep position. The camber changes were assumed to be present between the 50 and 85 percent radius positions. Typical results are shown in Figure 2. A blade with a four-to-one stiffness reduction (relative to that of the UH-60A blade) over the outboard half was examined at $\mu = 0.2$ and $\mu = 0.35$ for a $C_L/\sigma = 0.07$. No sweep and 20 degrees of sweep at the 93.5-percent radius were studied assuming the pitching moment coefficients of the UH-60A airfoils and pitching moments shifted by Δc_m = +0.C3 and +0.06. Results show that increased noseup pitching moment produces noseup steady twist and one/rev twist phased to pitch the advancing blade noseup. Tip sweep also produces noseup advancing blade twist but nosedown steady twist. At $\mu = 0.35$ and zero Δc_m tip sweep produces 2 degrees of nosedown steady twist and 3 to 4 degrees of advancing blade noseup one/rev twist. At $\mu = 0.35$ camber changes produce approximately 2 degrees of steady twist and 2 degrees of one/rev sine twist per 0.01 Δc_m. This level of elastic response was considered significant enough to demonstrate effects on rotor behavior. Any higher level of "elastic twist" might be impractical based on increases in the control inputs required for trim. Also, more extreme reductions in torsional stiffness might be expected to contribute to non n/rev aggravated vibration resulting from manufacturing dissimilarities between blades. Reference 12 examined, through analysis, the sensitivity of non n/rev vibration to dissimilarities in blade aerodynamics and structure for several levels of torsional stiffness. For a four-to-one GJ reduction on the outer half of the blade, there was little impact on predicted vibration.

Figure 3 compares predicted performance, blade loads and root torsion moments for the six configurations examined at the two advance ratios. Results showed that performance and blade loads are relatively insensitive to the elastic twist changes produced by tip sweep and camber at $\mu = 0.2$. At $\mu = 0.35$ tip sweep generally improves performance. A +0.03 change in pitching moment coefficient is likewise beneficial, but above Δc_m = +0.03 the effect is detrimental. Tip sweep

12. Blackwell, R. H., Aeroelastically Conformable Rotor Mission Analysis, Sikorsky Aircraft Division, United Technologies Corporation, USARTL TR-79-5, Applied Technology Laboratory, U.S. Army Research and Technology Laboratories, Fort Eustis, Virginia March 1979, AD A067338.

and noseup Δc_m reduce vibratory flatwise moment as would be expected based on the reduction in advancing blade twist. Vibratory root torsion moments were reduced by tip sweep at low values of Δc_m and by moderate increases in Δc_m.

Based on these results, conformable rotor blades employing -12 degrees of built-in twist, a four-to-one reduction in GJ outboard of 50 percent radius and tabs capable of providing up to +0.06 Δc_m were specified for fabrication. A straight tip and a constant chord swept tip with 20 degrees of sweep at the 93.5 percent radius were chosen.

MODEL BLADE DESIGN AND FABRICATION

In order to explore the effects of torsional stiffness, tip sweep and camber, two blade sets differing only in torsional stiffness and capable of accepting various tip sections were fabricated. Each blade incorporated bendable trailing edge tabs and was capable of accepting alternate tips. Relative to the conventional stiffness baseline blade, the ACR blade incorporated a nominal 4-to-1 reduction in torsional stiffness outboard of the 50 percent radius.

The model blades were designed to be representative of the UH-60A blades with the exception that -12 degrees (versus -16 degrees) of built-in twist was used. A four-bladed, articulated rotor having a 5.5-percent hinge offset and a Lock number of 9.0 was selected. Aerodynamic design features taken from the UH-60A are a solidity of 0.082 and the BLACK HAWK SC 1095 and SC 1095R8 airfoil sections. Blade weight; torsional inertia; and flatwise, edgewise, and torsional stiffnesses were established by scaling UH-60A blade properties although no attempt was made to match the detailed mass and stiffness distributions of the full-scale blades. The blade chordwise center of gravity was designed to be at the quarter chord.

In order to take advantage of the closer simulation of full-scale Reynolds numbers afforded by testing in Freon, the blades were designed for operation at full-scale Mach numbers in Freon at a density of 0.006 slug/ft^3. The use of Freon as a test medium simplifies some elements of the design of a model rotor, but in the case of the ACR, it created two difficult inter-related problems. The primary problem was to obtain an adequately low outer blade torsional stiffness while maintaining other properties at conventional values. An indication of this problem was the fact that the 0.005-inch-thick fiberglass cloth used as the outer blade skin contributed more than 50 percent of the desired torsional stiffness. The second difficulty was to provide enough weight in the blade to achieve mass, torsional inertia and C.G. scaling without increasing blade stiffnesses.

A general assembly drawing of the ACR and baseline blades is shown in Figure 4. The blades have a 56.22-inch radius, a 3.625-inch chord and a -12 degree twist. The blades have an SC 1095 airfoil section inboard of the 50 percent and outboard of the 85-percent radius stations. The SC 1095R8 airfoil, which includes increased leading-edge camber, is used between the 50- and 85-percent span stations. An

adjustable 7.5-percent chord trailing edge tab was also incorporated between the 50- and 85-percent span stations. Three 11-percent radius removable tips were provided. These included the constant chord 20 degree swept tip used on the UH-60A, a rectangular tip and a swept-tapered-anhedral tip. Cross-sectional views of the inner and outer model ACR blades are presented in Figure 4. It should be noted that the structural design developed for these model blades would have been totally inappropriate if the testing had been conducted in air. Similarly the model blade structural concept would not bear any resemblance to a full-scale aircraft design. The primary structural member of the blade is a central spar fabricated from unidirectional pre-preg fiberglass orientated at ±15° with respect to the spanwise axis. To reduce the outer spar torsional stiffness of the ACR blade, troughs were machined on the upper and lower surfaces. Unidirectional graphite straps were bonded to the spar to achieve the desired flatwise properties. A fatigue test was performed on the blade spar, which demonstrated the integrity of the graphite-fiberglass bond. Segmented lead and tungsten counterweights were bonded at the leading edge to provide mass balance about the quarter chord and to increase the torsional inertia to the required values. A fiberglass torque tube was wrapped around the spar on the inner half of the ACR blades and the entire length of the baseline blades to provide conventional blade torsional stiffness.

The blades incorporated internal flatwise, edgewise and torsion moment gages at the 26, 40, 52 and 79 percent radial stations. Two blades were instrumented. Dummy spanwise wiring was added to the other blades to minimize weight and stiffness differences between instrumented and non-instrumented blades.

Individual 0.012-inch-thick trim tabs (stainless steel for the ACR and aluminum for the baseline blade) which increased chord length by 7.5-percent were bonded into a recess on the lower surface of the inboard sections. Individual tabs and weights were used to minimize any increase in edgewise stiffness. A fixture was provided for bending the trim tabs. The tab was sized, based on the data shown in Reference 13, to produce a +0.06 change in c_m for an 8-degree deflection. According to the reference this requires a 7.5-percent chord tab.

---

13. Prouty, R. W., A State-of-the-Art Survey of Two-Dimensional Airfoil Data, Journal of the AHS, Volume 20, No. 4, October 1974, pp. 14 - 25.

Three interchangeable tip configurations were fabricated: a constant chord 20-degree swept tip with the sweep beginning at the 93.5-percent radial station, a rectangular tip, and a swept-tapered anhedral tip. The anhedral tip has a leading-edge sweep angle of 20 degrees between 93.5- and 96-percent radius and a sweep angle of 35 degrees outboard of 96-percent radius. Twenty degrees of anhedral are incorporated at 96-percent radius. Each tip consisted of a tapered fiberglass inner cavity, foam cast to contour, a powdered tungsten counterweight, and an outer cover of fiberglass impregnated with film adhesive. The tips were essentially balanced to the quarter-chord line of the main part of the blade. For attachment to the blades, the tips were slipped over the protruding tapered spar tip sections, aligned and then secured with a 1-inch-wide aluminum strap (0.010 inch in thickness) wrapped chordwise around the blade and bonded at the 89-percent span joint station. Figure 5 shows a completed blade and a sample of each of the tips.

Spanwise stiffness distributions for both the ACR and baseline blades were experimentally determined. The technique of using a point light source and series of miniature mirrors attached along the blade span was utilized. The change in the reflected position of the light from a given mirror is related to the slope of the blade deflection under load at a given spanwise position. These slopes were then related to the local spanwise stiffness properties using elementary beam equations. The stiffness properties of the two blade sets are compared in Figures 6 through 8. Figures 9 and 10 present the mass and torsional inertia properties of the two model blades.

Blade natural frequencies calculated based on measured inertia and stiffness properties are compared in Figures 11 and 12. These results were calculated using the natural frequency section of the Normal Modes Blade Aeroelastic Response Analysis (Y200 Program). As shown the flatwise and edgewise frequencies of the two blade sets are essentially identical. The torsional frequency of the ACR blades on a rigid control system is 4.5/rev, while that of the baseline blades is 6.7/rev at normal operating speed of 670 RPM. The corresponding frequencies are 4.3/rev and 6.0/rev based on the stiffness of the wind tunnel model control system (3750 in.-lb/rad).

Nonrotating blade natural frequencies were measured in order to verify the calculated frequencies and also to determine blade-to-blade dissimilarities in structural properties. Tests were conducted by mounting the blades in a cuff identical to that used in the wind tunnel model and then mounting the hub to a massive structural beam. A miniature

accelerometer was used to measure motion at the tip. A miniature load cell was used to measure excitation force delivered to the blade by an electromagnetic shaker. Wave-, form of the acceleration and load cell force were displayed on an oscilloscope to monitor resonant response. Torsional freedom was locked out at the control horn by a rigid bracket for the duration of the test. Full flap and lag freedom was allowed. No lag dampers were installed.

Frequency measurements were made on each of the eight test blades. Nonrotating frequency and blade weight measurements shown in Table 1 indicate that blade-to-blade differences were very slight. The variation in total blade weight and in nonrotating frequencies were typically less than 1 percent.

Nominal nonrotating frequencies of the model blades are compared in Figures 11 and 12 with calculated frequencies. Generally good agreement is shown. This agreement suggests that measured mass and stiffness properties are accurate and that the calculated blade frequencies used in the correlation study described later in this report are reliable.

WIND TUNNEL TEST PROGRAM

TEST FACILITY AND PROCEDURE

Test Facility

The test program was conducted in the Langley Research Center Transonic Dynamics Tunnel (TDT). The TDT is a continuous-flow tunnel with a slotted test section, and is capable of operation over a Mach number range from 0 to 1.20 at stagnation pressures from .01 to 1 atm. The tunnel test section is a 16 ft square with cropped corners and has a cross sectional area of 247 ft^2. Either air or Freon-12 may be used as a test medium in the TDT. For this investigation, Freon-12 at a nominal density of 0.006 $slugs/ft^3$ was used as the test medium.

Model Description

The basic model used in this investigation was the Langley Research Center Aeroelastic Rotor Experimental System (ARES). The ARES is powered by a variable frequency synchronous electric motor rated at 35kw output at 12000 RPM. The motor is connected to the rotor shaft through a belt-driven, two-stage speed reduction system. Rotor speed is controlled by varying the line frequency to the electric motor. Figure 13 shows the ARES model with the ACR blades installed.

The ARES control system and pitch attitude are remotely controllable from the wind-tunnel control room. The pitch attitude is changed using a hydraulic actuator and an electric servo system. Blade collective pitch as well as lateral and longitudinal cyclic pitch are imparted to the rotor through the model swashplate. The swashplate is moved by three hydraulic actuators. The pitch horns used on the ARES model provide 25° of pitch-flap coupling.

Instrumentation provisions on the ARES allow continuous measurement of model control settings, rotor forces and moments, blade loads, and pitch link loads. Model pitch attitude is measured by an accelerometer, and rotor control positions are measured by linear potentiometers connected to the swashplate. Rotor blade flapping and lagging are measured by rotary potentiometers mounted on the rotor hub and geared to the blade cuff. The rotating blade data are transferred to the fixed system through a 60-channel, horizontal disk slip-ring assembly. Rotor forces and moments are measured by using a six-component strain-gage balance

mounted below the pylon and drive system. The balance is fixed with respect to the rotor shaft and pitches with the fuselage. Fuselage aerodynamic forces and moments are not sensed by the balance.

Data Reduction Procedure

Balance data were processed to provide rotor performance measurements. Balance interactions, deadweight tares and aerodynamic rotor hub tares are removed from the data. Some difficulty was experienced with regard to repeatability of performance data. This difficulty was evidenced by significant shifts between pre- and post-test wind off zero readings. The source of the shift and the nature of the variation during the run are not known. Attempts were made to minimize the impact of this problem by referencing data to a linear variation between pre- and post-test zero readings and by repeating test conditions. A scatter band on the data of ±4 percent in torque for fixed lift and drag is estimated based on repeated test points.

Dynamic data for the twelve blade strain gages, the pitch link load, root flap, lag and pitch angles, and the six components of balance load were recorded on FM tape. Blade bending moment data were reduced by subtracting from the raw data the gage readings measured for a wind-off dynamic zero condition. Blade torsion moments, as discussed in the following section, were reduced by subtracting the dynamic zero data for the ACR blade with the rectangular tip. Pitch link load and balance data are referenced to zero load for a wind-off static zero condition. Root flap, lag and pitch angles were referenced to a physical calibration. Dynamic data were converted to digital format and processed to give mean and peak-to-peak statistics and the first eight harmonic components.

Test Procedure

Data were taken at advance ratios of .20 to .45, shaft angles of attack of +5 degrees to -15 degrees, and hover tip Mach numbers of .62, .65, and .68. For each test point, the rotor rotational speed and tunnel conditions were adjusted to give the desired values of tip Mach number and advance ratio. The model was then pitched to the desired shaft angle. Blade collective pitch was changed to obtain a variation in rotor lift, and at each collective pitch setting, the cyclic pitch was used to remove rotor first-harmonic flapping with respect to the shaft. Data were then recorded at each value of collective pitch. The maximum value of collective pitch attained was determined in most instances by blade load limits.

Derivatives of flapping and of rotor forces with respect to control inputs and shaft angle were measured at selected trim points. The procedure used was first to trim the rotor to chosen lift and propulsive force coefficients and then to successively apply ±2 degree perturbation in each of the independent variables without disturbing the other inputs from their trim settings.

TEST RESULTS

Configurations Tested

The following five configurations were tested under this program (Contract DAAJ02-77-C-0047):

1. ACR blade with swept tip.
2. ACR blade with swept tip and 4° trailing edge up (TEU) tab deflection.
3. ACR blade with swept anhedral tip.
4. ACR blade with rectangular tip.
5. Baseline blade with swept tip.

In addition to these configurations, three additonal ACR configurations were tested by personnel of the Army Structures Laboratory and Applied Technology Laboratory during a February 1980 Transonic Dynamics Tunnel entry. Results of that test will be published by ATL. The additonal ACR configuration tested were:

1. ACR blade with rectangular tip and 4° TEU tab deflection.
2. ACR blade with swept tip and 8° TEU tab deflection.
3. ACR blade with swept tip and 6° TEU tab deflection.

A limited amount of data from the second tunnel entry is included in this report in instances where the additional data help clarify the trends and phenomena measured during the contractual test.

Blade Torsional Response Data

One of the primary objectives of the program was to define the dynamic twist produced by the several variables tested. The results which are presented below are not represented to be profound. In many cases the trends are obvious. The reason for reducing the data in this fashion is to provide a systematic listing of dynamic twist amplitudes so that the impact of the twist on rotor loads and performance can be traced. Previous results had generally suggested that one/rev response which decreased advancing blade twist and increased retreating blade twist would have generally beneficial effects. Results were reduced in a form which permitted clear evaluation of this hypothesis. The test plan included an attempt to estimate dynamic twist by taking stroboscopic motion pictures of the advancing blade. Due to difficulties experienced with the camera system these attempts were not successful. Instead, dynamic twist was estimated from the torsion moment strain gage data. A short data reduction program was written which calculated the relative torsional deflection between strain gage locations based on measured moments and measured torsional stiffness properties. This program was used with the harmonic components of blade moments to estimate steady, one/rev and two/rev elastic response. In order to permit comparison of the different blades, data were not reduced by referencing each moment to its dynamic zero reading but rather to the dynamic zero reading for the rectangular tip ACR blade with no tab deflection. Using the individual dynamic zeros would, of course, have eliminated the basic effects of changes in camber and sweep from the data. Using no dynamic zeroes would have retained unwanted signals due to bending moment interactions and centrifugal force effects. It was justified by reference to the analysis that the straight ACR blade at the dynamic zero condition produces approximately zero moment and zero dynamic twist.

Sample estimates of dynamic twist are shown in Figures 14 and 15. Plotted are blade steady elastic twist and one/rev lateral twist for an advance ratio of 0.3, shaft angle of -5 degrees and C_L/σ of 0.08. As desired, ACR twist is concentrated on the outer half of the blade. Steady elastic twist values range from approximately -3 to +4 degrees for the configurations tested. One/rev lateral twist results range from configurations which increase advancing blade twist by 1.4 degrees (the rectangular tip ACR blade) to those which decrease advancing blade twist by 3.3 degrees (the 8 degree trailing-edge-up tab ACR blade).

The elastic twist program examined the variation with flight condition of the steady, one/rev and two/rev twist at the tip for each of the configurations. Results were generally in agreement with pre-test analysis. Figures 16 through 20 display the buildup with C_L/σ of steady and one/rev twist for five rotors at an advance ratio of 0.3 and -5 degree shaft angle. The one/rev plots show the amplitude and azimuthal position for peak noseup one/rev tip twist. Points are connected in order of increasing blade loading. Figure 21 compares the one/rev elastic twist produced by several configurations at a $C_L/\sigma = 0.08$ and $\mu = 0.30$. Figure 22 compares two/rev elastic twist for the same configurations and flight condition. From these elastic twist data the following observations can be made.

1. The baseline blade experienced nosedown steady twist of approximately two degrees. One/rev twist was less than one degree.

2. The rectangular ACR blade produced nosedown steady twist and one/rev twist which was nosedown on the advancing blade. This blade also produced a significant amount of two/rev twist phased to increase pitch at advancing and retreating blade positions.

5
F

3. Nosedown steady twist increases with rotor lift for all swept tip blades. Tip sweep tends to drive the position for noseup one/rev twist toward the advancing blade (see Figure 21). For the blades tested the untwisting of the advancing blade was approximately one degree at $\mu = 0.3$.

4. Noseup camber produced noseup steady elastic twist and one/rev twist which was noseup at the advancing blade positon.

5. The anhedral swept tip tested produced nosedown steady twist which was generally similar to that of the swept tips. One/rev twist was basically advancing blade nosedown.

Plots similar to Figures 16 through 20 were prepared for all test conditions. Results were used to describe the twist variations with advance ratio, lift and propulsive force. Figures 23 through 25 present summary plots of these data. Results are shown for three combinations of C_L/σ and equivalent full-scale aircraft flat plate area. Plots include steady tip twist, one/rev lateral twist and the blade twist

at ψ = 90° due to steady plus one/rev components. In terms of producing low advancing blade twist the blades are ordered in the following way at high advance ratios.

1. ACR blade with 4 degree TEU tab deflection.
2. Baseline blade with swept tip.
3. ACR blade with swept tip.
4. ACR blade with anhedral swept tip.
5. ACR blade with rectangular tip.

As shown the steady elastic twist generally becomes nosedown with increased airspeed. Changes in propulsive force of the magnitude considered had a secondary effect on elastic twist amplitudes. The changes in elastic twist produced by torsional stiffness, camber, tip sweep and anhedral are collected in Figures 26 through 27 for a representative C_L/σ and flat plate drag area. Figure 26 shows that reducing blade torsional stiffness from the baseline to the ACR level generally caused increased twist. This is to be expected based on the basic nosedown section pitching moment of the SC 1095 airfoil. The independent effect of a noseup camber change on the conformable blade (Figure 27) is to produce noseup steady and noseup advancing blade one/rev twist which increase with airspeed. At the .08 blade loading condition sweep produces a small noseup advancing blade twist (less than one degree) (Figure 28). In comparison to the swept tip conformable blade, the principal effect of adding anhedral is to increase steady nosedown twist at high speed (Figure 29).

5
B

Rotor System Loads

Blade flatwise, edgewise and torsion moments were compared for the configurations tested. Results generally supported the expectation of reduced loads for those configurations which reduced advancing blade total twist.

The variation of blade moments with lift coefficient and shaft angle is illustrated in Figures 30 through 34 for the five configurations tested. Flatwise loads were generally maximum at the 53-percent radius; torsion and edgewise loads at 27-percent radius. Therefore these stations are shown. The figures show that edgewise moments build up with blade loading and forward tilt of the shaft. Flatwise moments are generally insensitive to shaft angle and C_L/σ. Torsion

moments are relatively constant until blade loading (C_L/σ) reaches approximately 0.10, at which point high frequency components become significant. Figure 35 compares all configurations at an advance ratio of 0.3 and -5 degree shaft angle. Figure 35a shows all blades having the same swept tip. Included in Figure 35a are the blade loads of a -16 degree twist conventional stiffness baseline UH-60A model blade which was tested on the ARES model in the Transonic Dynamics Tunnel in 1978 (Reference 9). The ranking of ACR configurations in terms of reducing blade flatwise moments follows directly from the advancing blade elastic twist angle. The highest loads were measured on the rectangular tip ACR blade and the lowest on the 8-degree tab ACR configuration. This rotor produced up to a 50-percent reduction in flatwise loads relative to the -12 degree baseline stiffness blade and a 70-percent reduction relative to the -16 degree twist UH-60A model blade. These results are in qualitative agreement with the pretest analysis in which tip sweep and noseup pitching moment were shown to reduce vibratory flatwise loads.

The significance of the blade load reductions achieved by the ACR blades cannot be assessed without considering the associated effect on hover performance. To have a useful effect, the ACR must produce hover and forward flight twisting which permits a more favorable tradeoff between hover performance and forward flight loads than that possible with a conventional stiffness (fixed twist) design. Ideally, the goal is to have a torsionally soft blade of low built-in twist which winds up in hover to achieve high twist and good hover performance and which untwists on the advancing side in forward flight to produce very low twist and low blade loads. Figure 36 compares the model blade data in this regard. Blade vibratory bending moments measured at an advance ratio of 0.3 are plotted against hover figure of merit. Because the model blades were not tested in hover, the hover data are based on analysis. A version of the Sikorsky Circulation Coupled Hover Analysis program which treats blade flexibility was used. This analysis is described in Reference 2. The -12 degree twist swept-tip baseline blade tested under this program and the -16 degree twist UH-60A blade tested under a previous program show the tradeoff which is present with conventional stiffness blades. Results shown for the -12 degree twist swept-tip ACR blades illustrate benefits in terms of reduced blade moments for a fixed figure of merit or improved figure of merit for fixed loads. Twenty-five to 35 percent reductions in bending moments or one percent improvements in figure of merit are shown to be possible.

Blade vibratory edgewise bending moments are compared in Figure 37 for the 0.3 advance ratio, -5 degree shaft angle condition. Edgewise loads on the rectangular tip ACR blade are approximately 25 percent higher than the other configurations which are approximately the same as one another. Vibratory root torsion moments are compared for the same conditions in Figure 38. The rectangular tip ACR blade experienced the highest loads. The 6- and 8-degree tab ACR configurations which produced the most significant noseup advancing blade elastic twist had the highest torsion moments at high blade loading as a result of elevated one/rev and two/rev loads.

The effects of the dynamic twist on blade flatwise and torsion moments are illustrated by the time histories shown in Figures 39 and 40. Figure 39 illustrates the effect of changes in torsional stiffness and camber. It shows clearly that reducing the torsion stiffness from the baseline to conformable blade levels causes increased advancing blade twist and aggravated tip down bending in the second quadrant. Driving the section pitching moment coefficient noseup with reflex deflection of the tab reduced the effective advancing blade twist by approximately 8 degrees, thereby causing a significant reduction in advancing blade bending. Figure 40 shows the source of the high flatwise loads experienced by the rectangular tip ACR blade. Relative to the swept tip blade, additional nosedown twist was produced between ψ = 150 and 210 degrees. This is shown in Figure 40 to have caused increased downward bending over the nose and a higher subsequent upward bending on the retreating side of the disc. It should also be noted that the rectangular blade produced higher 3/rev and 4/rev elastic twist angles and flatwise loads than any of the other configurations.

The effects of torsional stiffness, tip sweep and camber on the harmonic content of flatwise and torsion moments are illustrated in Figure 41. Relative to the rectangular tip ACR blade, addition of tip sweep or noseup section pitching moment reduced flatwise moments at one, two and three/rev. The rectangular tip ACR blade had generally highest torsion moments at all harmonics.

The 0.3 advance ratio data described above was combined with data at 0.3, 0.4 and 0.45 to form the plots shown in Figures 42 through 44. Here the vibratory loads are shown for four combinations of lift coefficient and aircraft equivalent flat plat drag area. As shown, differences between configurations are insignificant at a 0.2 advance ratio. Where data are available, the trends described earlier for μ = 0.3

apply to the $\mu = 0.4$ condition. Vibratory blade loads from Figure 44 were evaluated in relation to advancing blade total twist (built-in twist plus estimated elastic twist from Figure 25). Typical results shown in Figure 45 illustrate the trend for reduced flatwise moments with reduced advancing blade twist. Edgewise and torsion moments, as noted earlier, are slightly higher for the configurations which produce significant one/rev lateral twist.

Vibratory Hub Loads

Data from the balance gages which sense rotor forces and moments were harmonically analyzed to provide an indication of the effects of the various rotor configurations on vibratory hub loads. The balance is not dynamically calibrated so the indicated force and moment values can only be used to determine trends. Also, the forces and moments are measured at the balance, which is 20.25 inches below the hub, and not at the hub itself.

In most cases, the measured vibratory loads projected beneficial effects of tip sweep and reflex tab deflection on fixed system response for the ACR blades. However, vibratory loads were generally higher, for the low torsion stiffness rotor than for the baseline rotor. Typical results are shown in Figures 46 and 47. The higher vibratory loads produced by the ACR may be traceable to higher levels of torsional response at 4/rev on the ACR blades due to closer proximity of this harmonic to the torsional natural frequency (4.3/rev). Highest vibratory loads were measured with the rectangular tip ACR blade. As noted above this configuration had the highest 3 and 4/rev elastic twist components. The principal observation is that the vibration appears to be sensitive to alterations in the airload distributions which can be produced by changes in blade torsional response. A future design, perhaps having the torsional natural frequency below 4/rev, may lead to partial cancellation of the airload contribution to fixed system vibration.

Rotor Performance

The pretest analysis projected that there would be significant effects of tip sweep and camber on rotor aerodynamic performance at advance ratios above 0.2. L/D_E improvements on the order of 10 percent with the addition of tip sweep and 20 percent with a +0.03 increase in pitching moment coefficient were predicted. Rotor performance data were reduced to permit comparison of configurations at advance ratios of 0.2, 0.3, 0.4 and 0.45. Results are presented in

Figures 48 through 51. As noted earlier, experimental difficulties were experienced with regard to balance force and torque measurements. Variations in measured torque for fixed lift and drag were typically on the order of ±4 percent for repeated test conditions. Most of the configuration to configuration differences measured were of the same order of magnitude as this uncertainty. Differences greater than the uncertainty band were, however, measured in several instances. These results permit the following conclusions to be drawn:

1. Blades with reflex camber had superior performance for moderate lift and propulsive force coefficients at $\mu = 0.3$, 0.4 and 0.45. At high lift and propulsive force coefficients no significant gains were measured (Figure 49).

2. At an advance ratio of 0.3 and for positive propulsive force conditions, the ACR blade with the swept tip required less power than the rectangular tip ACR blade and the baseline blade.

3. The performance effect of anhedral was favorable at $\mu = 0.2$ but unfavorable at $\mu = 0.4$ and 0.45.

The significant reductions in power experienced with noseup section pitching moment and the increase in power required on the anhedral tip blade generally follow trends of advancing blade twist. Figures 23 through 25 showed blades with reflex tab deflection to have the lowest advancing blade twist and the anhedral blade to have the highest. In light of these favorable trends and the fact that there were some problems experienced in measuring performance, further testing should be conducted to increase confidence in the results.

Control Derivatives and Trim Requirements

In considering the use of blades which produce significant torsional response, the possible effects on aircraft stability and control characteristics must be considered. The variation of blade torsion response with the application of controls or with airspeed, for example, will obviously affect the rotor contribution to aircraft stability and control derivatives. The amplitude and phase relation between applied cyclic and actual blade pitch change including dynamic twist may alter the basic flapping response to cyclic pitch inputs. Washout of steady and one/rev pitch inputs by dynamic twist must be compensated for by applying additional control. Reference 1 illustrated that in some cases the required inputs might exceed the capability of a

conventional control system. The tunnel test provided the opportunity to define effects on control inputs required for trim and to measure rotor control and angle of attack derivatives. Derivatives were measured for the conformable blades with swept tips, swept tips and 4 degree reflex tab deflection and with rectangular tips; derivatives were also measured for the baseline blades with swept tips at an advance ratio of 0.3, shaft angle of -5 degrees and a blade loading of 0.07. Rotor steady forces and moments were recorded for independent ±2-degree changes in θ_{75}, A_{1C}, B_{1C} and shaft angle. A_{1C} and B_{1C} are the inputs in an axis system defined by the position of the swashplate actuators and the geometry of the pitch horn. Positive A_{1C} increases pitch when the blade is at 212 degrees azimuth, positive B_{1C} increases pitch at $\psi = 302$ degrees. Rotor hub forces and moments were plotted versus the perturbation quantities to assess linearity and calculate derivatives. The derivatives of rotor forces and moments with cyclic pitch in the actuator axis system were transformed to provide derivatives in an axis system aligned with the freestream. Tables 2 through 5 present the final derivatives for the four configurations examined. The derivatives show no unusual behavior of the ACR blades. The derivative of normal force with collective is lower for the ACR swept tip blades as would be suggested by the increased nosedown steady elastic twist with collective for these blades. The ACR blade with the rectangular tip had a $\Delta N/\Delta\theta_{75}$ derivative which was comparable to that of the baseline. Rotor axial force and pitching moment variations with collective were similar for the configurations examined. The one/rev flapping and hub pitching and rolling moments produced by cyclic pitch were essentially the same for all configurations. Figure 52 illustrates the flapping response to one degree actuator inputs. These results show one/rev flapping of approximately one degree per degree of cyclic. The phase lag between pitch and flapping is between 70 and 90 degrees for the configurations tested. There was no significant variation in phase angle with torsion stiffness or blade geometry.

The control inputs required for trim were not significantly different for the baseline and conformable rotors. Results are illustrated in Figure 53. The trends are generally in agreement with expectations based on estimated elastic twist. Rotors producing increased steady nosedown twist require slightly higher collective pitch; rotors which untwist the advancing blade and twist the retreating blade require additional longitudinal cyclic pitch. Trim requirements of the conformable rotors tested were in no cases excessive.

CORRELATION STUDY

Upon completion of the data reduction and analysis, a correlation study was performed with the Normal Modes Blade Aeroelastic Response Analysis (Y200 Program). The purpose of the study was two-fold: First, the correlation study assessed the adequacy of the response analysis and pointed out areas in which refinement is desired. Second, exercise of the analysis improved understanding of the phenomena measured in the tunnel. The response mechanisms by which tip sweep and camber affect blade loads and performance were clarified by the analysis.

The Y200 Program was run assuming the hub to be fixed. The analysis used a nonuniform inflow distribution calculated by the UTRC Prescribed Wake Inflow Analysis. The two programs are coupled together so that blade response, inflow and circulation distributions are consistent between the two analyses. The procedure for linking the analyses is discussed in References 2 and 11. Flatwise, edgewise and torsion stiffness properties measured on the final blades were supplied to the analysis. Blade weight, torsional inertia and center-of-gravity distributions were determined from measurements on sample blade sections. Full-scale Reynolds Number data for the SC 1095 and SC 109R8 airfoils were used. Actual Reynold Numbers are approximately 40 percent of the full-scale values. No data are available to quantify differences in airfoil characteristics resulting from this effect. Twenty-four test points were examined for the ACR blades with swept and rectangular tips, with and without tab deflection and for the baseline swept tip blades.

The first aspect of the correlation examined was blade elastic twist. The calculated trends were in agreement with those measured in the wind tunnel; however, the predicted magnitudes of steady and one/rev twist were not always accurate. Figure 54 illustrates typical results. The trend with positive Δc_m for increased noseup steady and noseup advancing blade one/rev lateral twist is well predicted. The nosedown steady twist calculated to result from the addition of tip sweep is significantly greater than that estimated from the test data. Also, the predicted effect of tip sweep in producing noseup advancing blade twist was approximately twice the measured value. These results suggest that three-dimensional effects not modelled by the analysis reduce the strength of the airloads applied at the tip. The lateral component of one/rev twist for the conformable blade with the rectangular tip was overpredicted.

The advancing blade was predicted to experience a more extreme nosedown twist. This may be the result of overestimating the nosedown section pitching moment of the airfoil at high Mach number.

Blade vibratory flatwise bending and torsional moment trends were predicted adequately by the analysis. Sample flatwise moment time histories shown in Figure 55 for the ACR blade with the swept tip are in general agreement with test waveforms. Peak-to-peak levels are underpredicted for the higher advance ratios at which the test data show a more rapid buildup in 3/rev bending. The analytic results may reflect a calculated first flatwise mode further below 3/rev than was actually the case. Corresponding root torsion moment histories presented in Figure 56 show an overpredicted steady twisting moment and a one/rev moment of approximately the right phase but 30 to 40 percent lower amplitude than the test results. Edgewise moments were underpredicted by approximately 50 percent for all configurations. Waveform correlation was poor. Figure 57 compares the predicted and measured buildup of blade loads with lift coefficient for the swept tip ACR blade at an advance ratio of 0.3 and -5 degree shaft angle. The buildup of blade loads with lift coefficient is predicted although absolute loads are underpredicted.

The capability of the analysis for predicting the effects of tip sweep and camber changes on blade loads and rotor performance was evaluated at advance ratios of 0.2, 0.3 and 0.4. Typical results are shown in Figure 58. Blade load trends were well predicted in nearly all cases. The analysis generally predicted larger effects of sweep and camber changes on rotor performance than were measured as shown in Figure 55. It was not possible to judge the correlation of vibratory hub load prediction because no quantitative data were measured. Qualitatively, however, the rectangular tip ACR blades were predicted to have the highest vibratory loads followed by the swept tip ACR, the swept tabbed ACR and the baseline. This order is in agreement with the test results shown in Figures 46 and 47.

CONCLUSIONS

1. Blades can be designed to produce dynamic twist, which causes them to experience significantly lower forward flight blade loads than a conventional design while matching or improving hover performance.

2. Steady and one/rev dynamic twist can be controlled through blade design. Noseup blade pitching moment provides noseup steady twist and one/rev twist which is noseup on the advancing blade. Tip sweep provides nosedown steady twist and noseup twist in the second quadrant of rotor azimuth. For the blades tested, a change in pitching moment coefficient of +0.03 produced much larger dynamic twist than 20 degrees of sweep over the outer 6.5-percent span.

3. Blade vibratory flatwise bending moments and root torsion moments were significantly reduced by configurations which untwisted the advancing blade. For low stiffness blades having the same built-in twist, addition of tip sweep reduced flatwise bending moments by 20-percent and root torsion moments by 40 percent. For low stiffness blades having the same built-in twist and tip sweep, incorporating noseup pitching moment reduced flatwise vibratory loads by 60 percent without increasing root torsional moments. The -12 degree built-in twist swept tip ACR blade which would have a total twist in hover that is approximately the same as a -16 degree twist conventional stiffness blade achieves a reduction in flatwise blade moments of approximately 30 percent at an advance ratio of 0.3.

4. Relative to a rectangular tip low stiffness blade, addition of tip sweep or noseup section pitching moment reduced vibratory hub loads.

5. For the conformable blades tested, vibratory loads were equal to or greater than those produced by a conventional stiffness baseline blade of the same built-in twist.

6. Blades which experienced noseup twisting on the advancing blade improved aerodynamic performance. The most significant power savings, which were on the order of 10 to 12 percent, were achieved by a blade having noseup section pitching moment and tip sweep.

7. The control inputs required to achieve trim and the control derivatives of the conformable rotor were not significantly different from those of the baseline rotor.

8. A state-of-the-art blade response analysis adequately predicts all important trends of blade elastic response with torsional stiffness, tip sweep and camber changes.

RECOMMENDATIONS

Based on the results of this effort, it is recommended that:

1. The existing data be reviewed and a design analysis conducted to establish combinations of torsional stiffness, built-in twist, tip sweep (angle and radial position) and tab deflection (amount and position) which optimize blade loads and hover and forward flight performance.

2. An analysis be performed to identify blade design features and elastic response which reduce vibratory hub loads. Configurations which are indicated to have favorable effects on vibration should be fabricated and tested.

3. The aerodynamic and structural modelling of blades incorporating advanced tips (such as swept) be examined with a view toward improving agreement between measured and calculated blade dynamic twist.

4. Second-generation model rotor blades incorporating more nearly optimal features be built and tested in hover and at high advance ratio.

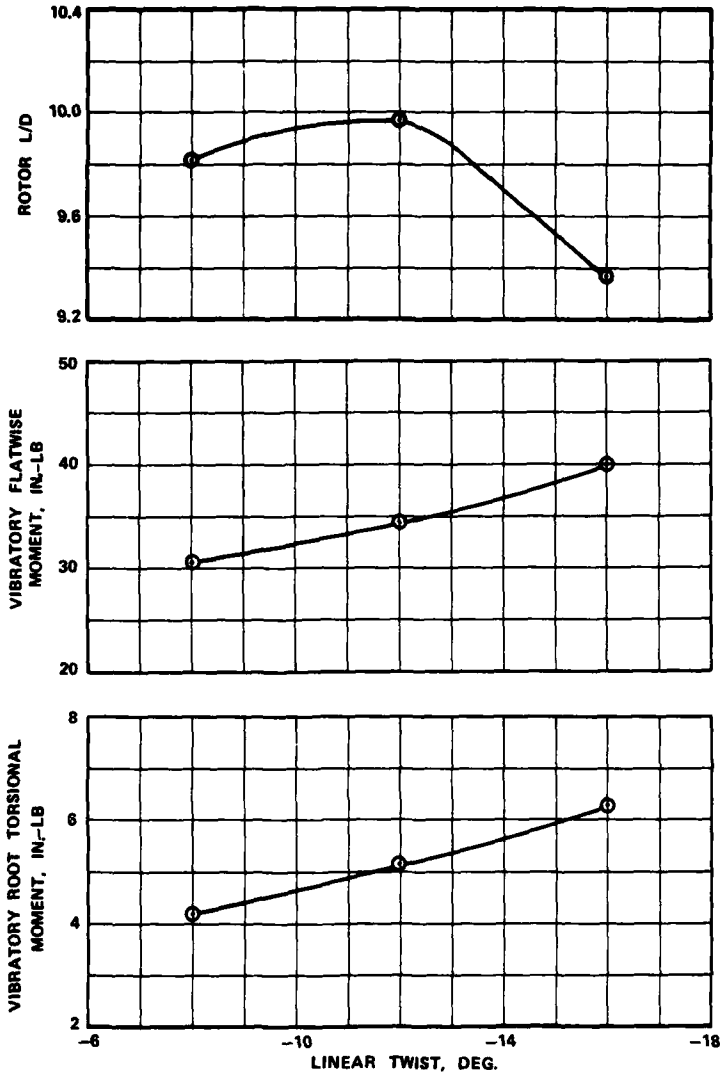

Figure 1. Calculated Variation of Conformable Rotor L/D_E, Blade Flatwise Moment and Root Torsional Moment with Blade Twist; $\mu = 0.35$, $C_L/\sigma = 0.07$.

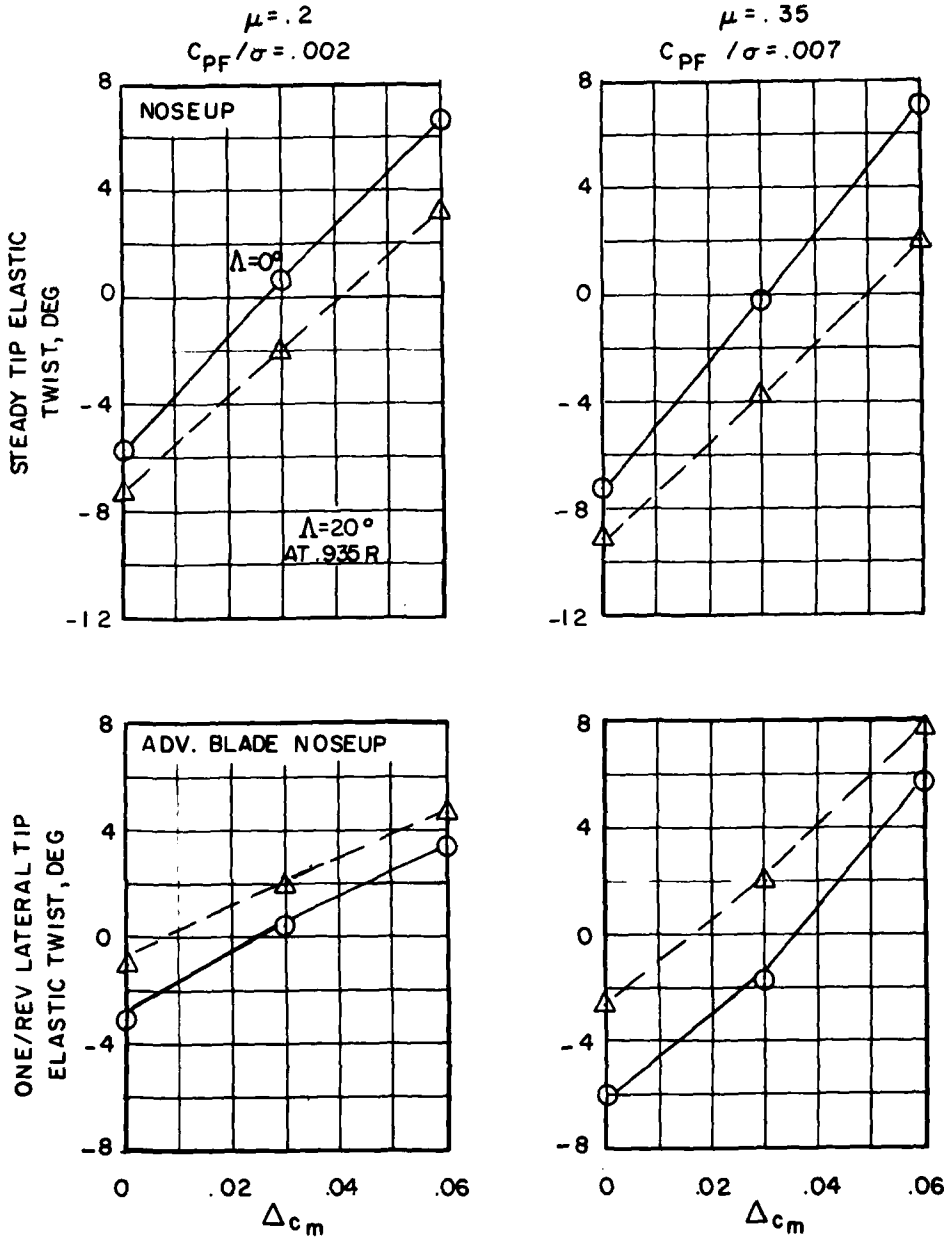

Figure 2. Calculated Variation in Steady and One/Rev Lateral Tip Elastic Twist With Section Pitching Moment Coefficient at C_L/σ = 0.07.

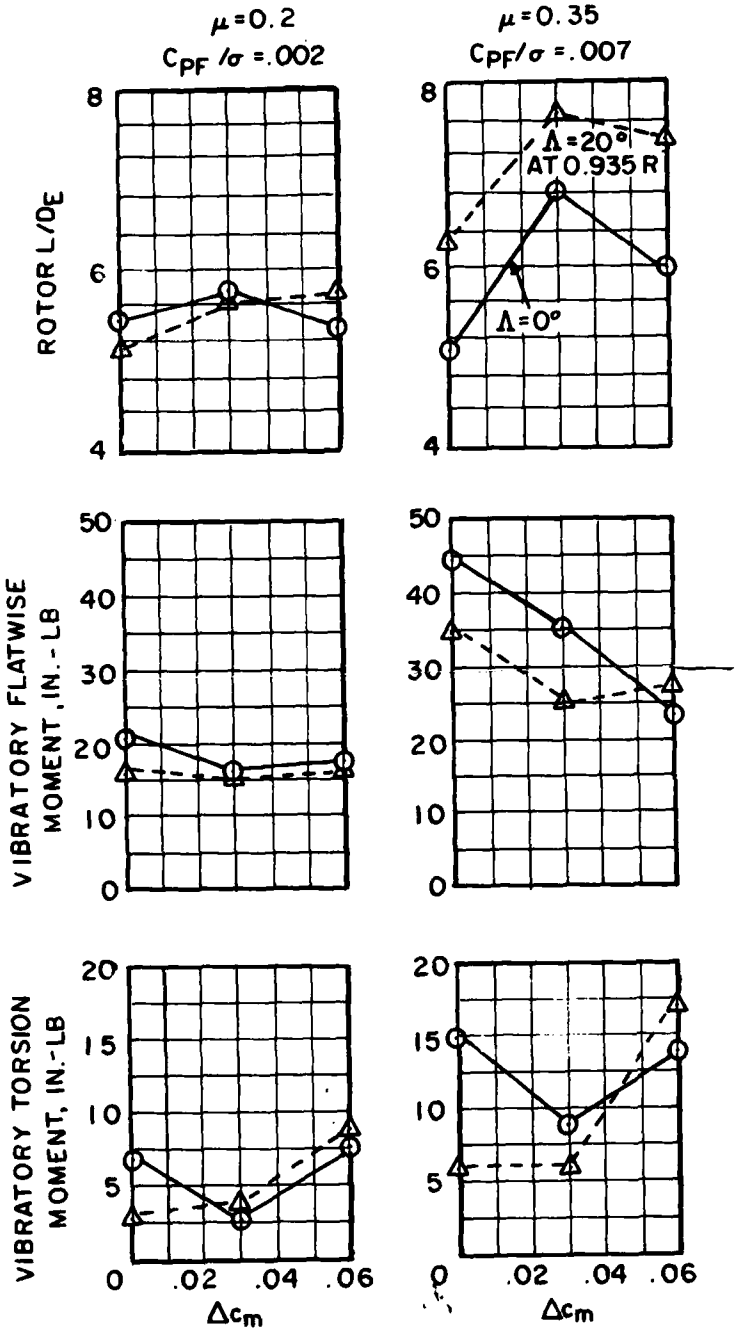

Figure 3. Calculated Effect of Tip Sweep and Section Pitching Moment Coefficient on Conformable Rotor L/D_E and Blade Moments at $C_L/\sigma = 0.07$.

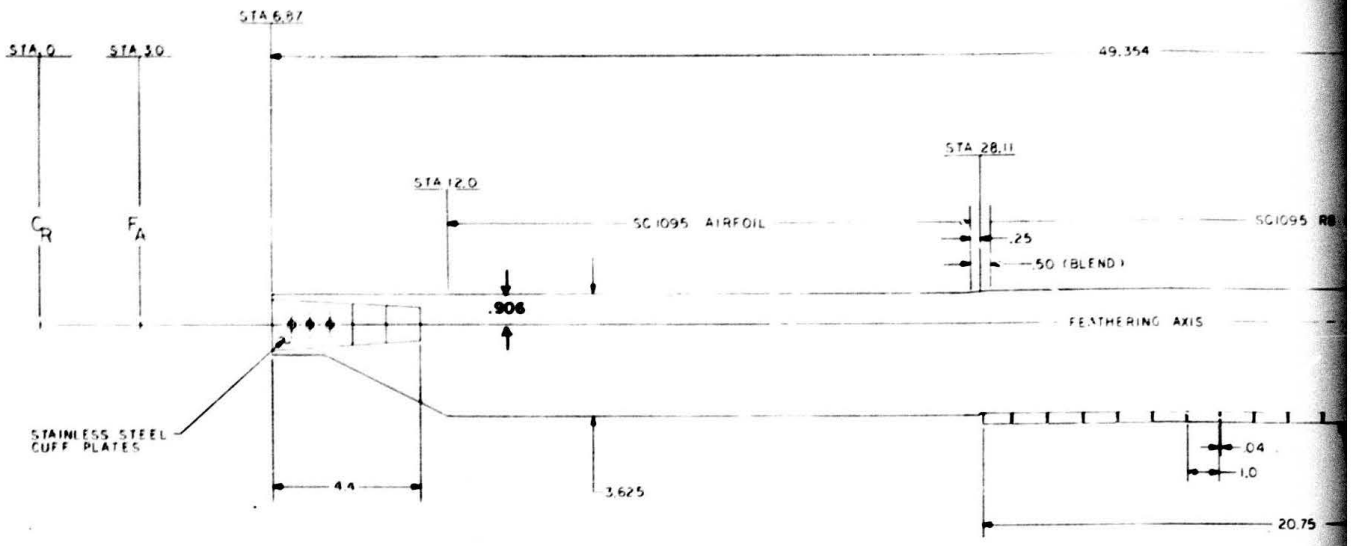

NOTE

ALL DIMENSIONS ARE DESIGN VALUES. ACTUAL INSTALLED ROTOR DIAMETER IS 56.284 INCHES DUE TO .030 ADDED TO TIPS FOR BALANCE WEIGHT AND TO .030 INBOARD OFFSET OF CUFF BOLT HOLES.

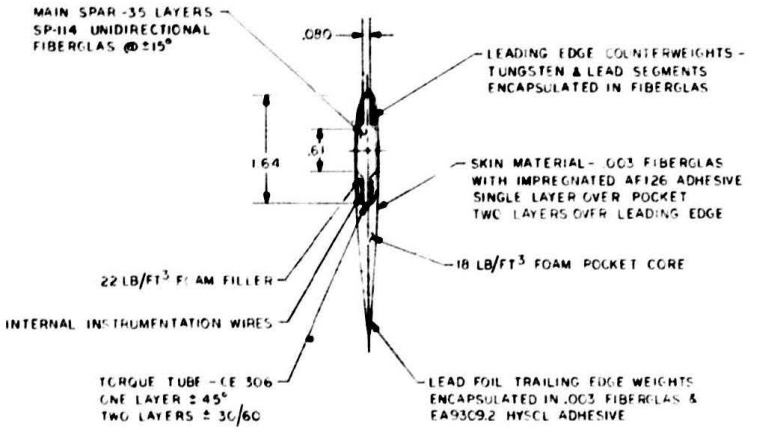

TYPICAL INBOARD SECTION
ACR & BASELINE BLADES

TYPICAL OUTBOA
BASELINE

Figure 4. Model Blade General Assembly Drawing.

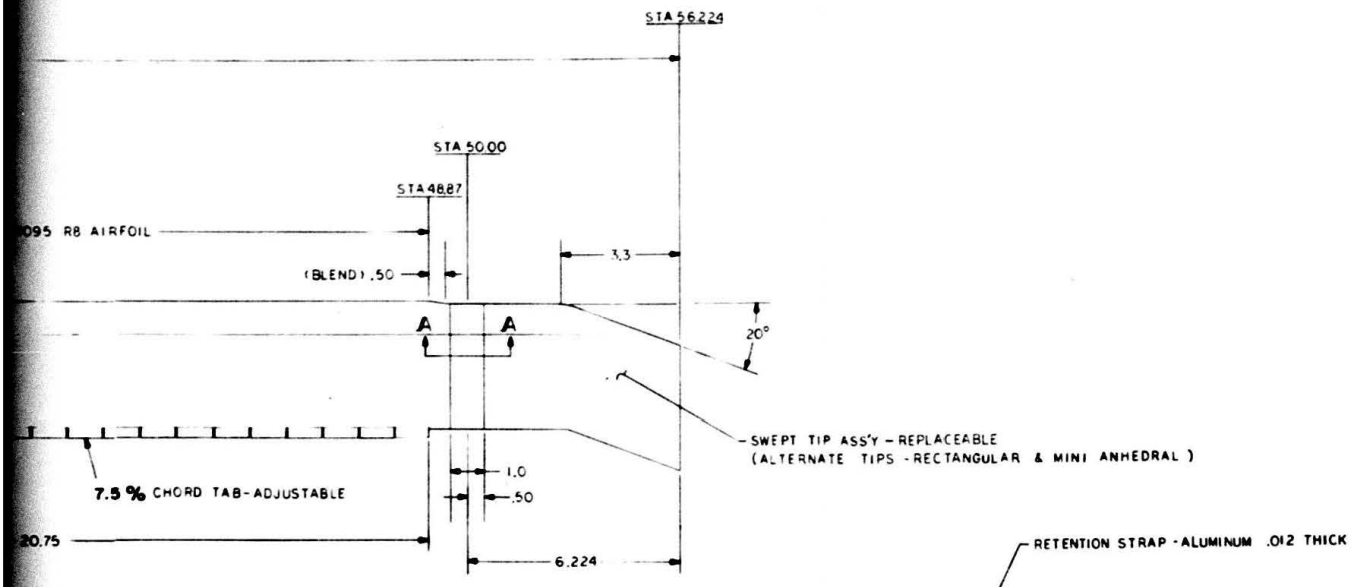

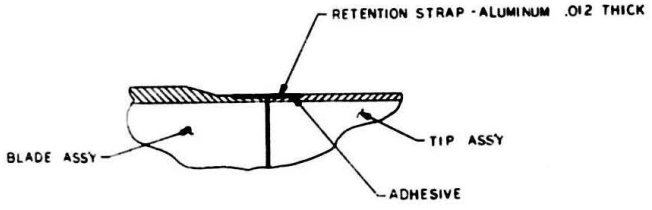

SECTION A-A

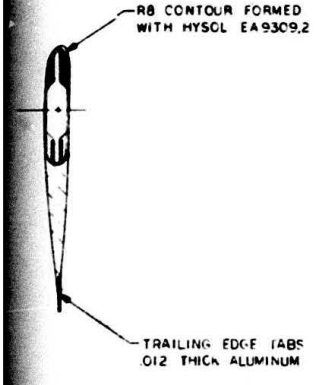

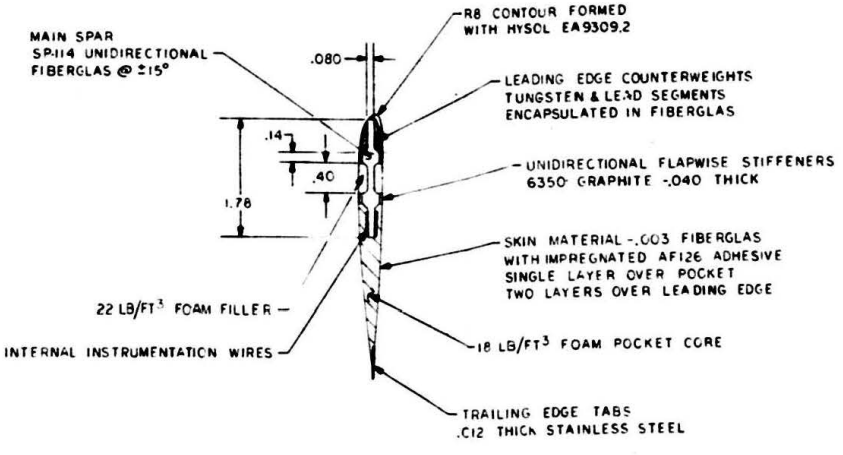

UTBOARD SECTION
ELINE BLADE

TYPICAL OUTBOARD SECTION
ACR BLADE

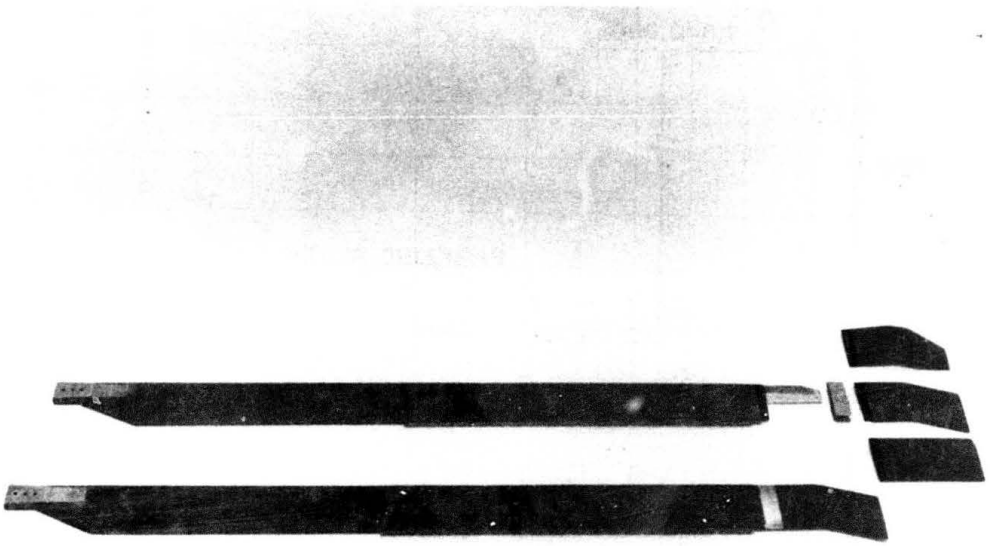

Figure 5. ACR Model Blade and Tips.

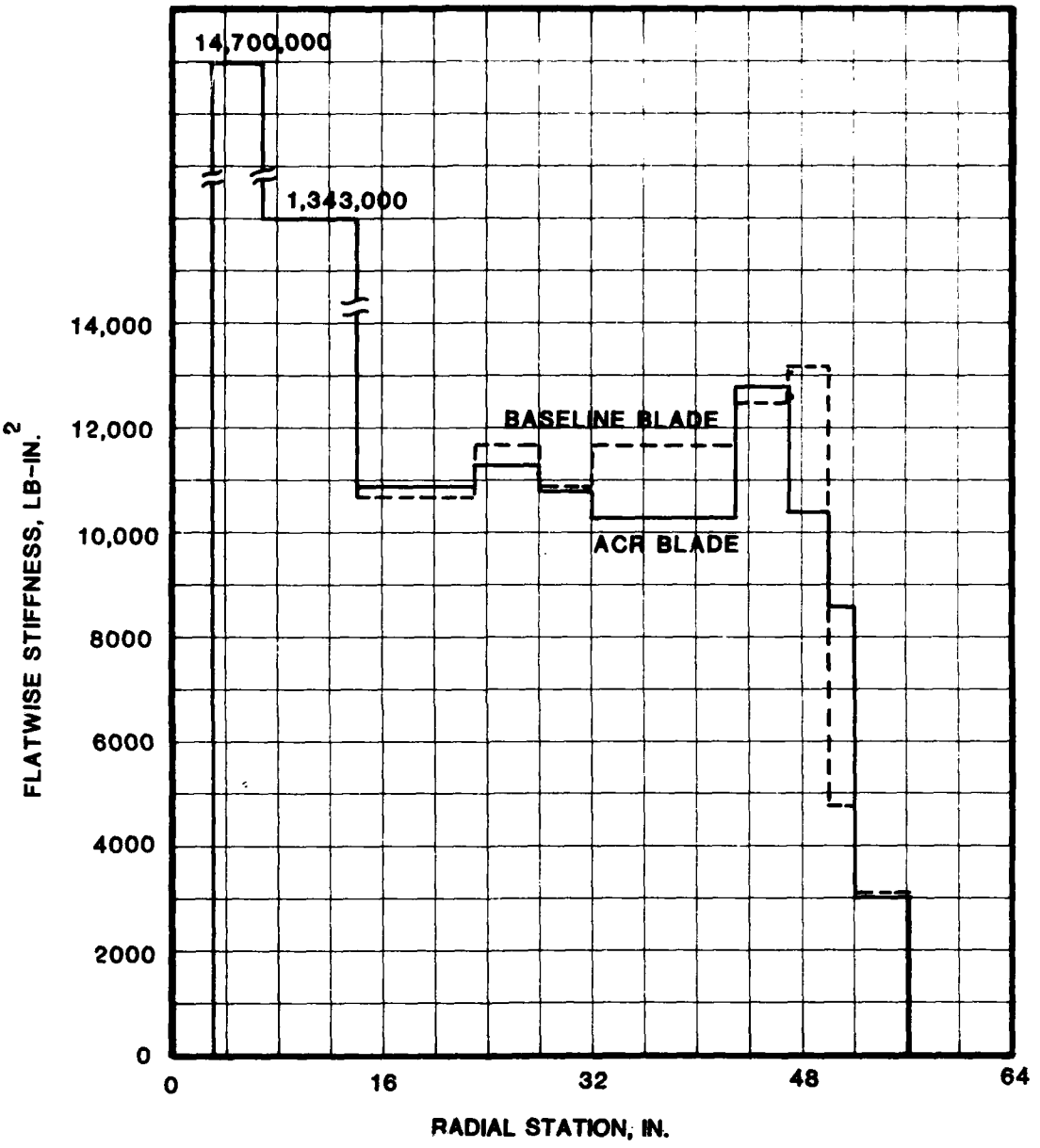

Figure 6. Comparison of ACR and Baseline Blade Flatwise Stiffness Distributions.

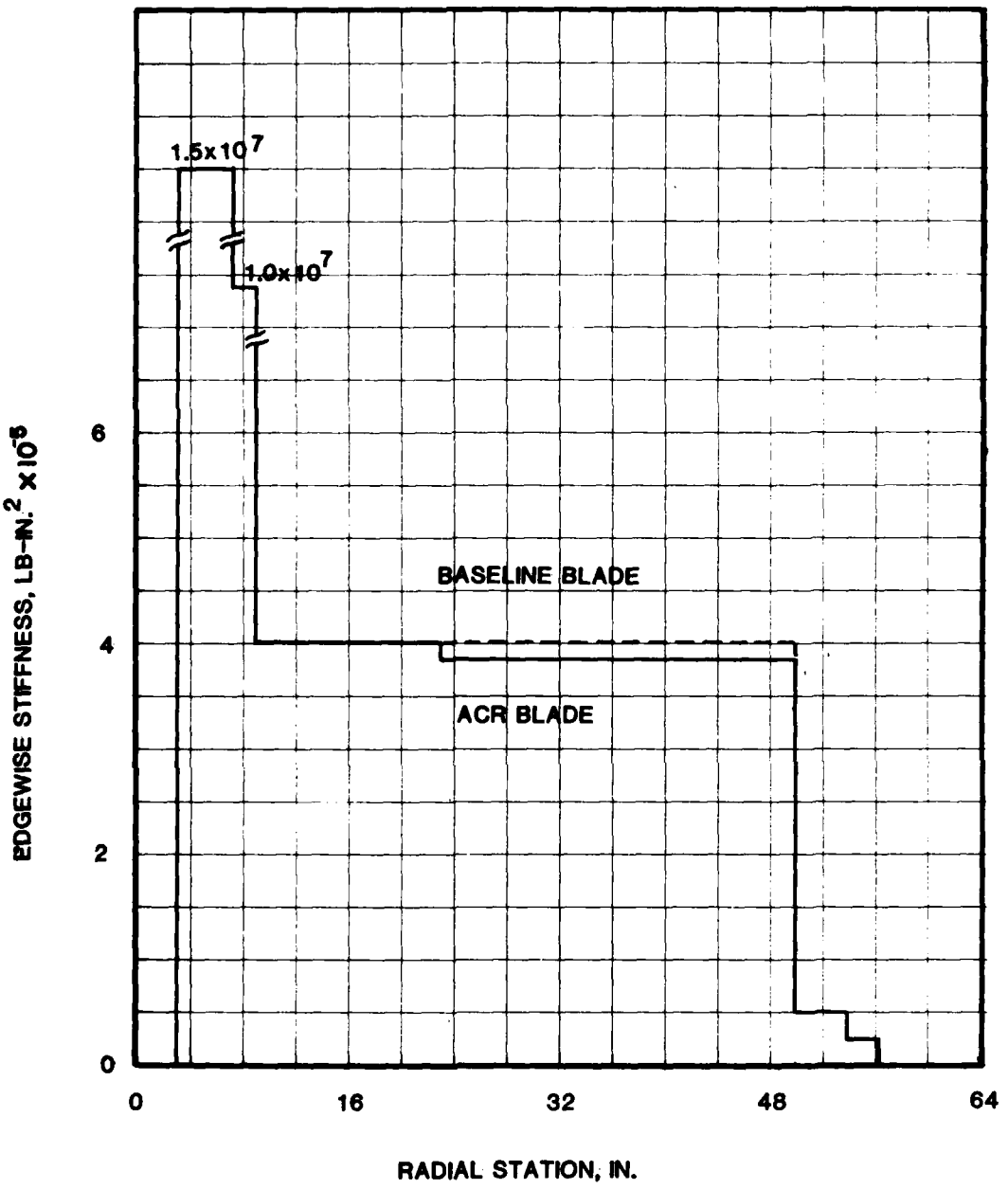

Figure 7. Comparison of ACR and Baseline Blade Edgewise Stiffness Distributions.

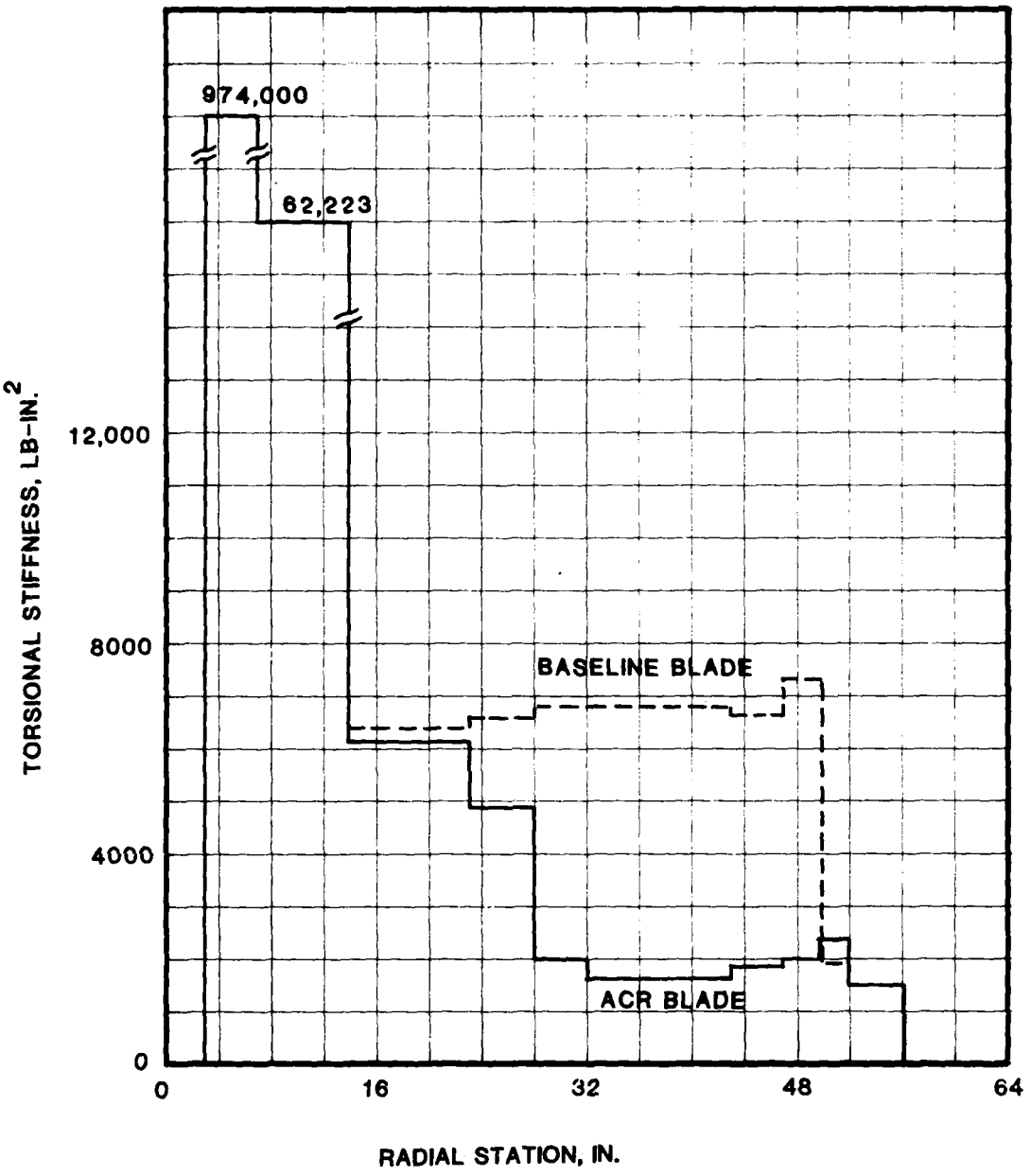

Figure 8. Comparison of ACR and Baseline Blade Torsional Stiffness Distributions.

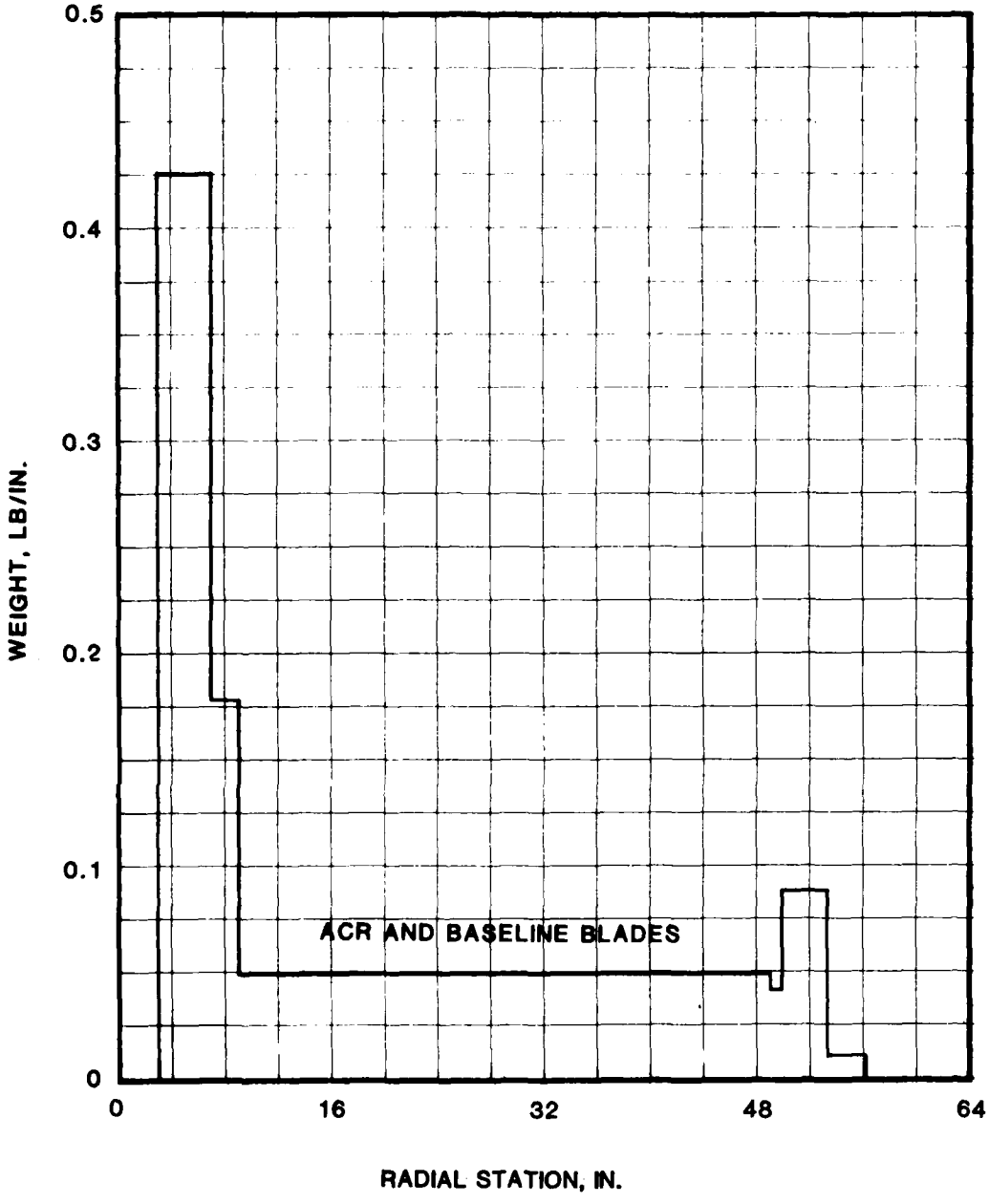

Figure 9. ACR and Baseline Blade Weight Distributions.

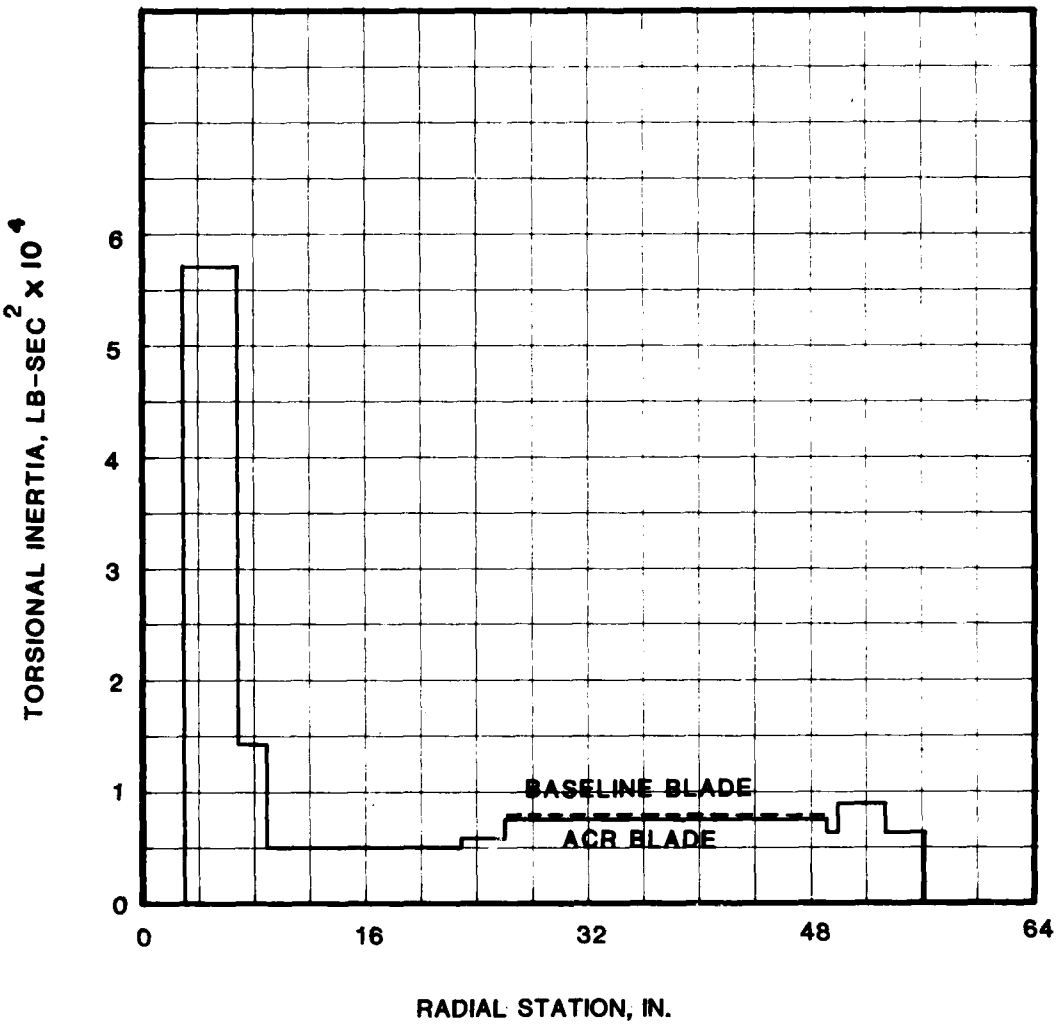

Figure 10. Comparison of ACR and Baseline Blade Torsional Inertia Distributions.

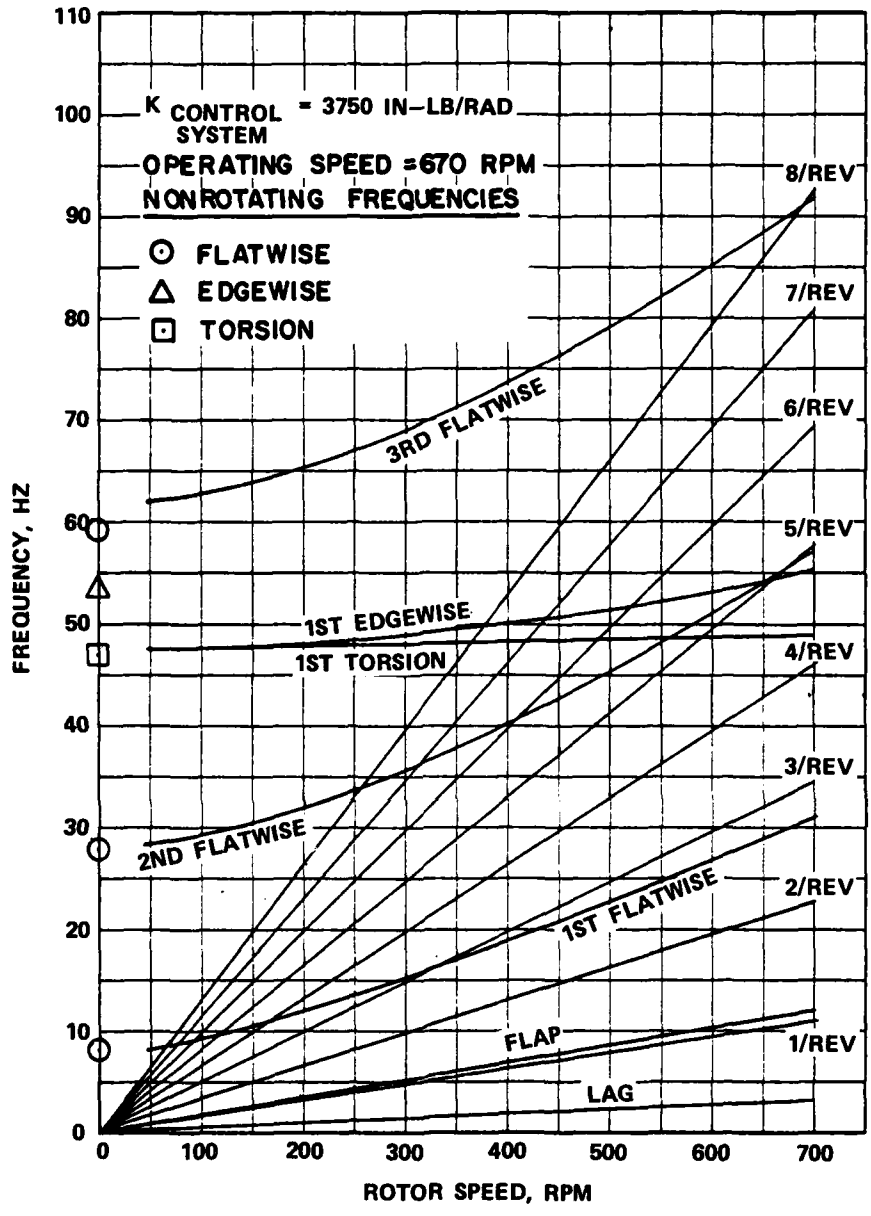

Figure 11. Natural Frequencies of ACR Model Blades.

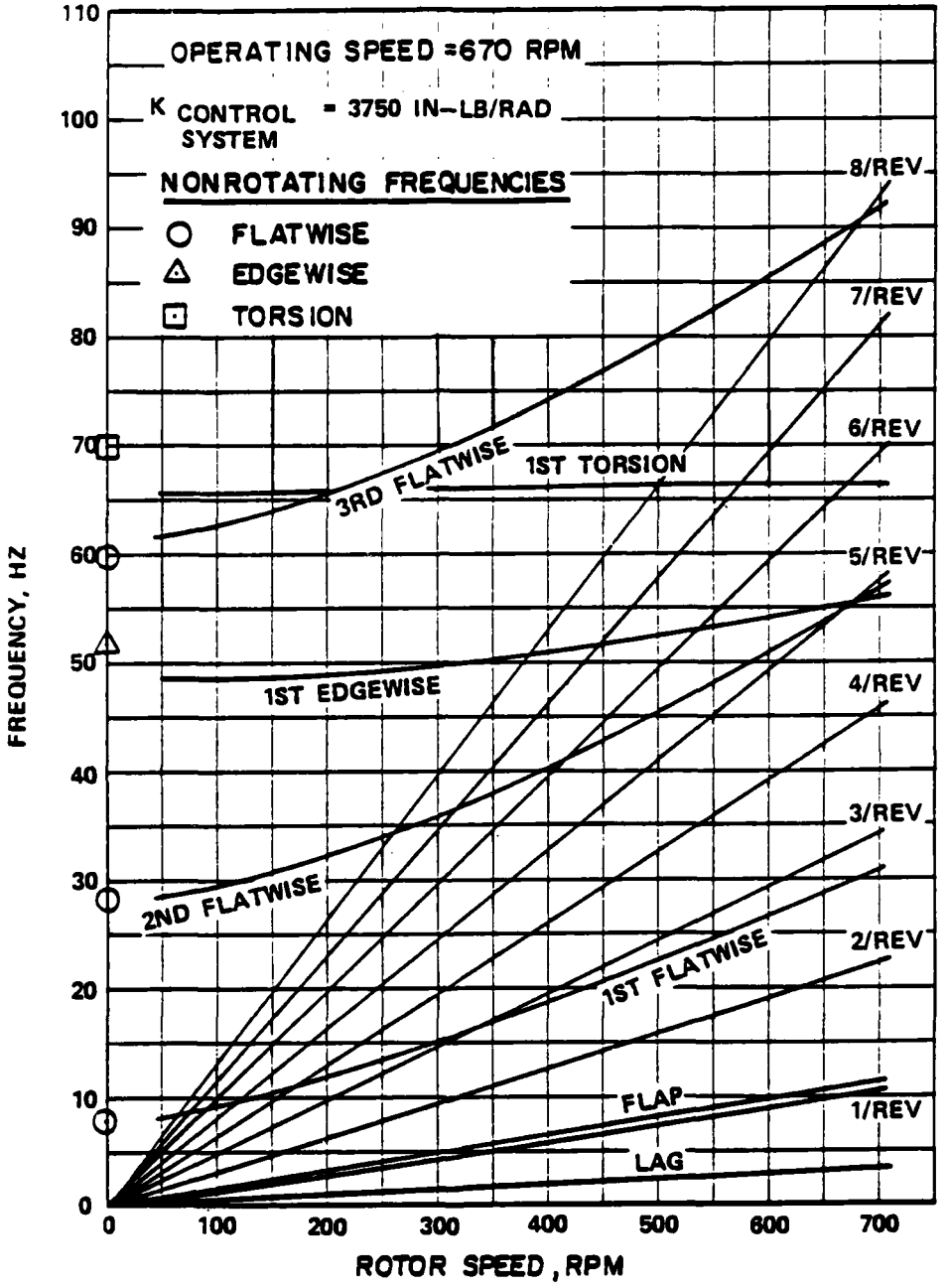

Figure 12. Natural Frequencies of Baseline Model Blades.

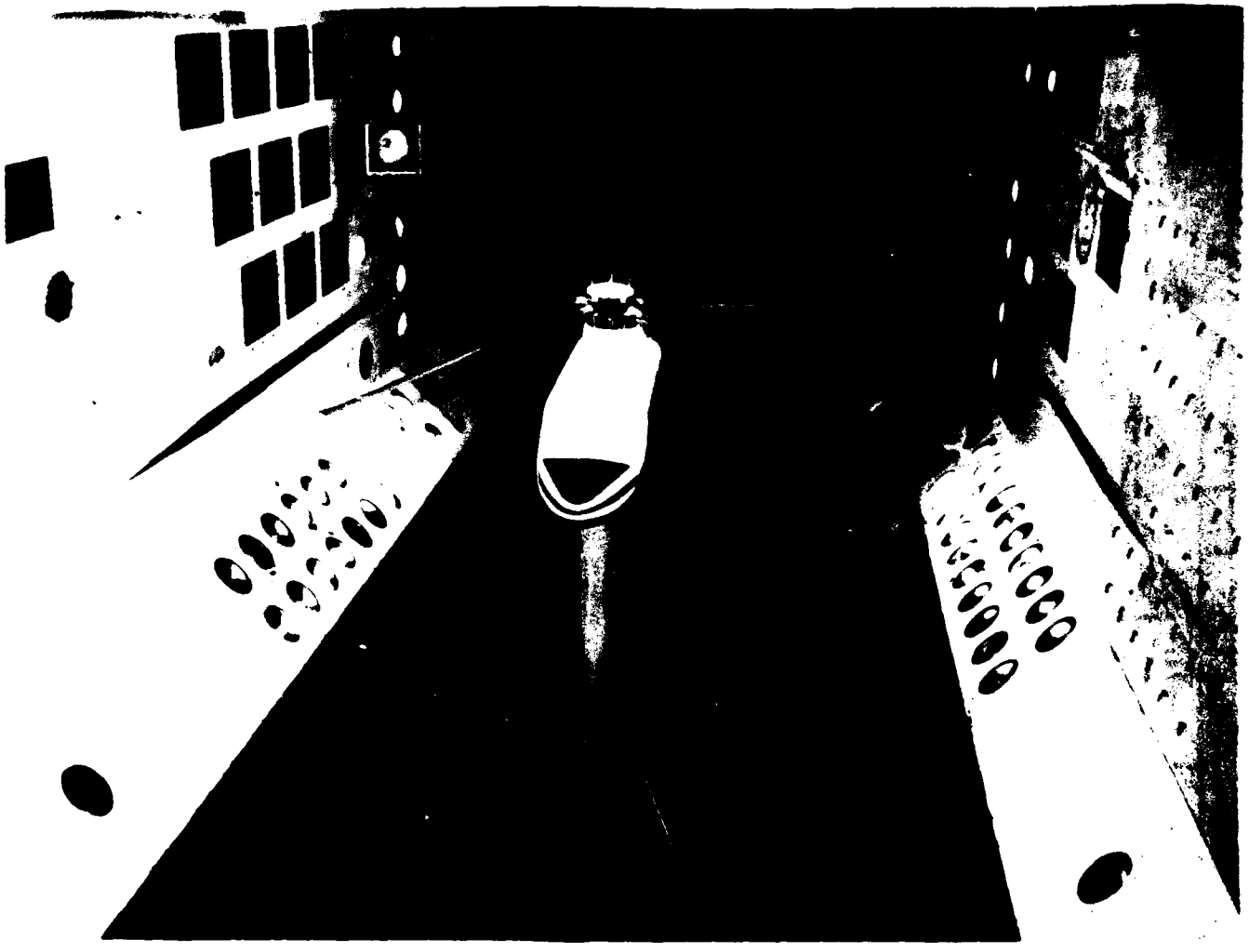

Figure 13. ACR Model Blades Installed on the Aeroelastic Rotor Experimental System in the Transonic Dynamics Wind Tunnel

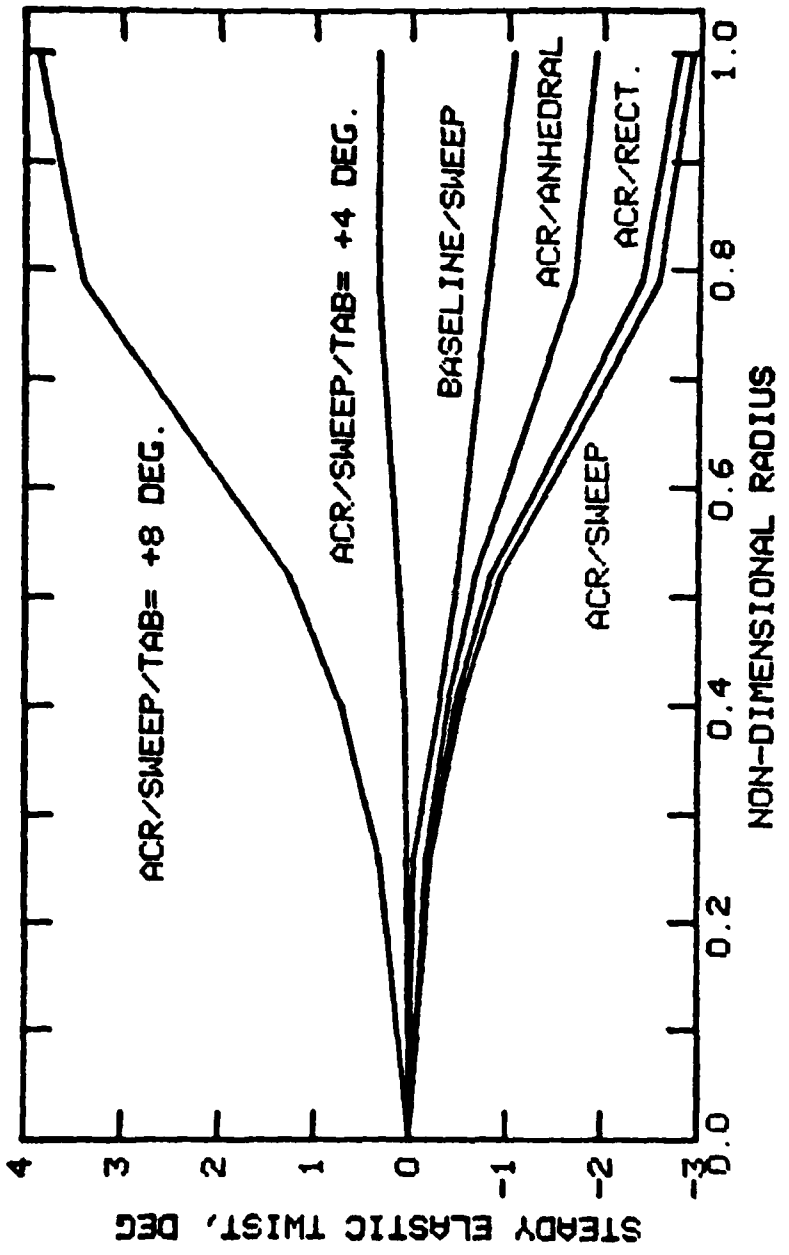

Figure 14. Semi-Empirical Steady Elastic Twist Distributions of Six Model Rotor Blades; $\mu = 0.3$, $C_L/\sigma = 0.08$, $\alpha_s = -5^0$.

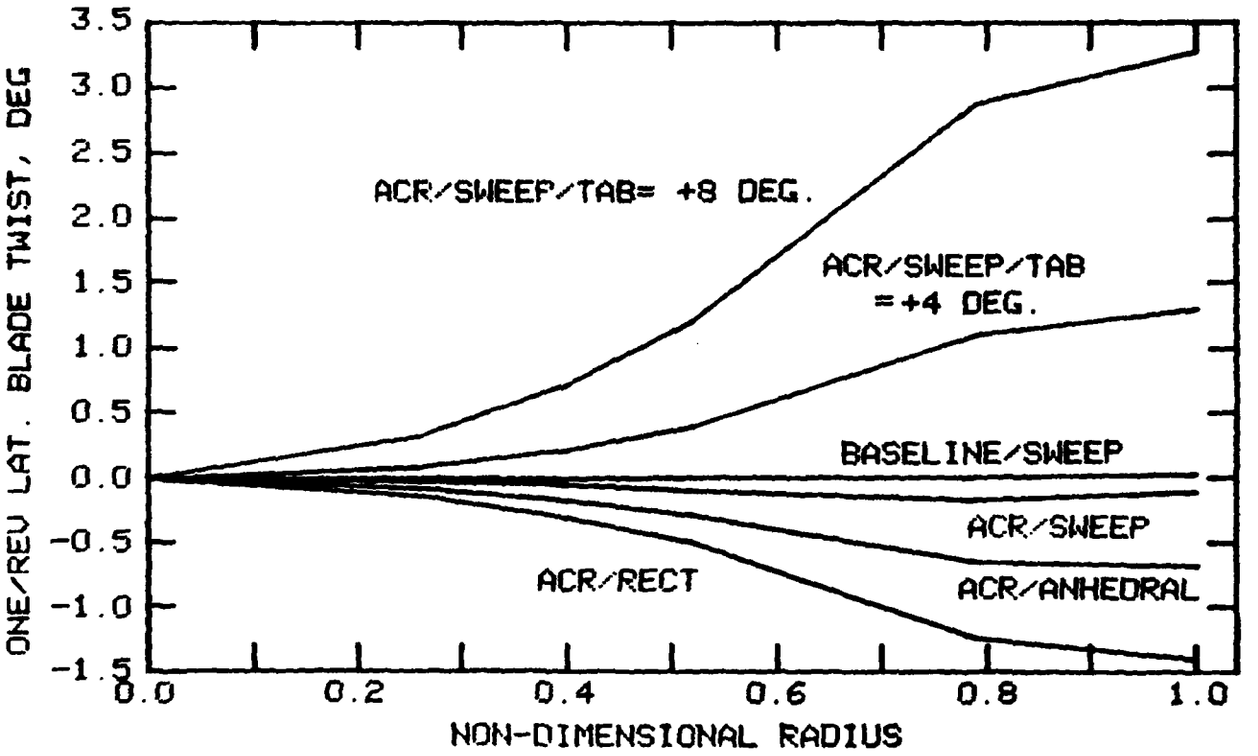

Figure 15. Semi-Empirical One/Rev Lateral Elastic Twist Distributions of Six Model Rotor Blades; $\mu = 0.3$, $C_L/\sigma = 0.08$, $\alpha_S = -5^o$.

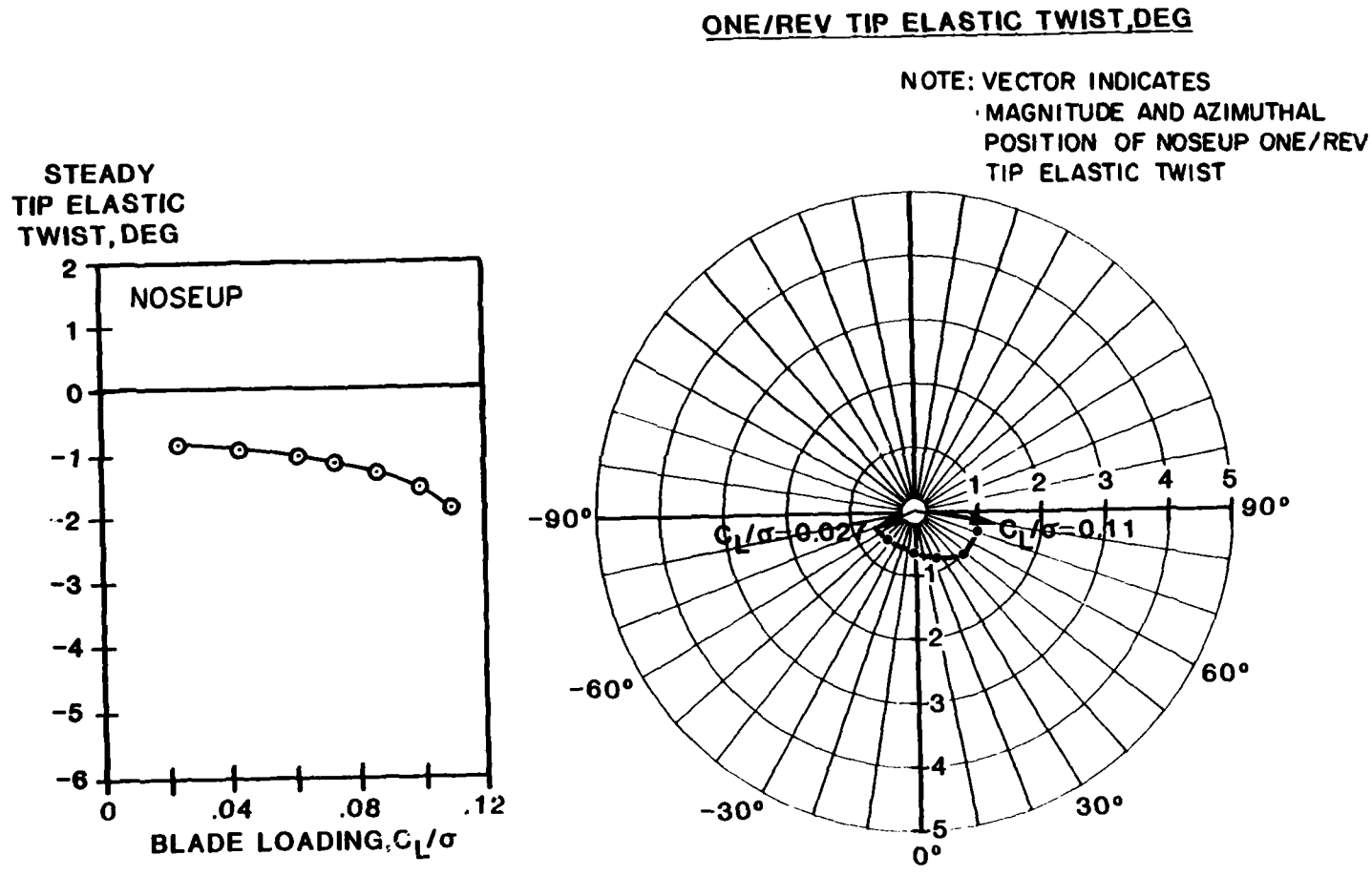

Figure 16. Steady and One/Rev Tip Elastic Twist of Baseline Model Rotor Blade; $\mu = 0.3$, $\alpha_s = -5^0$.

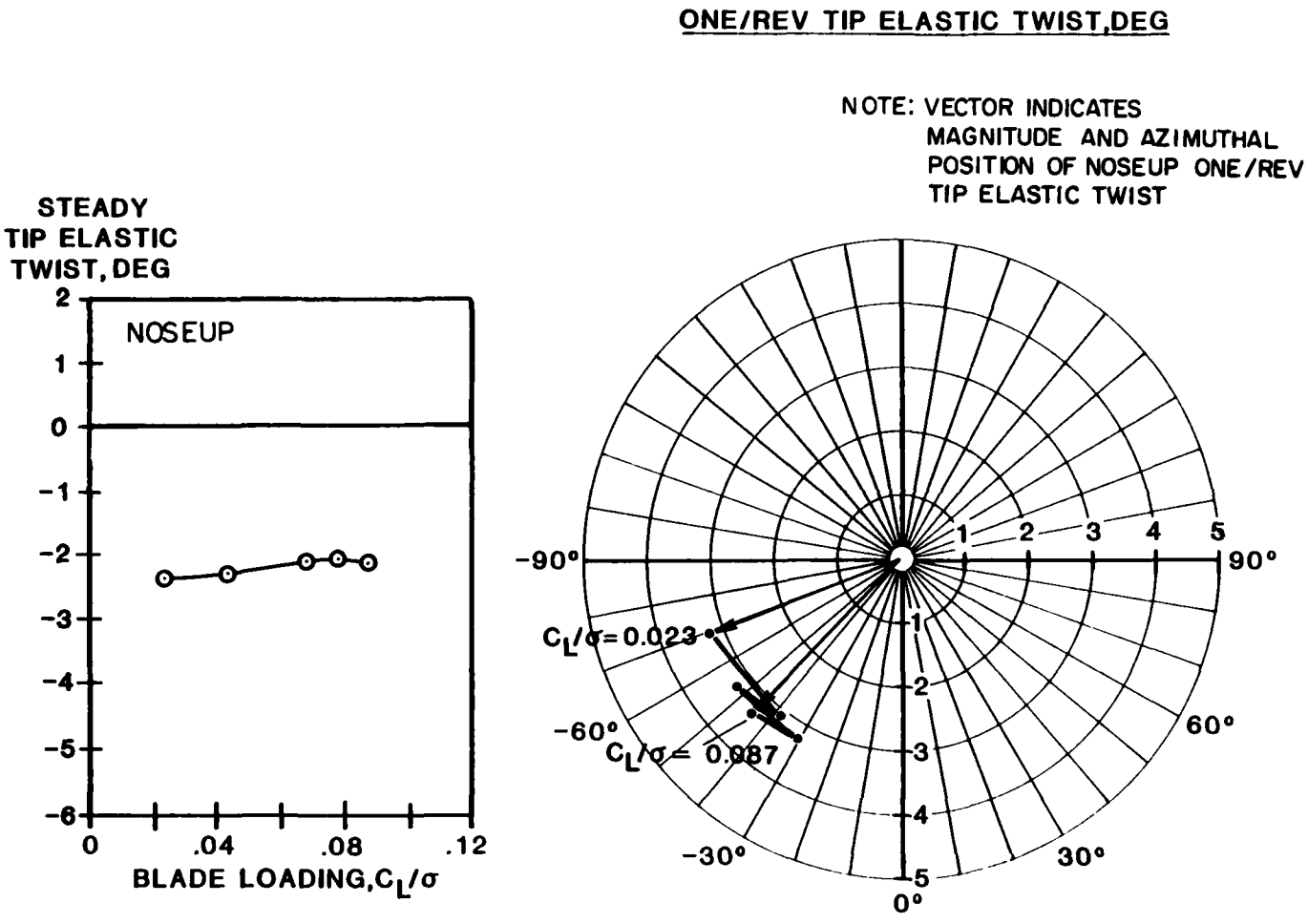

Figure 17. Steady and One/Rev Tip Elastic Twist of ACR Blade With Rectangular Tip; $\mu = 0.3$, $\alpha_s = -5^o$.

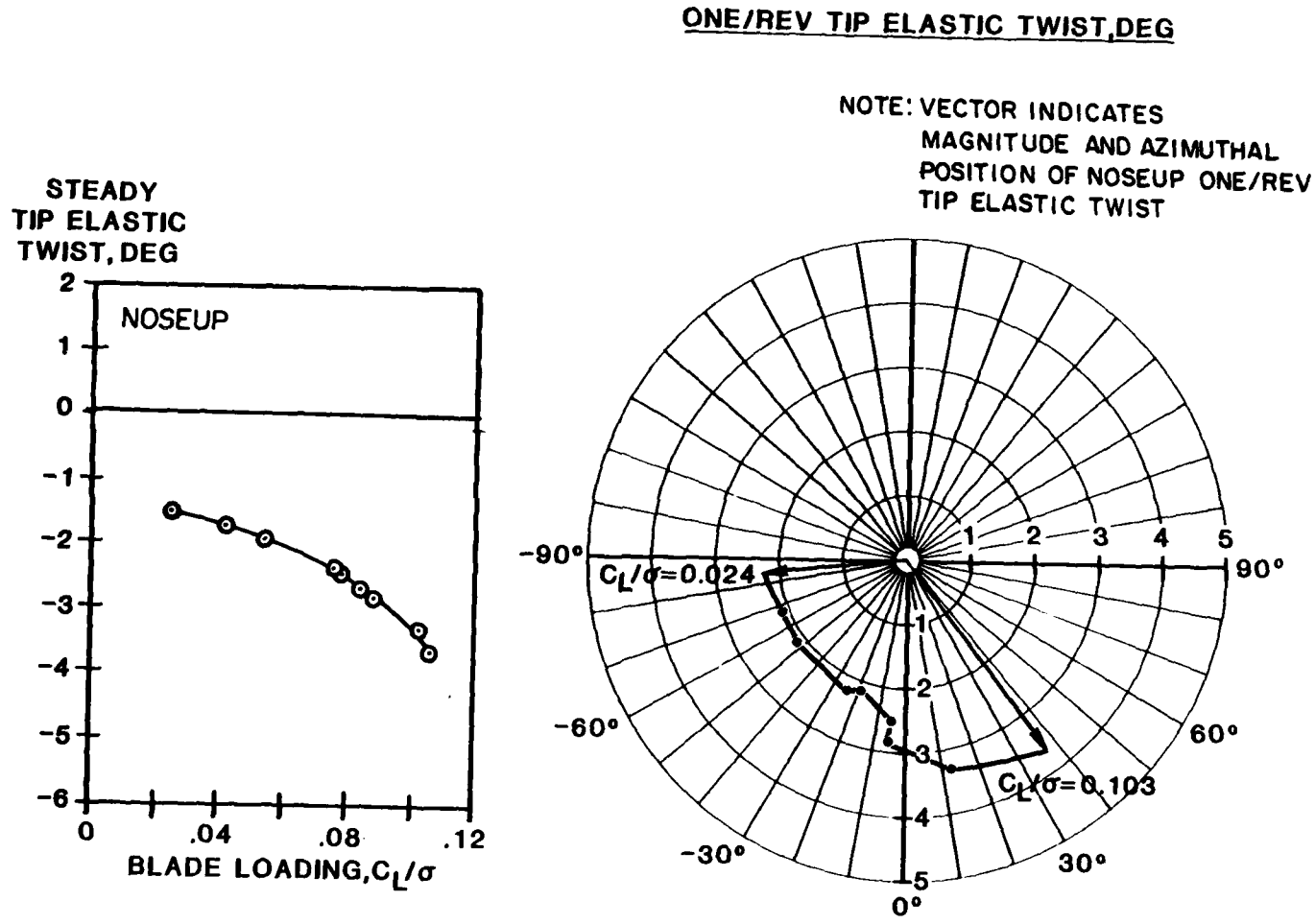

Figure 18. Steady and One/Rev Tip Elastic Twist of ACR Blade With Swept Tip; $\mu = 0.3$, $\alpha_s = -5^0$.

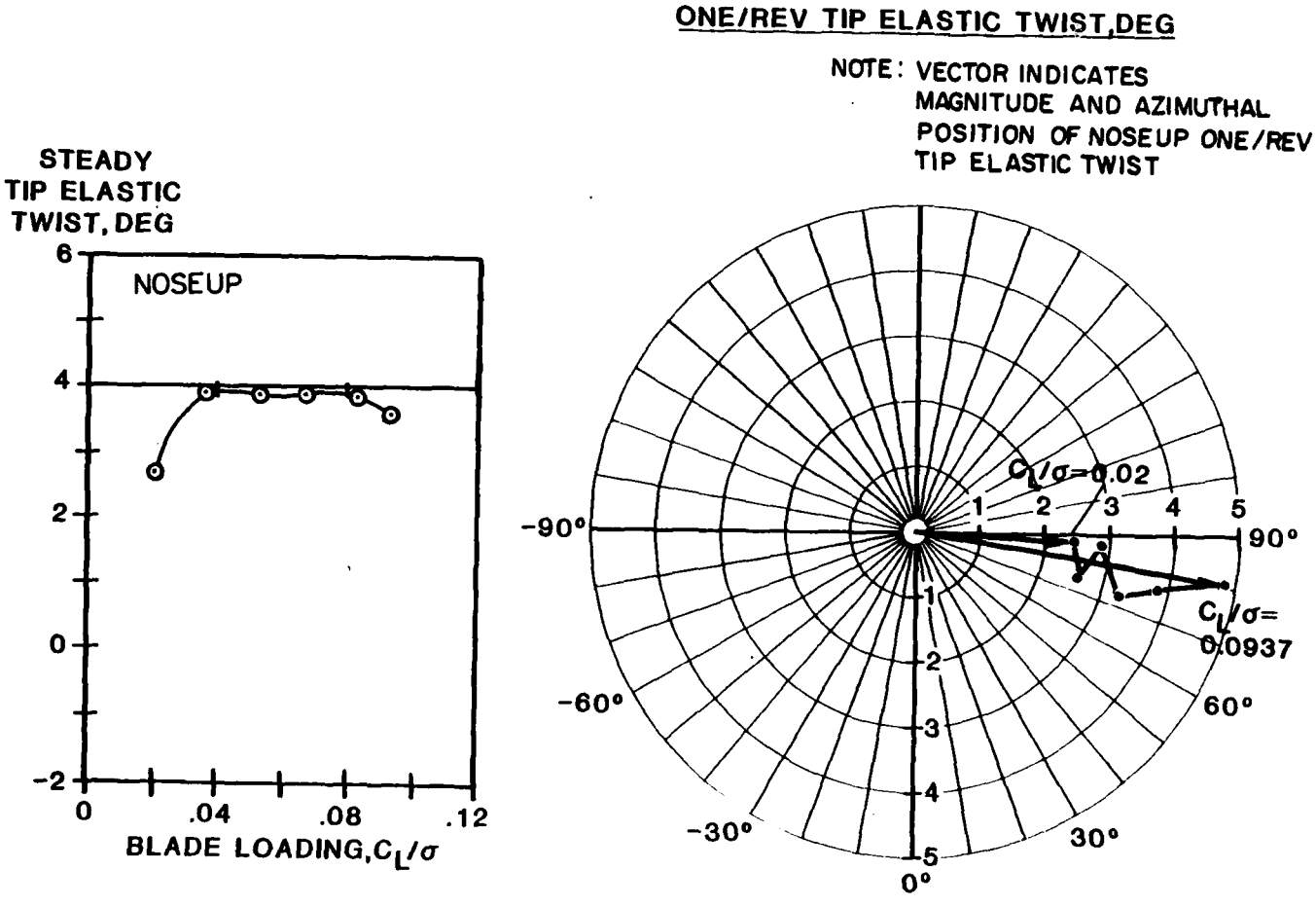

Figure 19. Steady and One/Rev Tip Elastic Twist of ACR Blade With Swept Tip and 8 degree Trailing Edge Up Tab Deflection; $\mu = 0.3$, $\alpha_s = -5^0$.

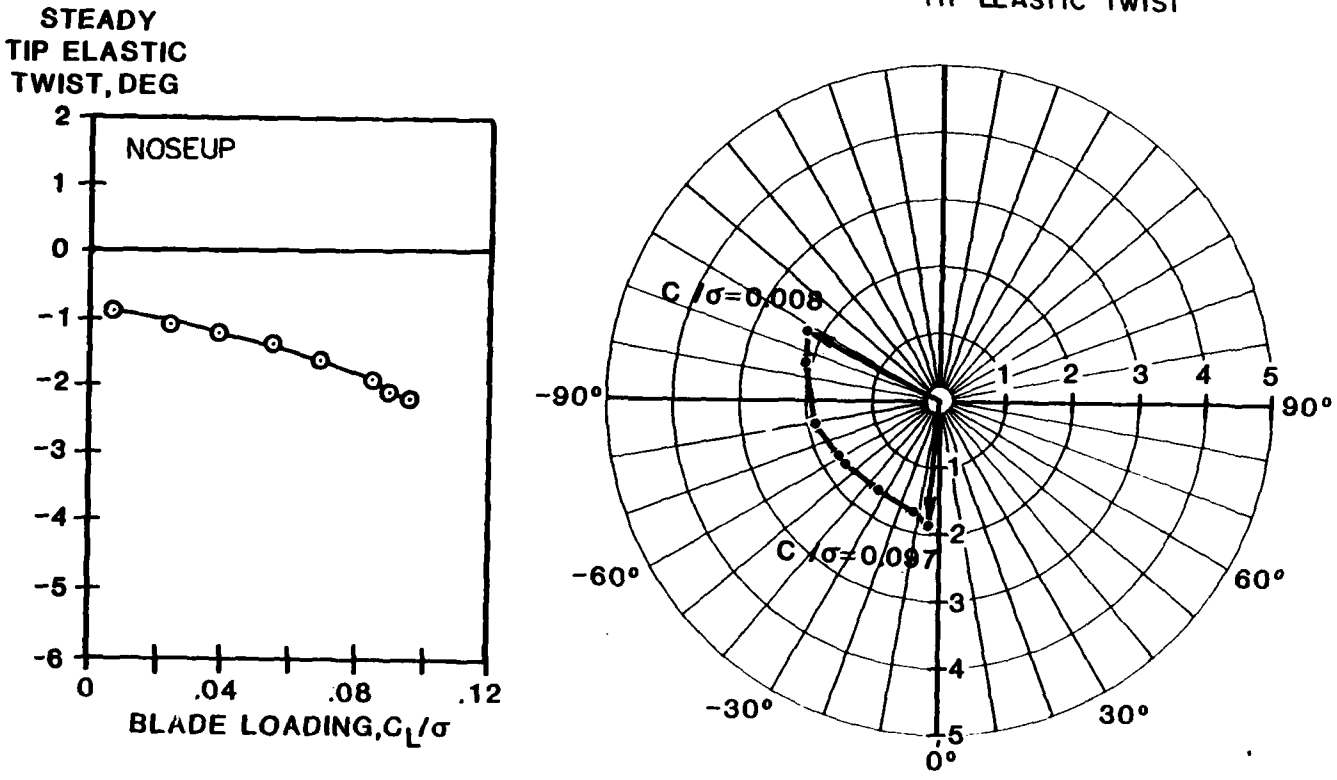

Figure 20. Steady and One/Rev Tip Elastic Twist of ACR Blade With Swept-Tapered-Anhedral Tip; $\mu = 0.3$, $\alpha_s = -5^0$.

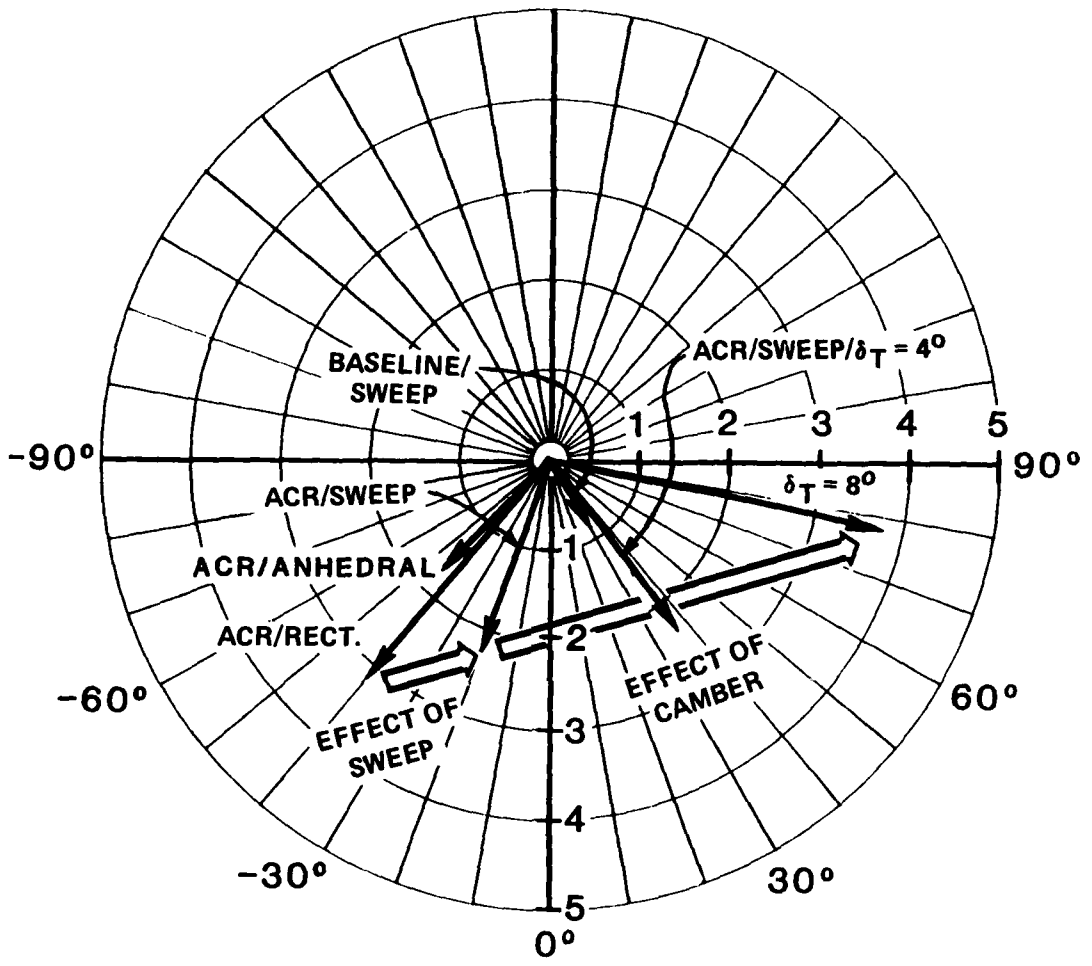

Figure 21. One/Rev Tip Elastic Twist of Six Model Rotors; μ = 0.3, α_s = -5°, C_L/σ = 0.08.

TWO/REV TIP ELASTIC TWIST, DEG

NOTE: VECTORS INDICATE MAGNITUDE AND AZIMUTHAL POSITIONS OF NOSEUP TWO/REV TIP ELASTIC TWIST

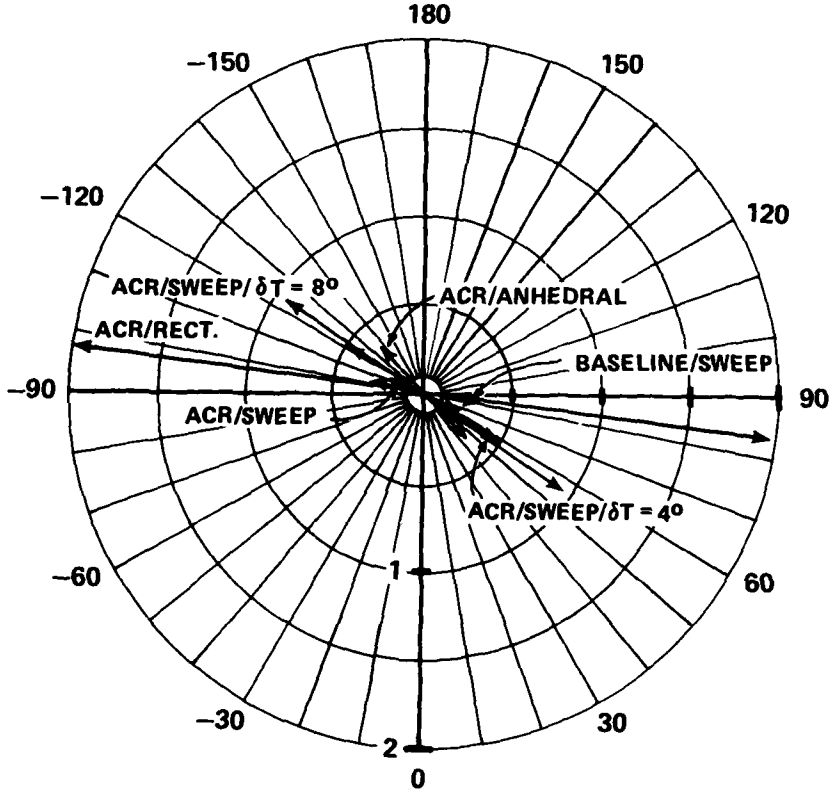

Figure 22. Two/Rev Tip Elastic Twist of Six Model Rotors; $\mu = 0.3$, $\alpha_S = -5^o$, $C_L/\sigma = 0.08$.

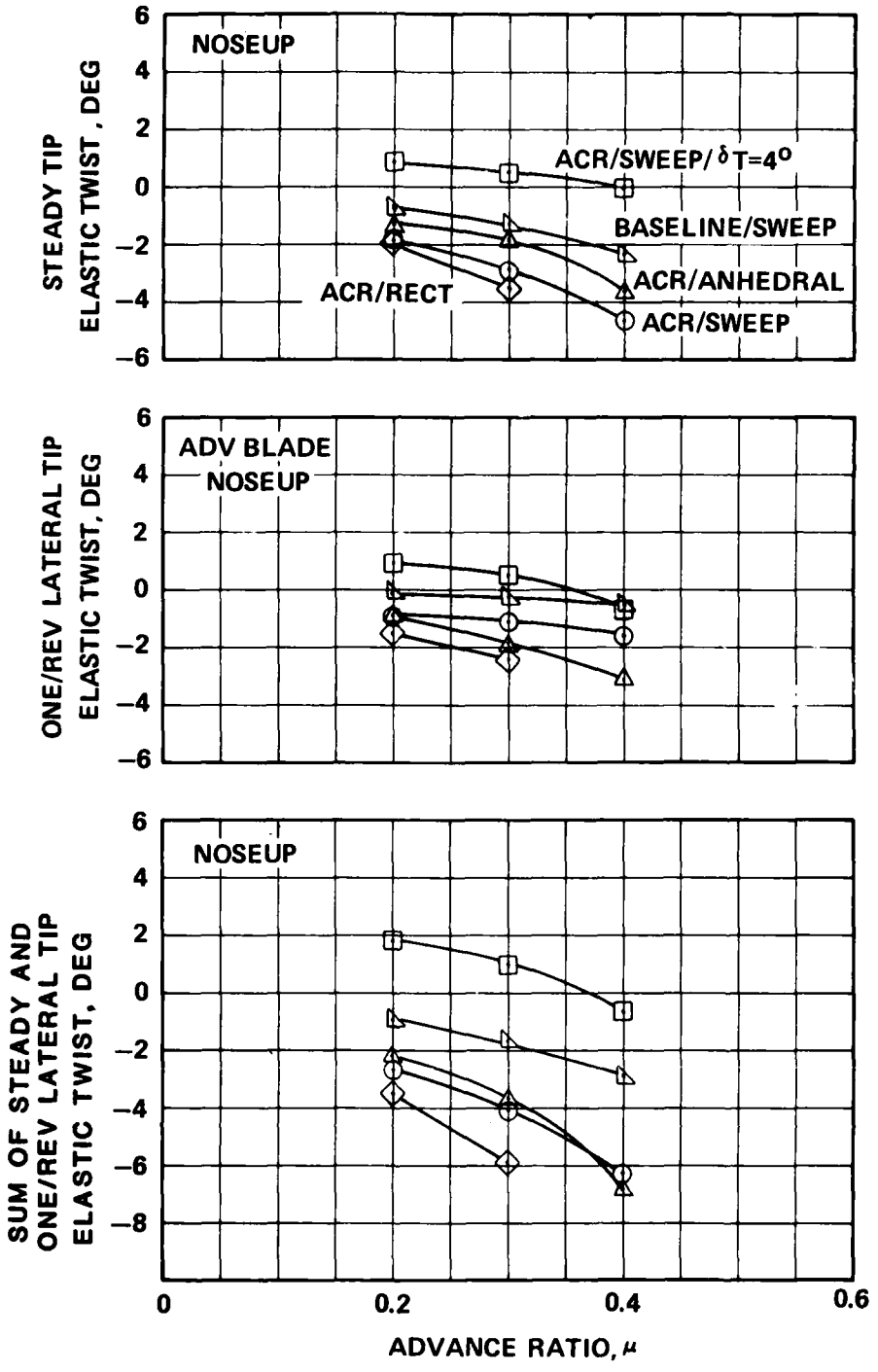

Figure 23. Variation in Model Rotor Blade Elastic Twist with Advance Ratio; $C_L/\sigma = 0.06$, $f = 15$ ft^2.

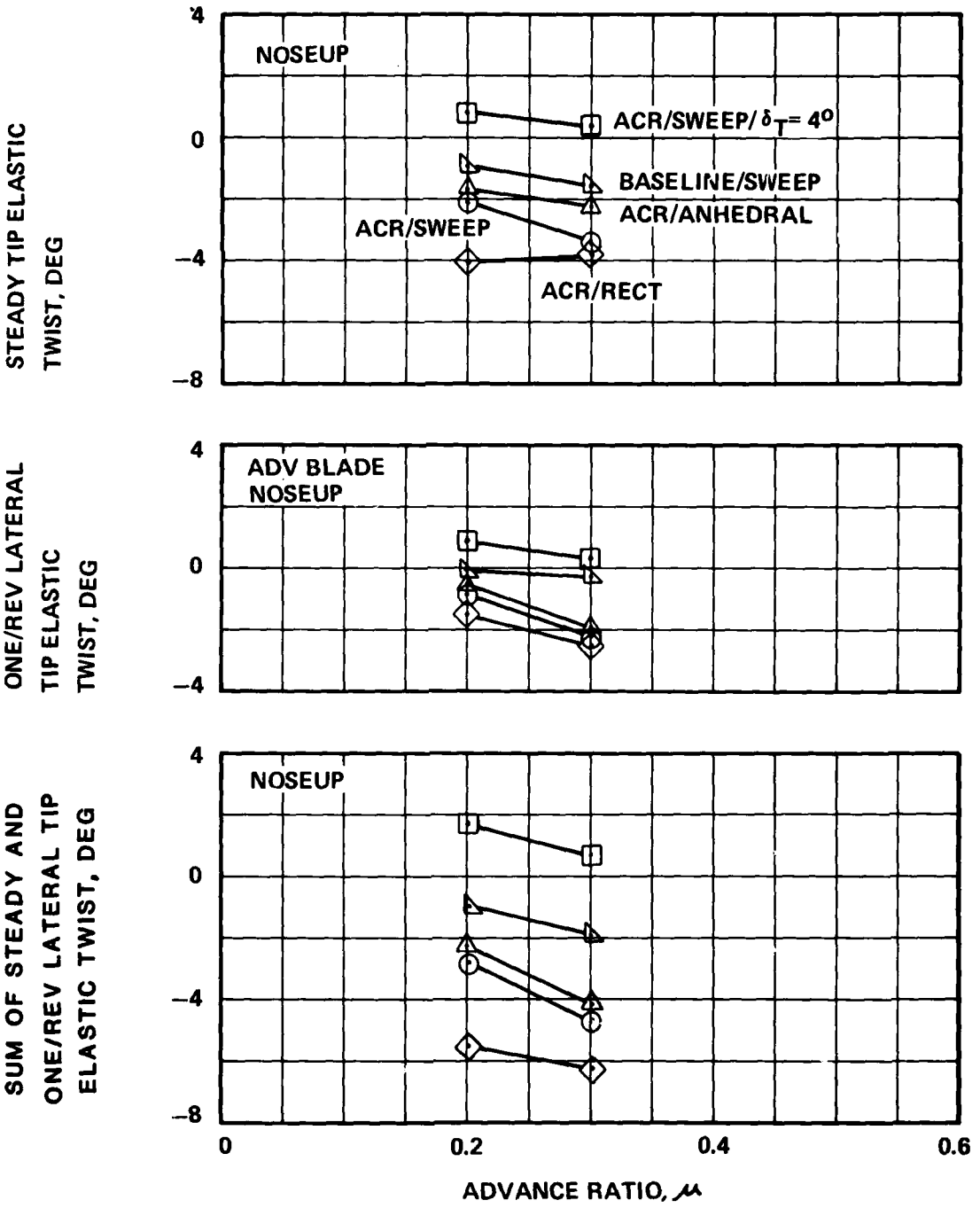

Figure 24. Variation in Model Rotor Blade Elastic Twist with Advance Ratio, C_L/σ = 0.06, f = 30 ft^2.

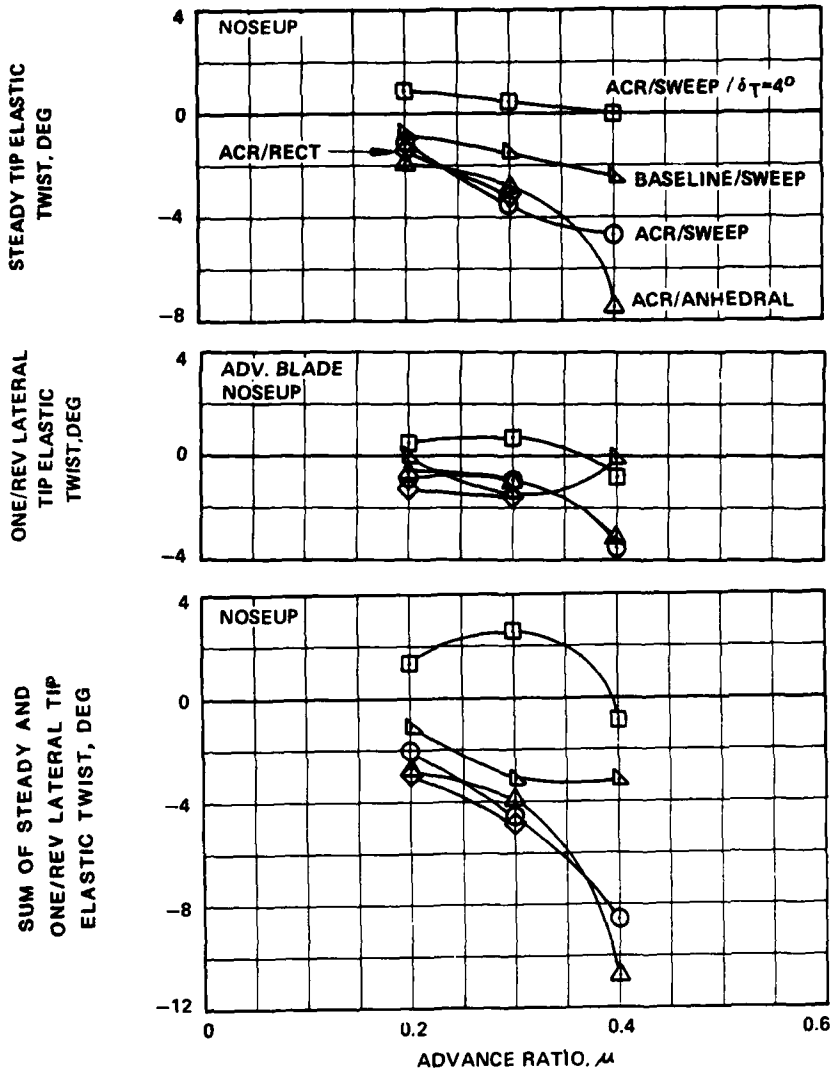

Figure 25. Variation in Model Rotor Blade Elastic Twist with Advance Ratio; C_L/σ = 0.08, f = 15 ft^2.

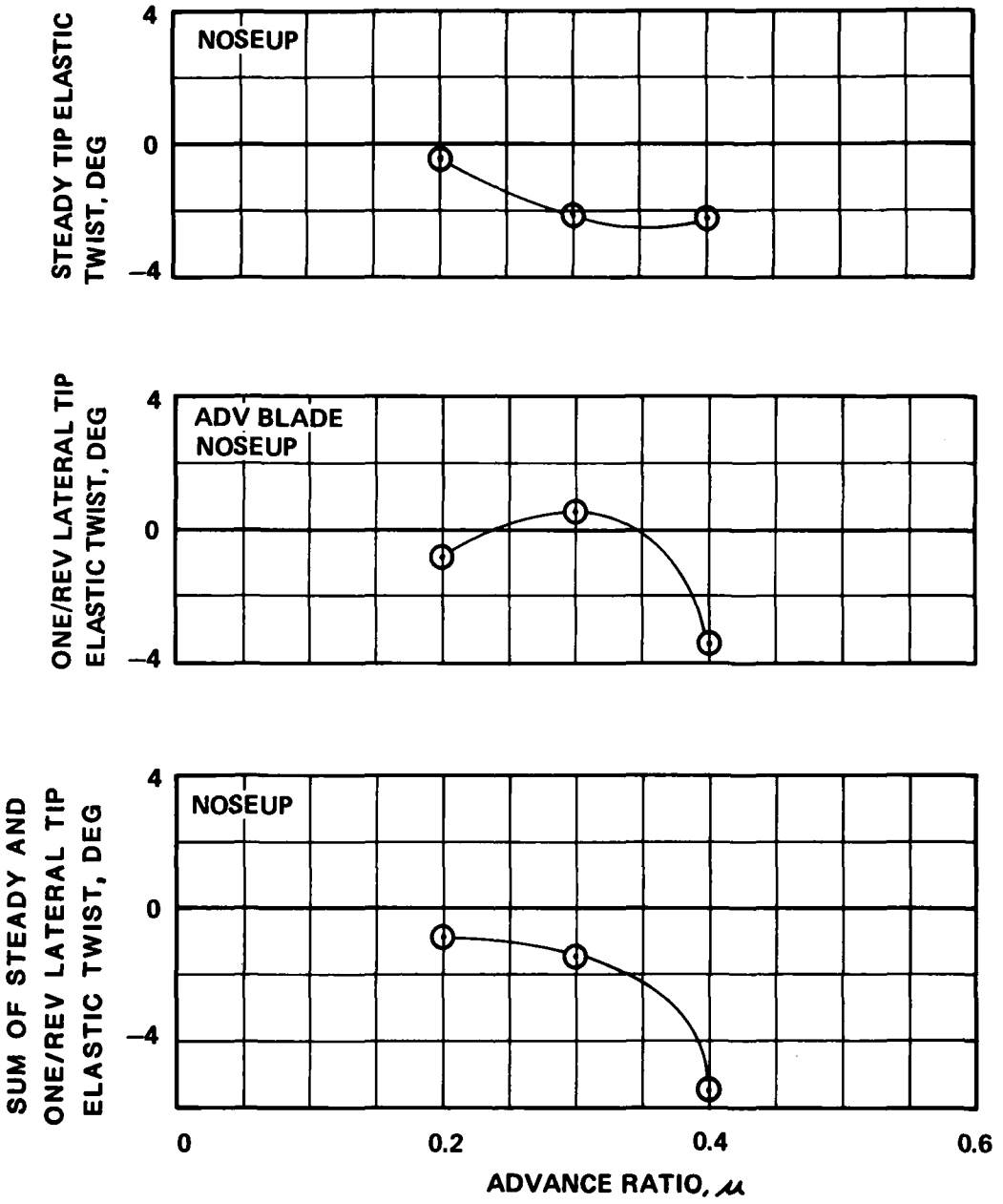

Figure 26. Elastic Twist Changes Produced by Reducing Torsional Stiffness on Swept Tip Model Blade; $C_L/\sigma = 0.08$, f = 15 ft^2.

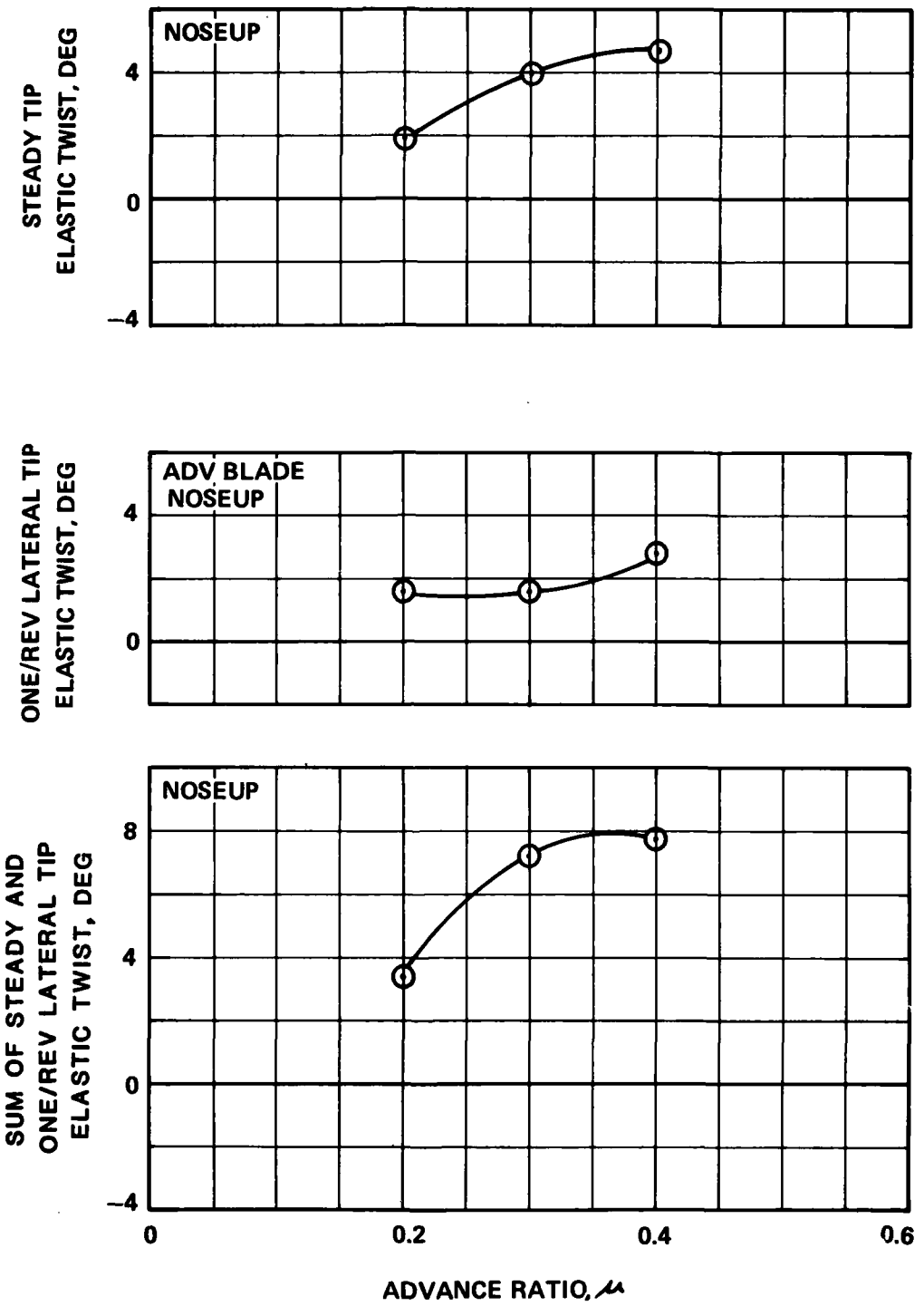

Figure 27. Elastic Twist Changes Produced by 4-Degree-Trailing-Edge-Up Tab Deflection on Swept Tip ACR Blade; C_L/σ = 0.08, f = 15 ft^2.

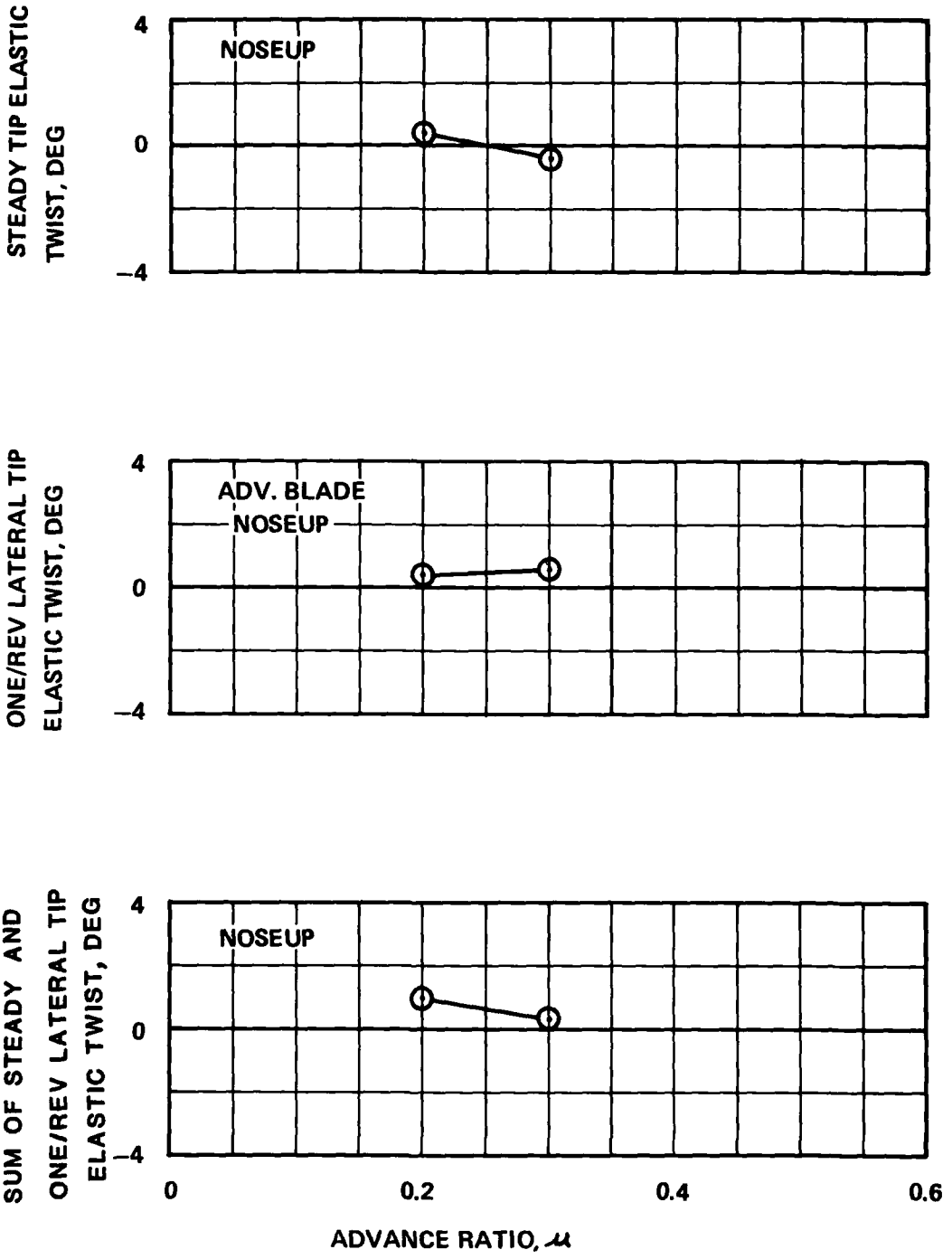

Figure 28. Elastic Twist Changes Produced by Tip Sweep on ACR Blade; $C_L/\sigma = 0.08$, $f = 15$ ft^2.

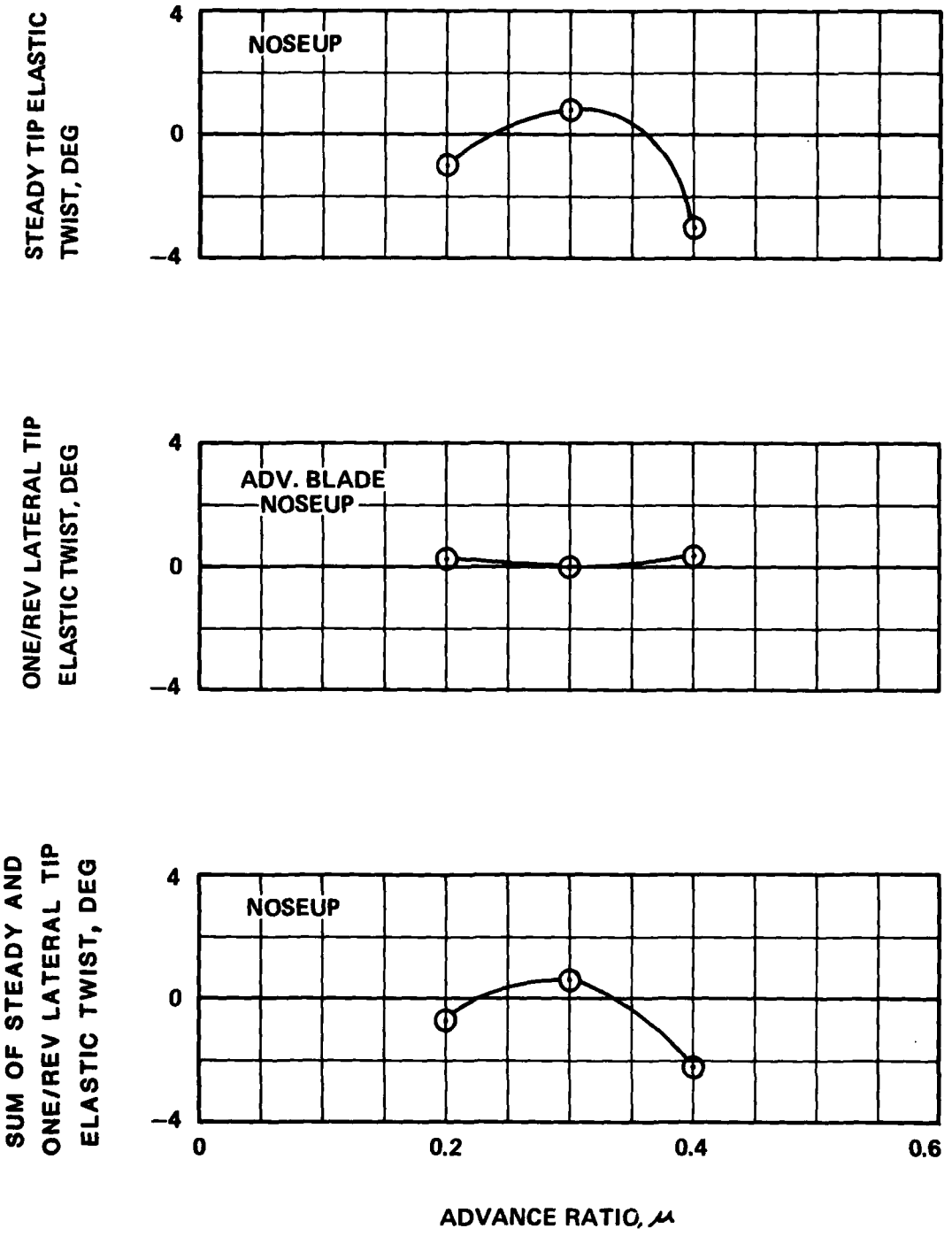

Figure 29. Elastic Twist Changes Produced by Anhedral on ACR Blade; $C_L/\sigma = 0.08$, $f = 15$ ft^2.

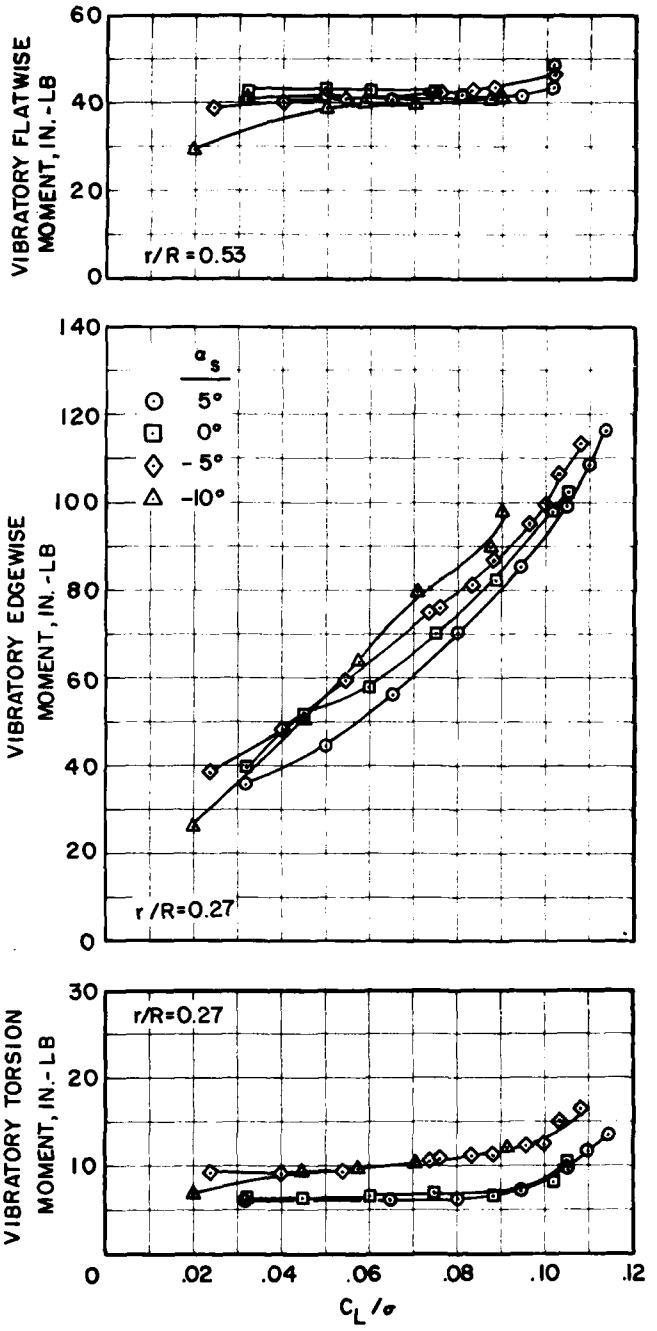

Figure 30. Vibratory Moments of ACR Blade with Swept Tip; μ = 0.3.

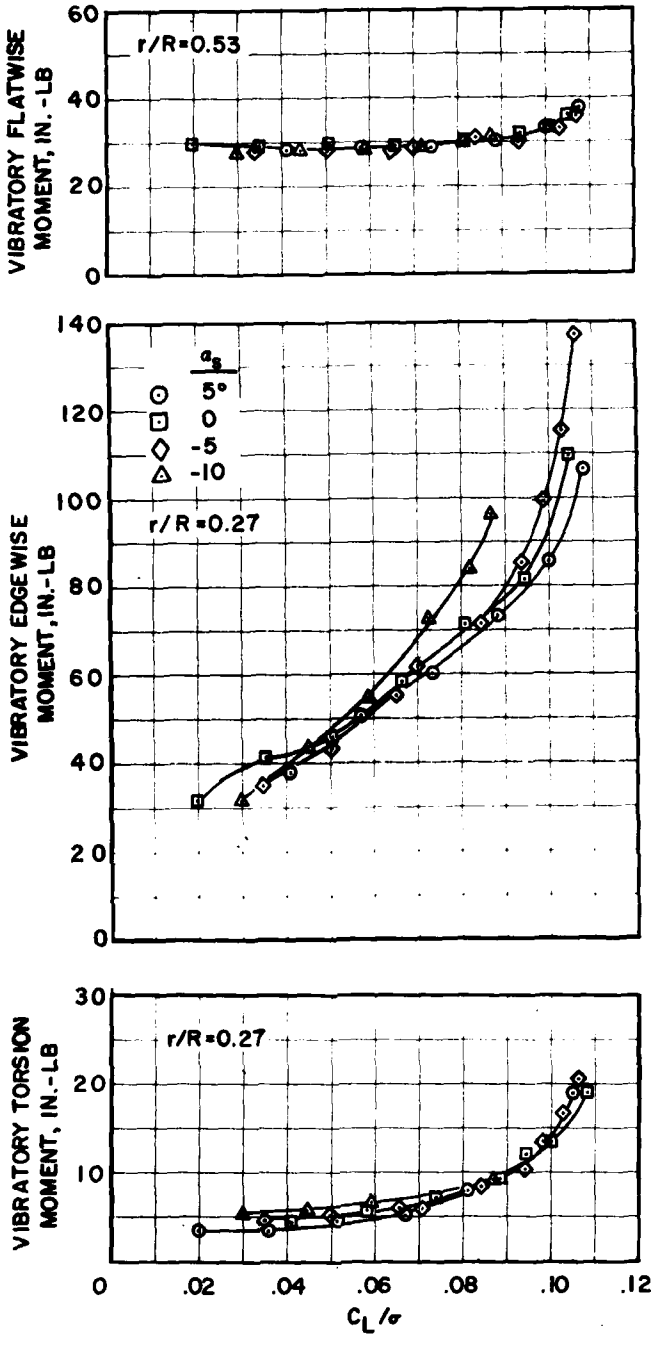

Figure 31. Vibratory Moments of ACR Blade with Swept Tip and 4 Degree Trailing Edge Up Tab Deflection; $\mu = 0.3$.

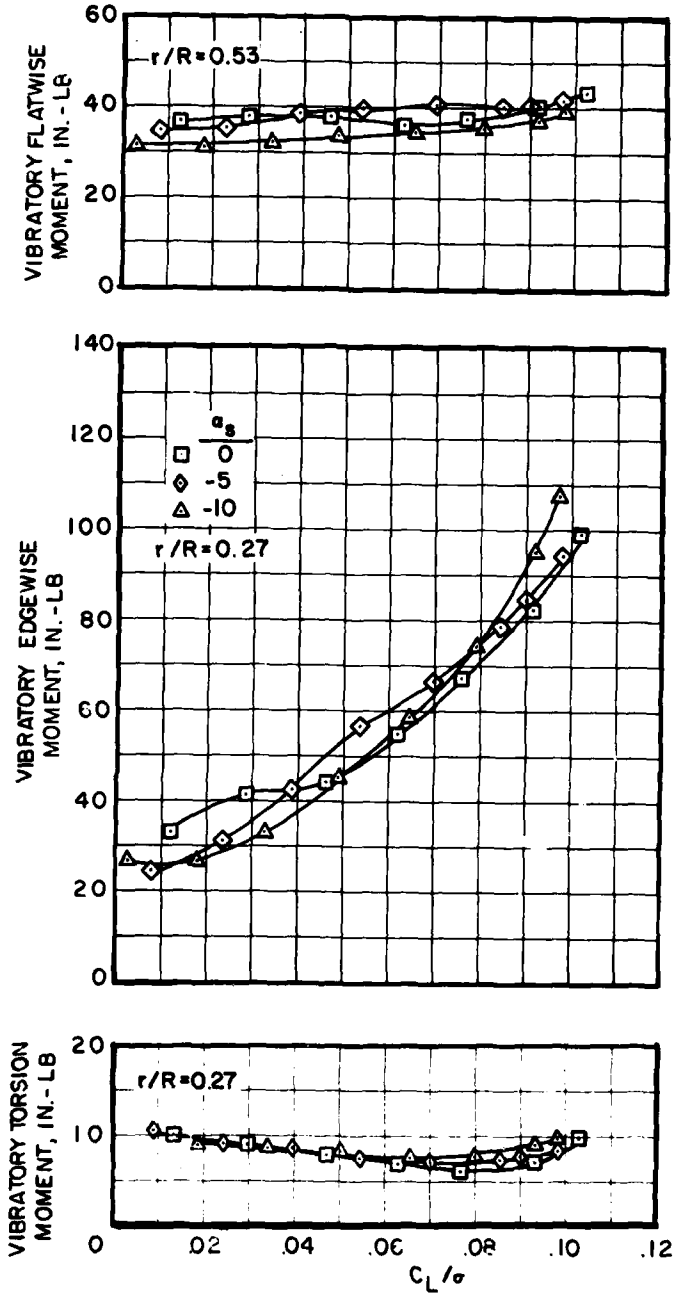

Figure 32. Vibratory Moments of ACR Blade with Swept-Tapered-Anhedral Tip; $\mu = 0.3$.

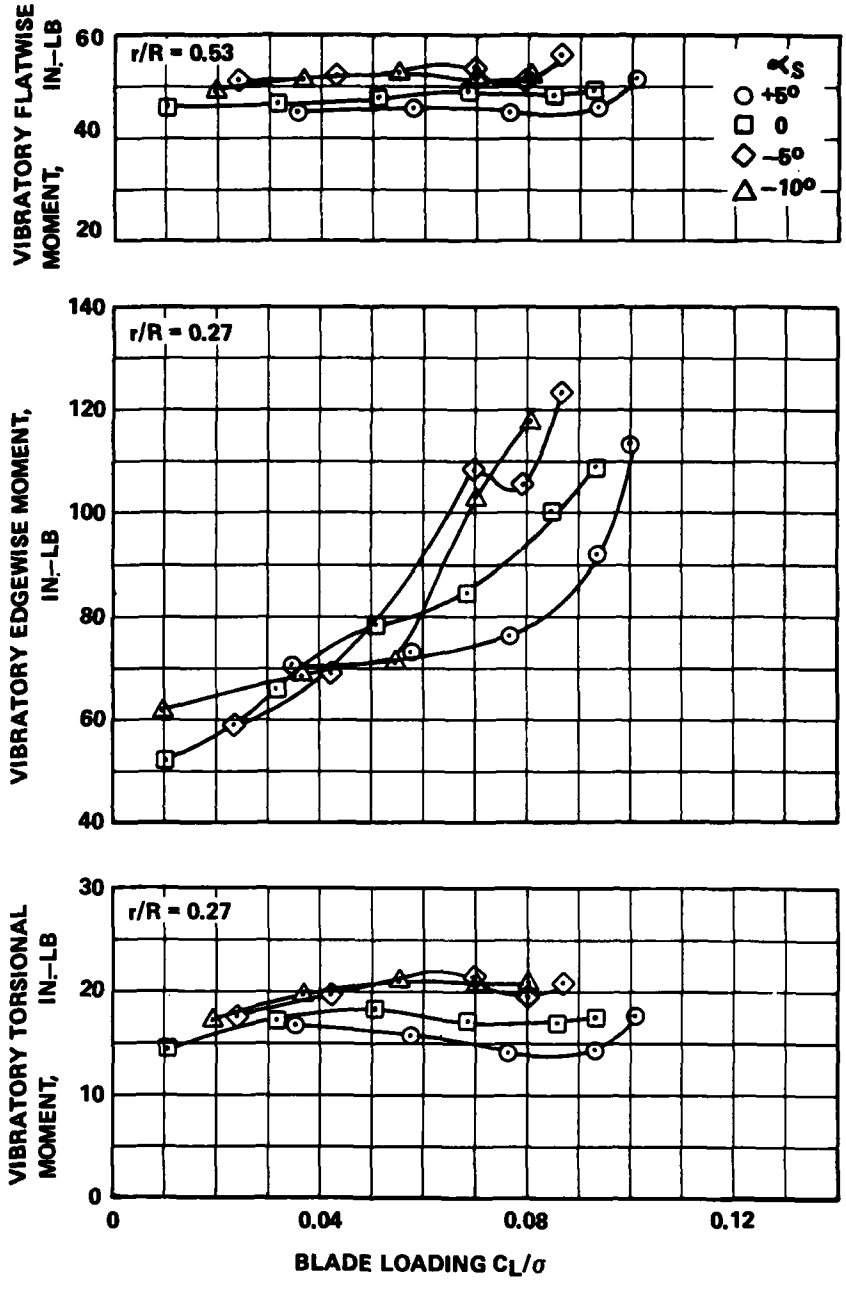

Figure 33. Vibratory Moments of ACR Blade with Rectangular Tip; μ = 0.3.

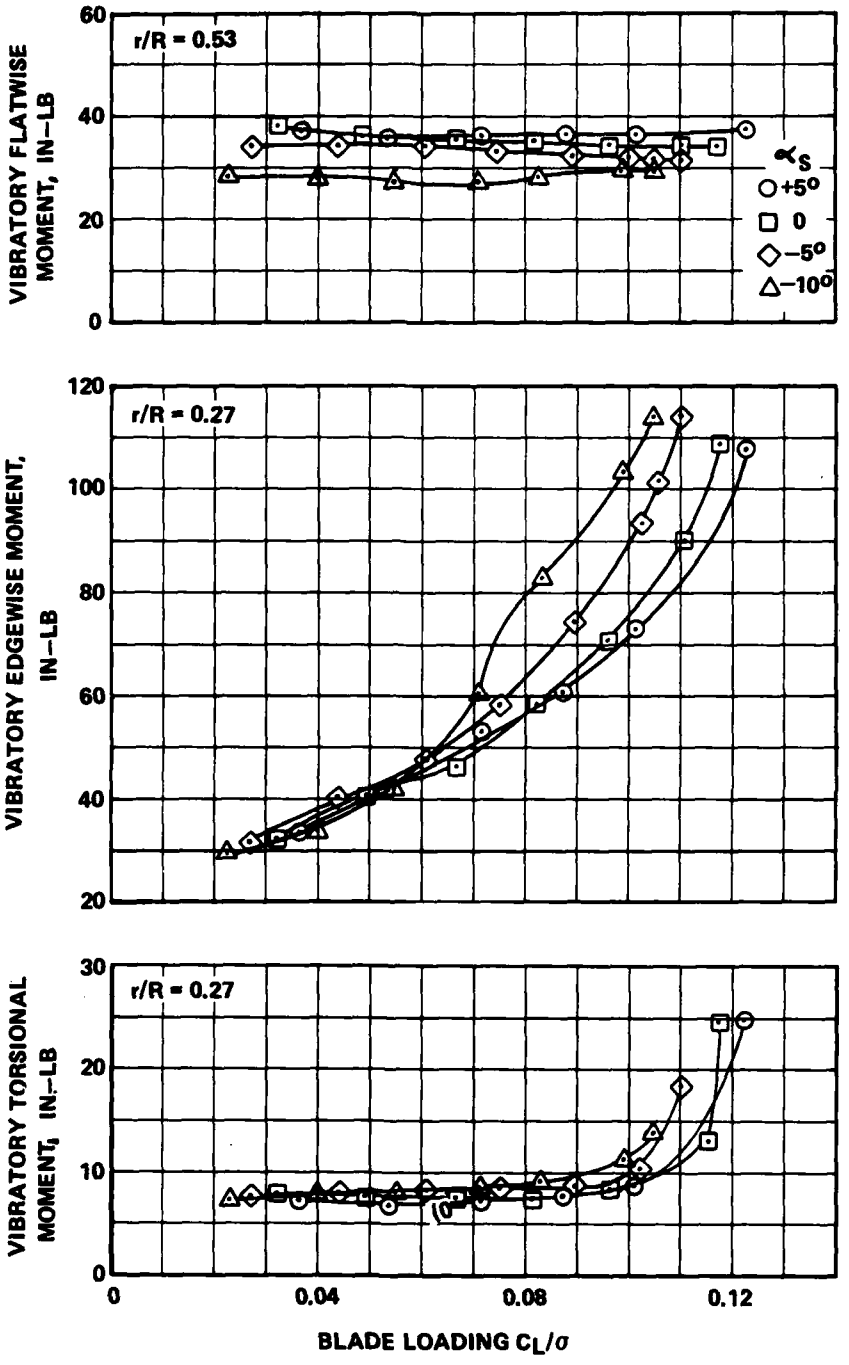

Figure 34. Vibratory Moments of Baseline Blade with Swept Tip; μ = 0.3.

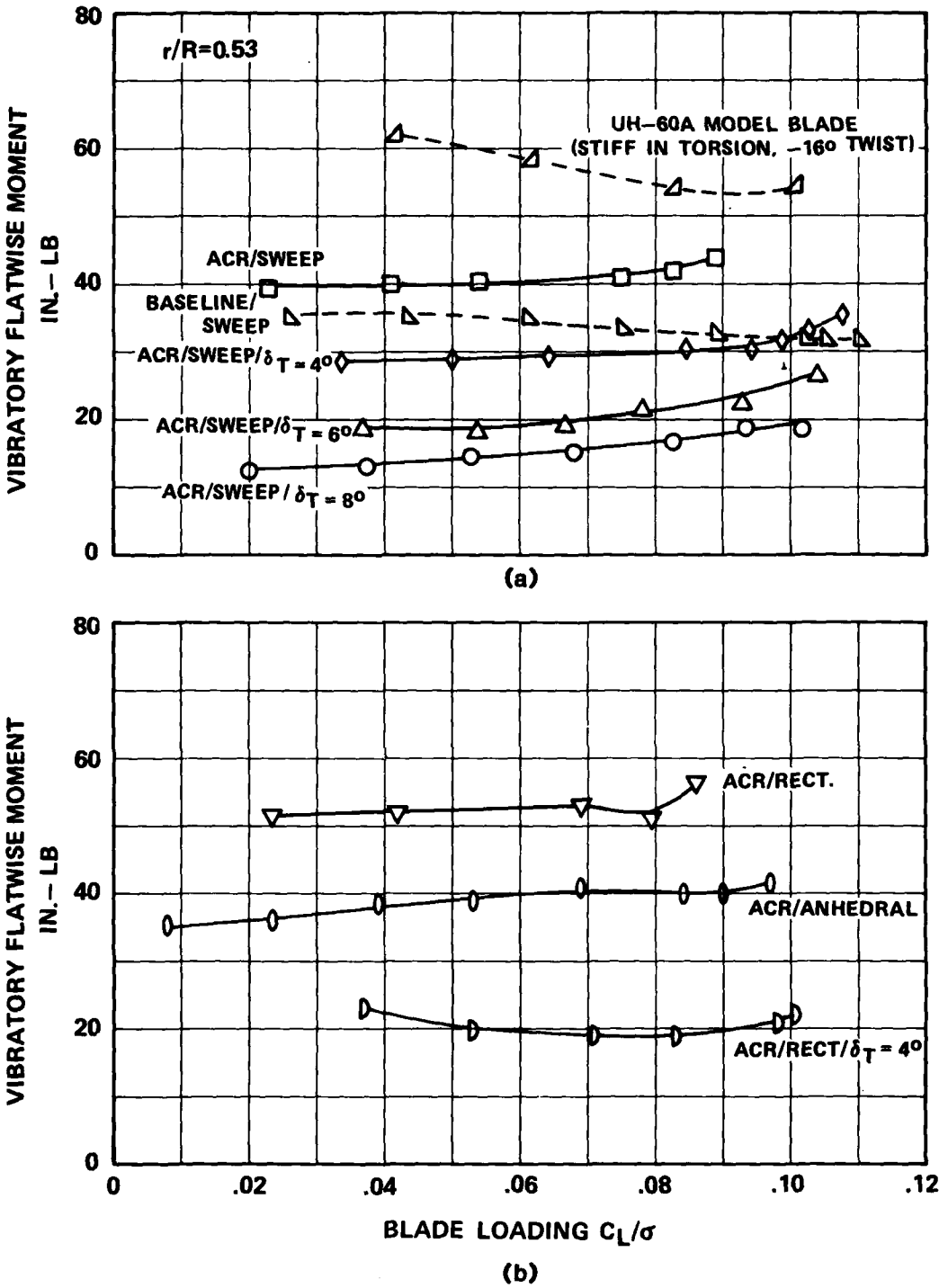

Figure 35. Vibratory Flatwise Moments of Nine Model Rotor Blades; $\mu = 0.3$, $\alpha_s = -5^o$.

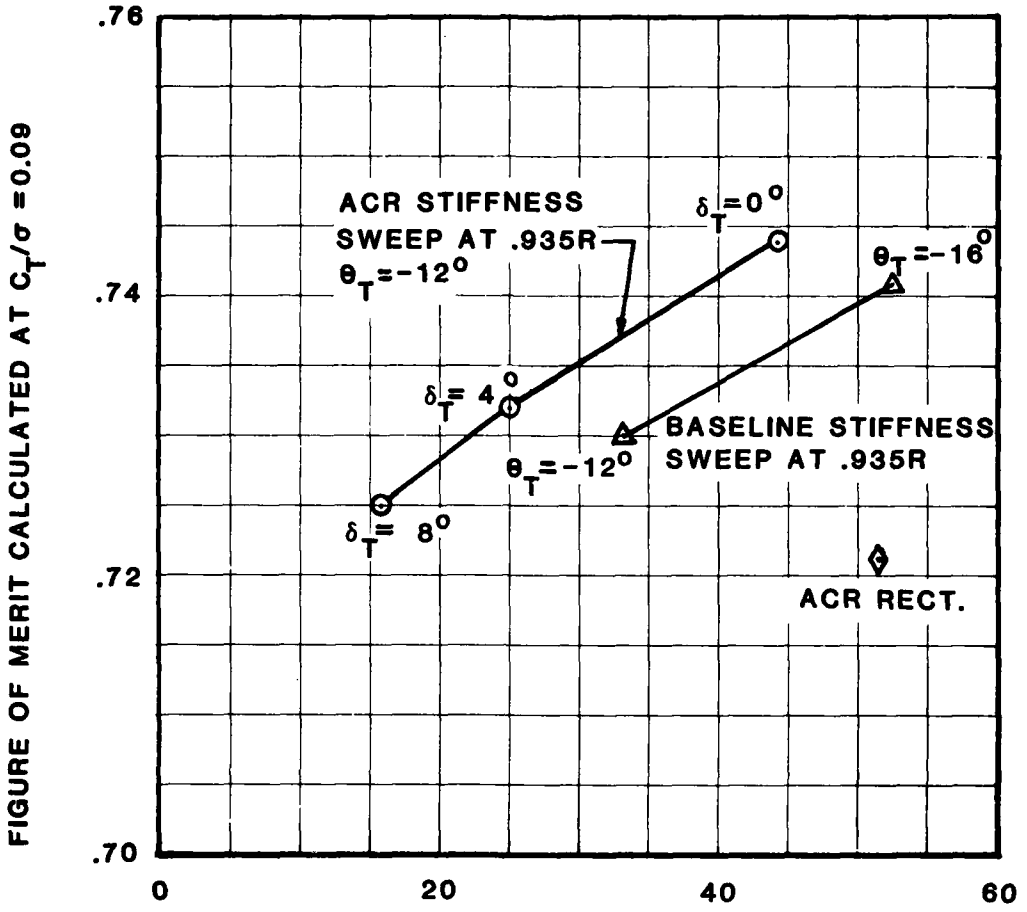

Figure 36. Tradeoff Between Hover Performance and Forward Flight Vibratory Flatwise Bending Moments for ACR and Baseline Rotors.

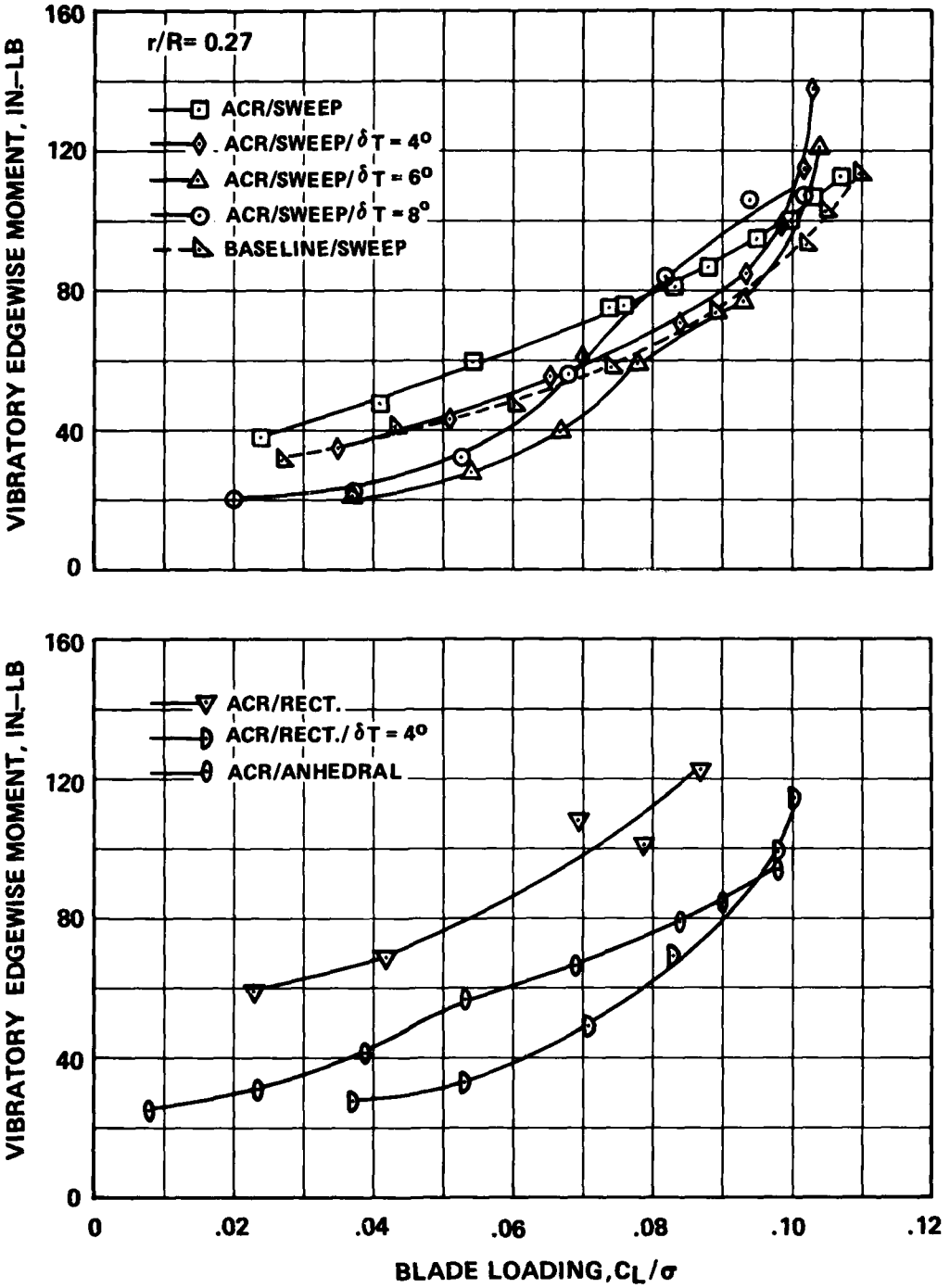

Figure 37. Vibratory Edgewise Moments of Eight Model Rotor Blades; $\mu = 0.3$, $\alpha_s = -5^o$.

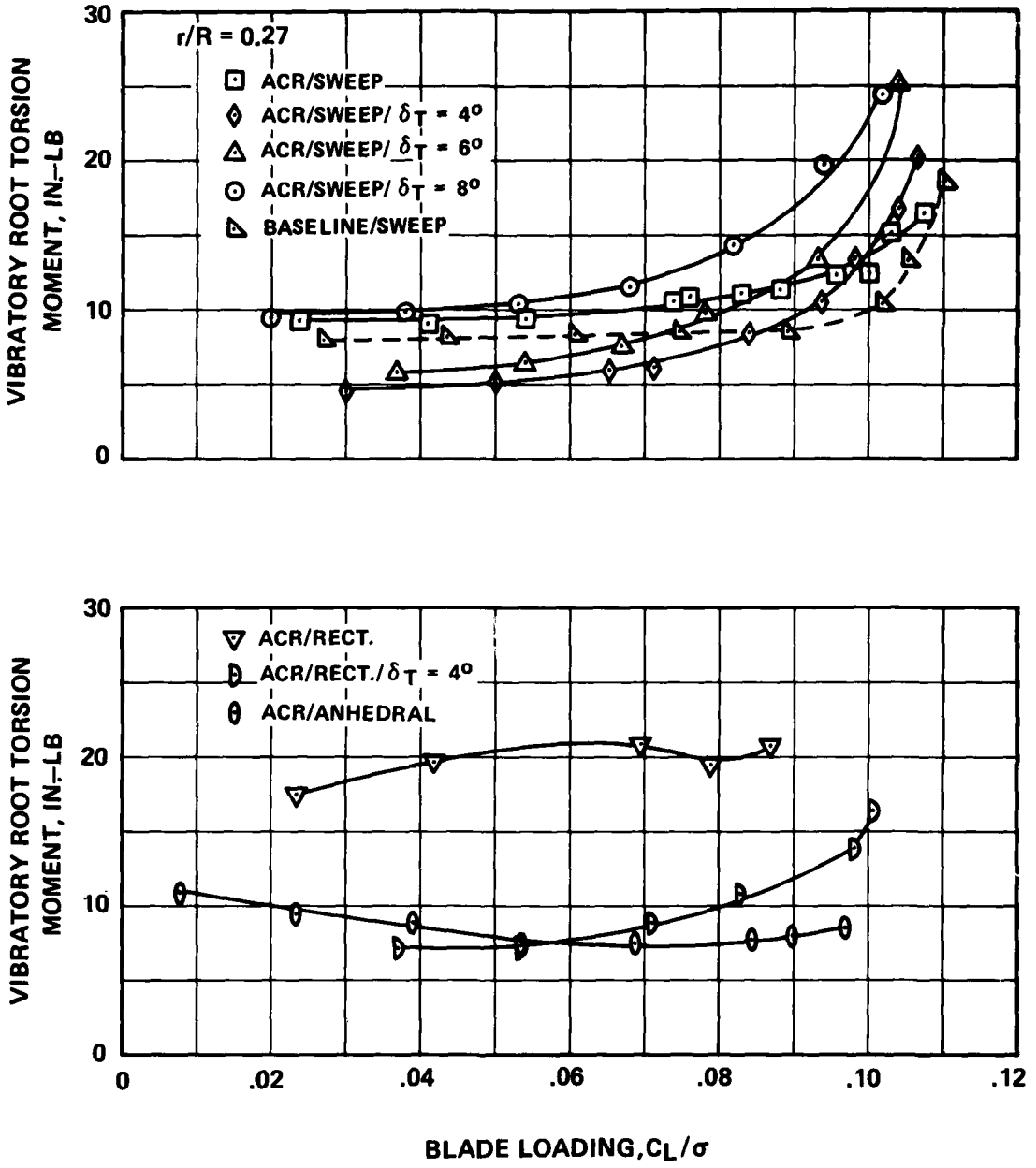

Figure 38. Vibratory Root Torsional Moments of Eight Model Rotor Blades; $\mu = 0.3$, $\alpha_s = -5^o$.

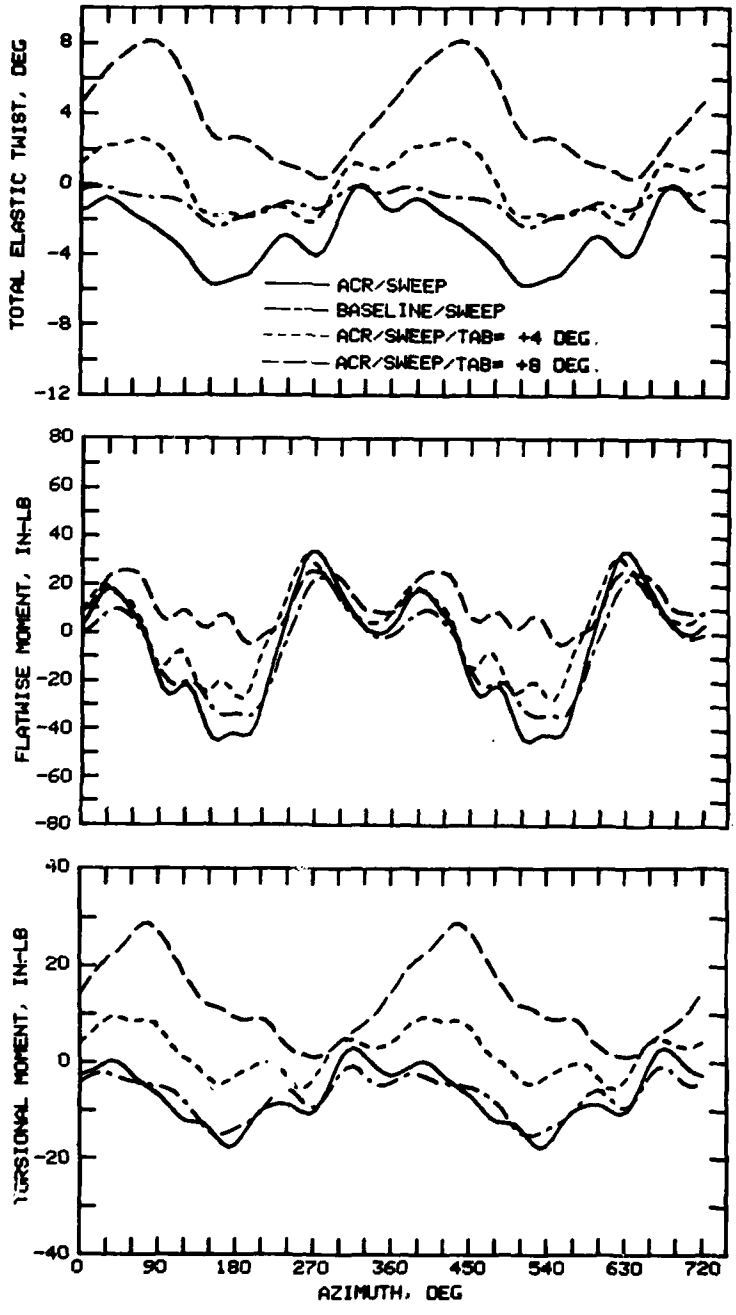

Figure 39. Time Histories of Elastic Twist and Blade Moments for Four Model Rotors; $\mu = 0.3$ $C_L/\sigma = 0.08$, $\alpha_s = -5^0$.

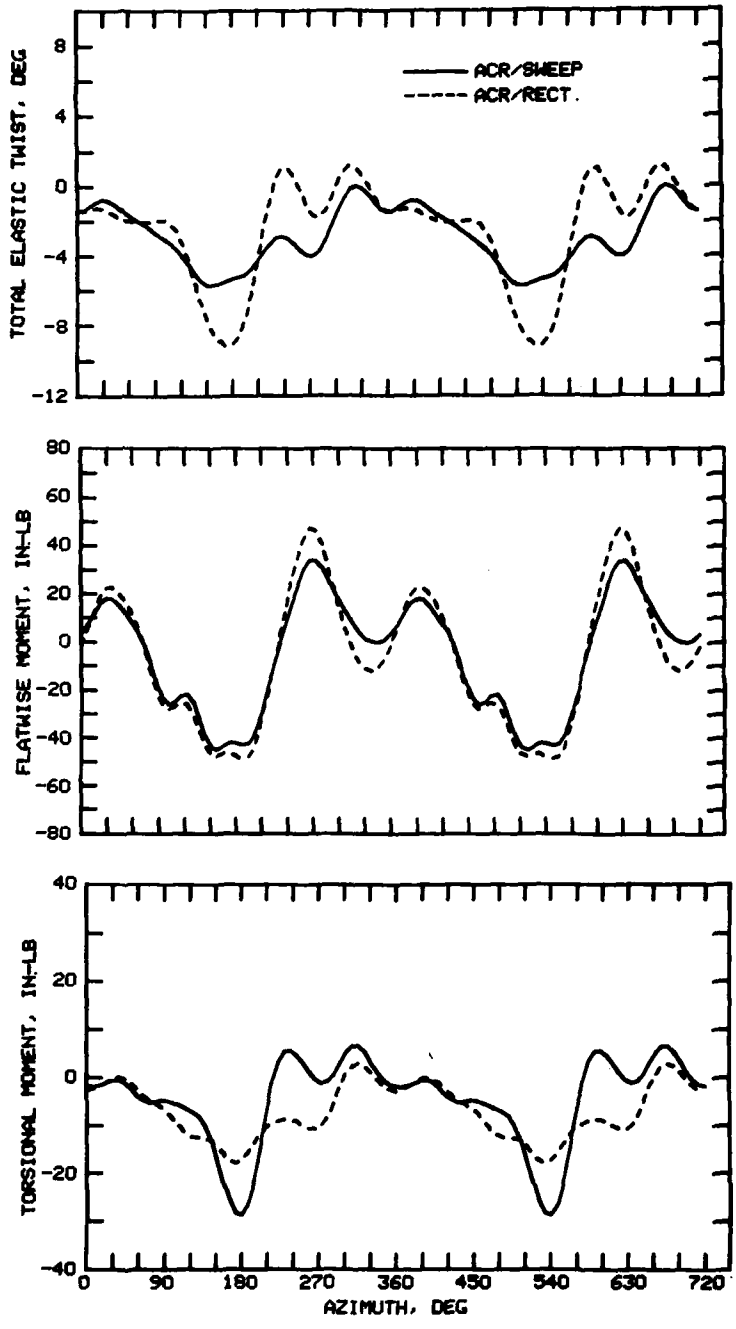

Figure 40. Effect of Tip Sweep on ACR Blade Elastic Twist and Blade Moments; $\mu = 0.3$, $C_L/\sigma = 0.08$.

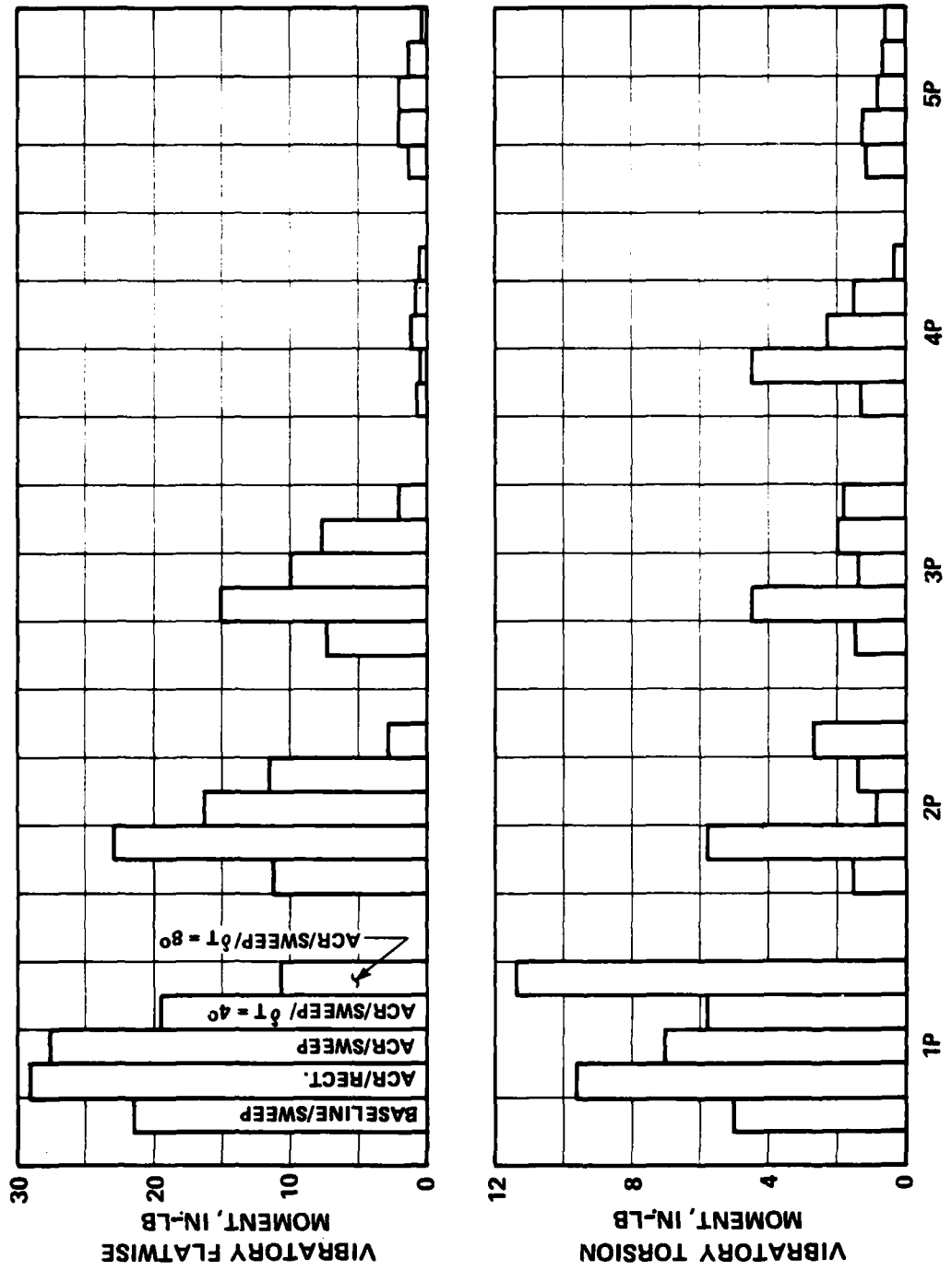

Figure 41. Harmonic Content of Flatwise and Torsion Moments for Four Model Rotors; $\mu = 0.3$, $C_L/\sigma = 0.08$, $\alpha_s = -5^o$.

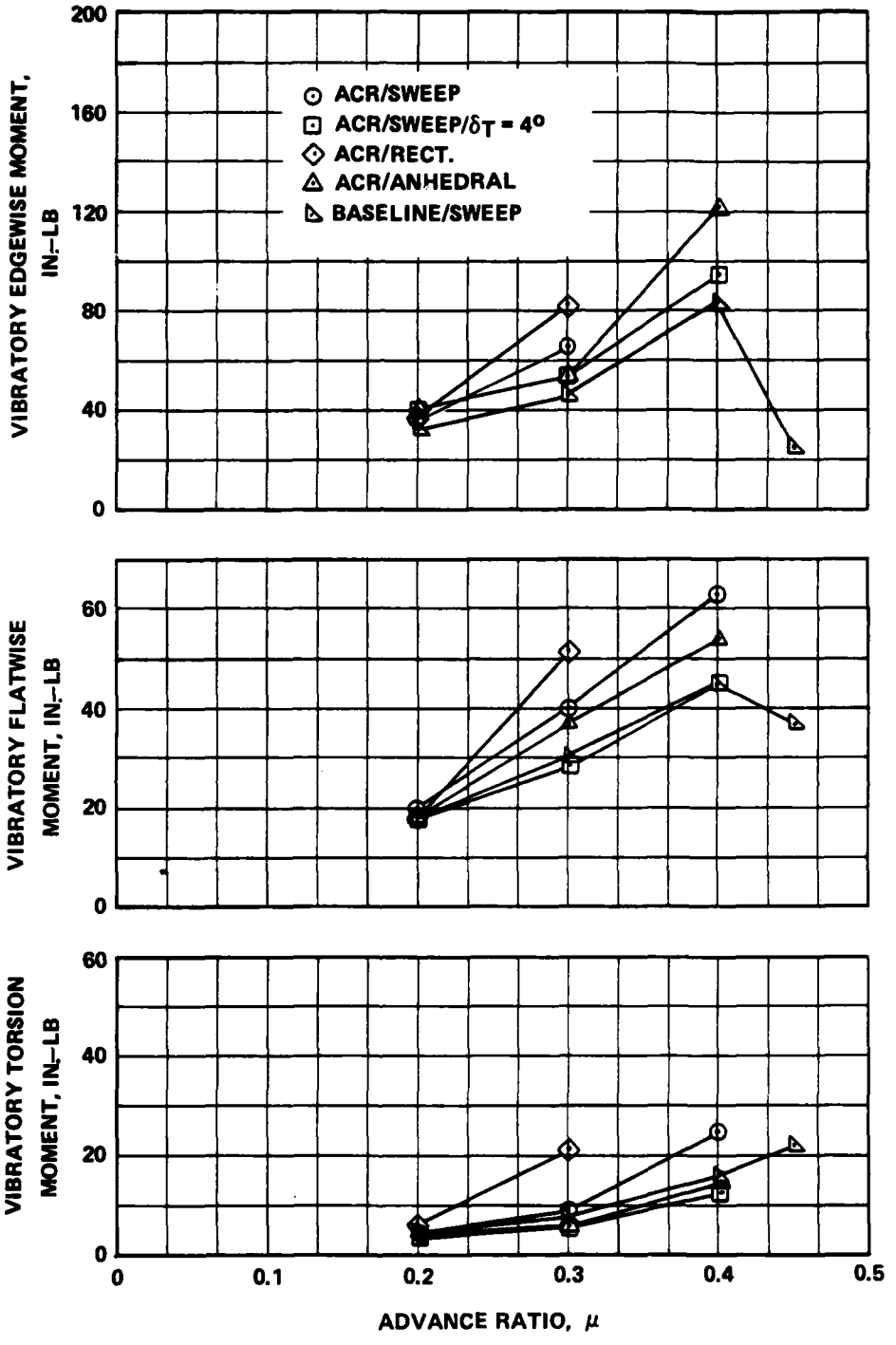

Figure 42. Variation of Model Rotor Blade Moments with Advance Ratio; C_L/σ = 0.06, f = 15 ft^2.

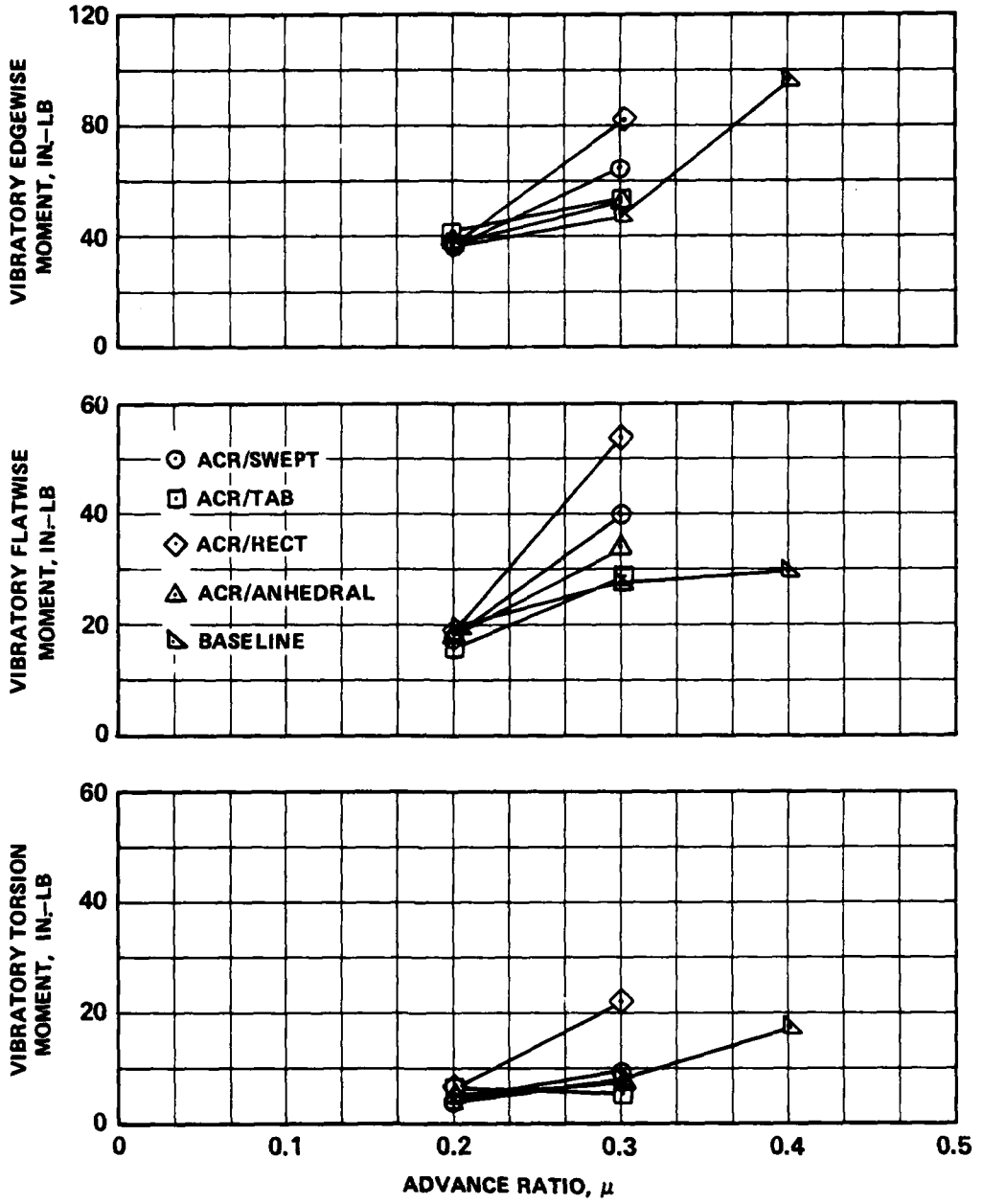

Figure 43. Variation of Model Rotor Blade Moments with Advance Ratio; $C_L/\sigma = 0.06$, $f = 30$ ft^2.

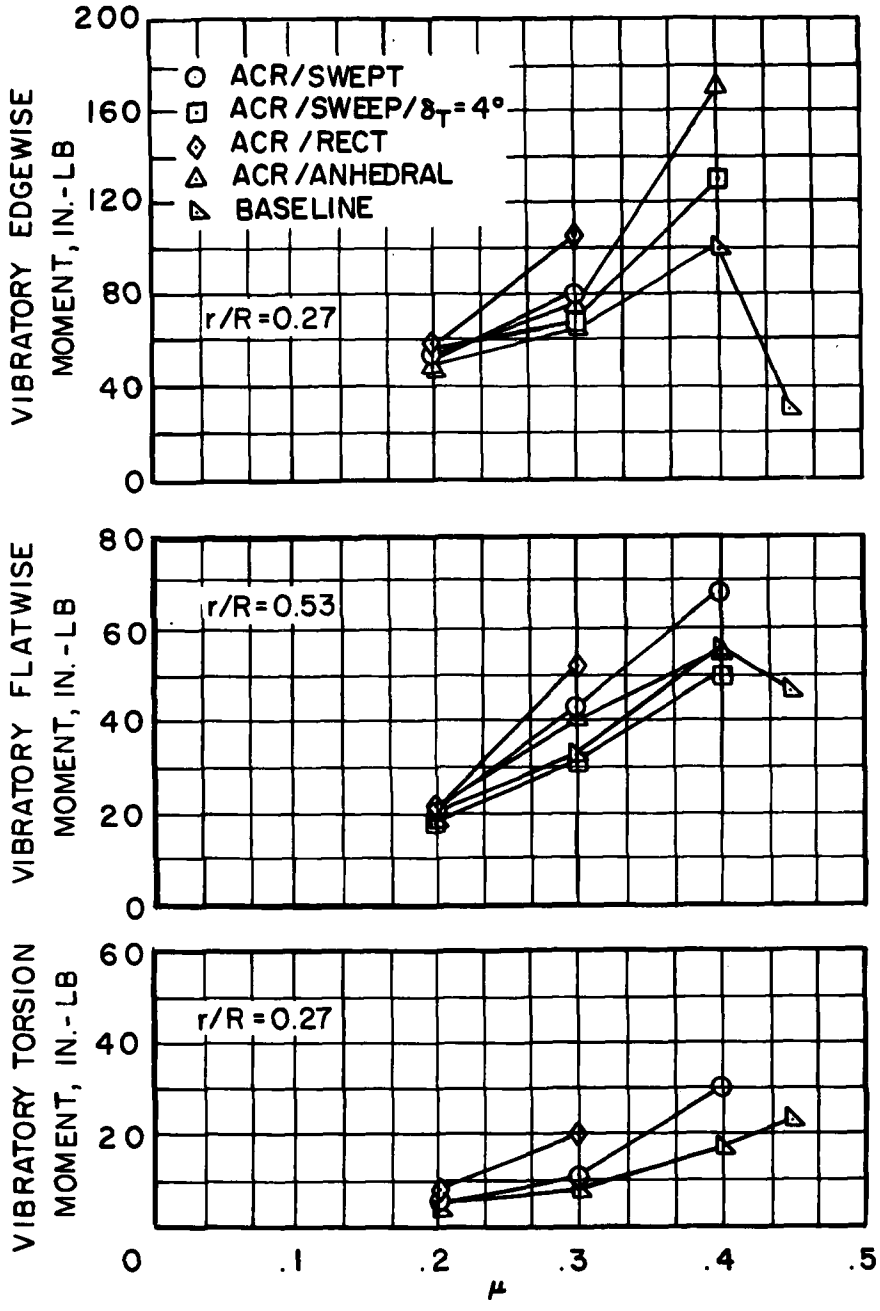

Figure 44. Variation of Model Rotor Blade Moments with Advance Ratio; C_L/σ = 0.08, f = 15 ft^2.

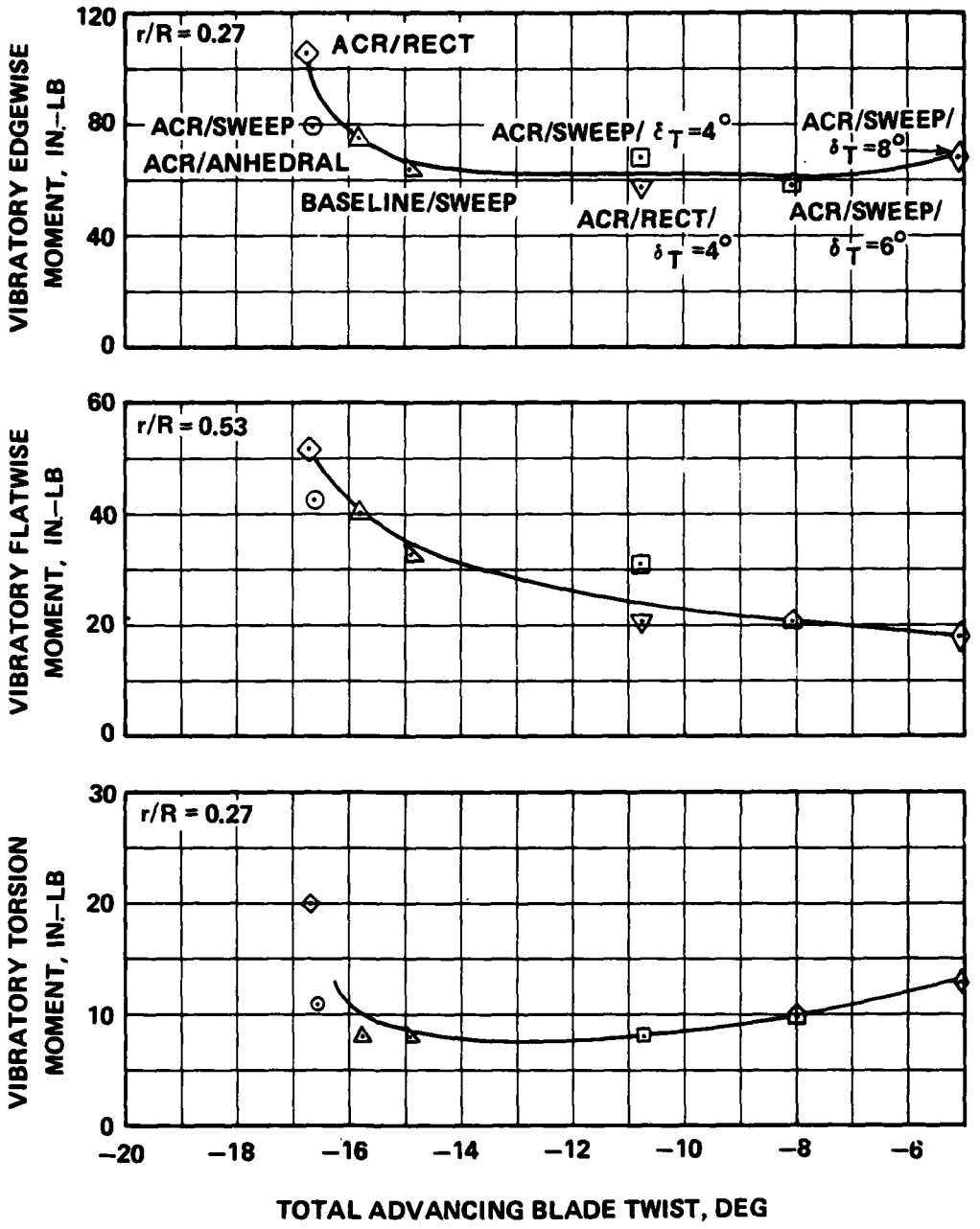

Figure 45. Variation in Vibratory Blade Moments with Advancing Blade Total Twist; $\mu = 0.3$, $C_L/\sigma = 0.08$, $f = 15$ ft^2.

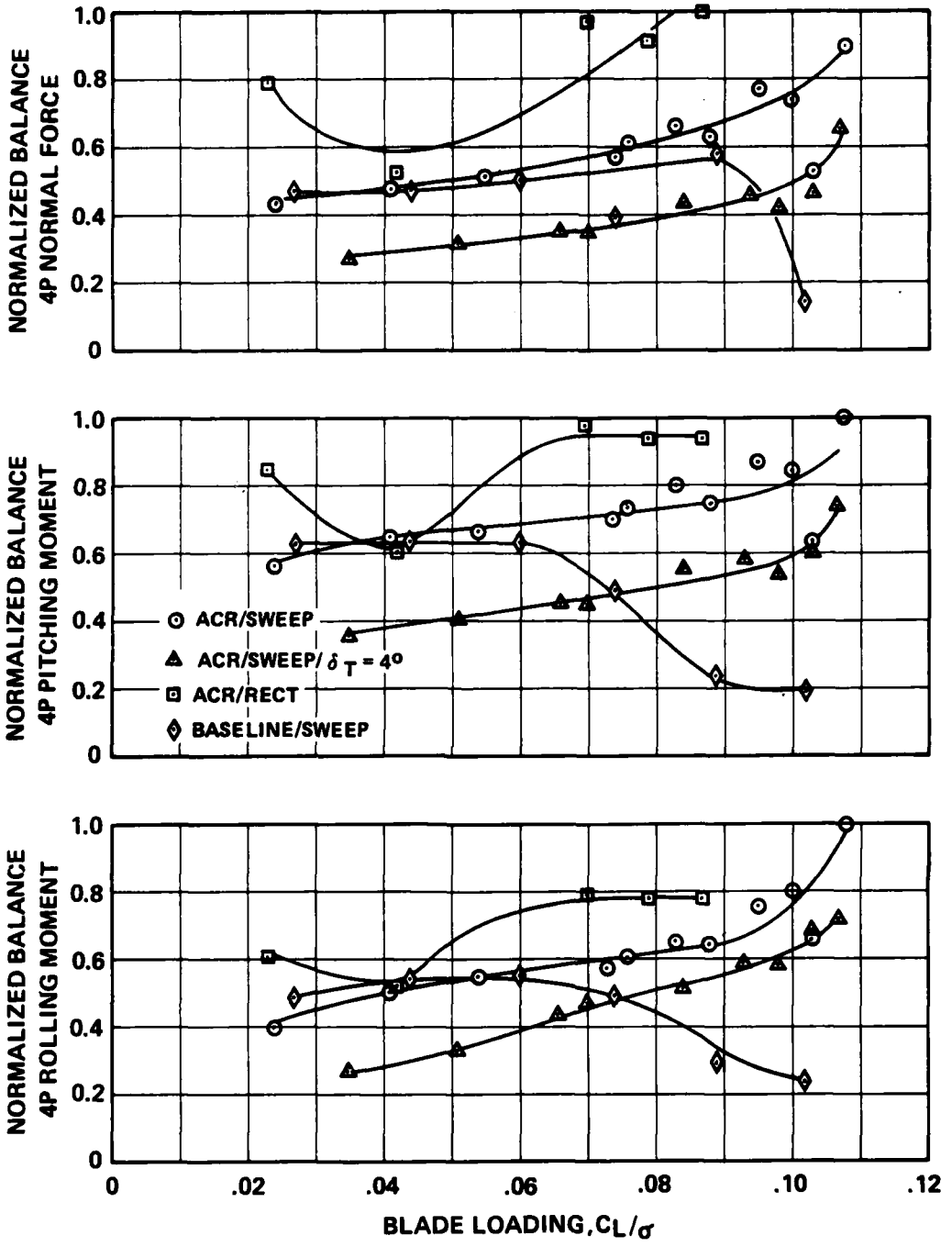

Figure 46. Normalized Vibratory Hub Loads for Four Model Rotors; $\mu = 0.3$, $\alpha_s = -5^o$.

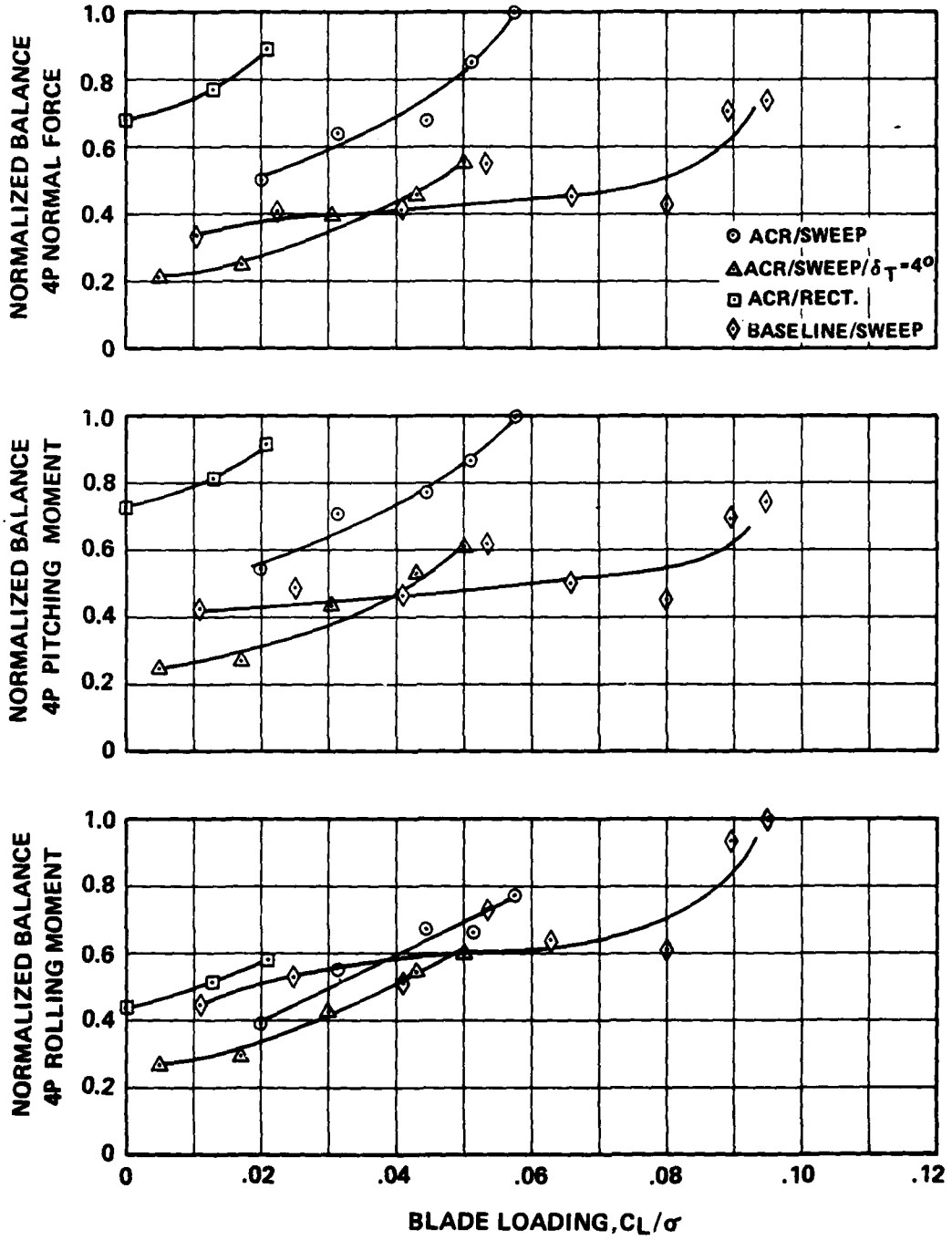

Figure 47. Normalized Vibratory Hub Loads for Four Model Rotors; $\mu = 0.4$, $\alpha_s = -10^0$.

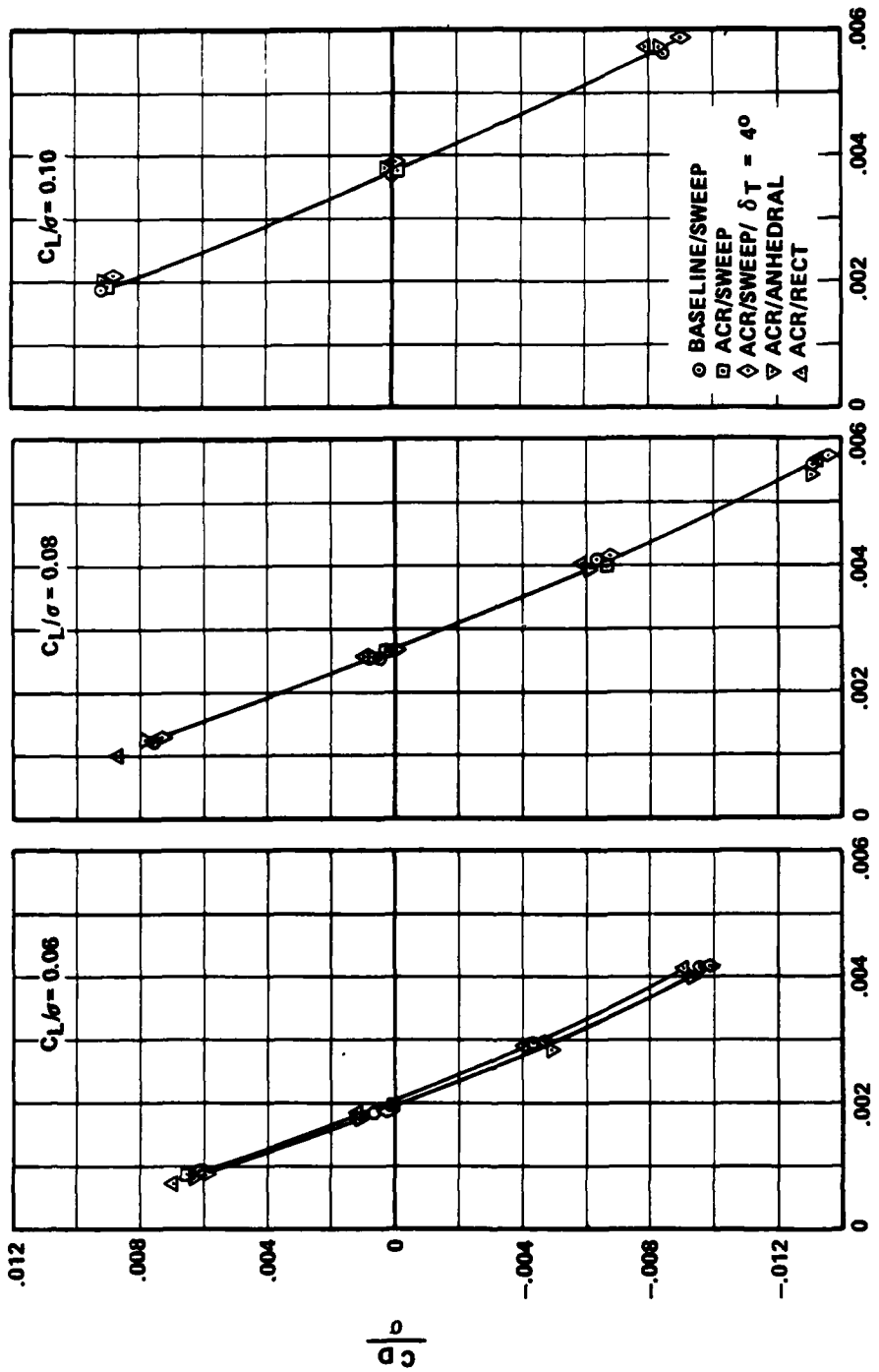

Figure 48. Model Rotor Performance at $\mu = 0.2$, $M_H = 0.65$.

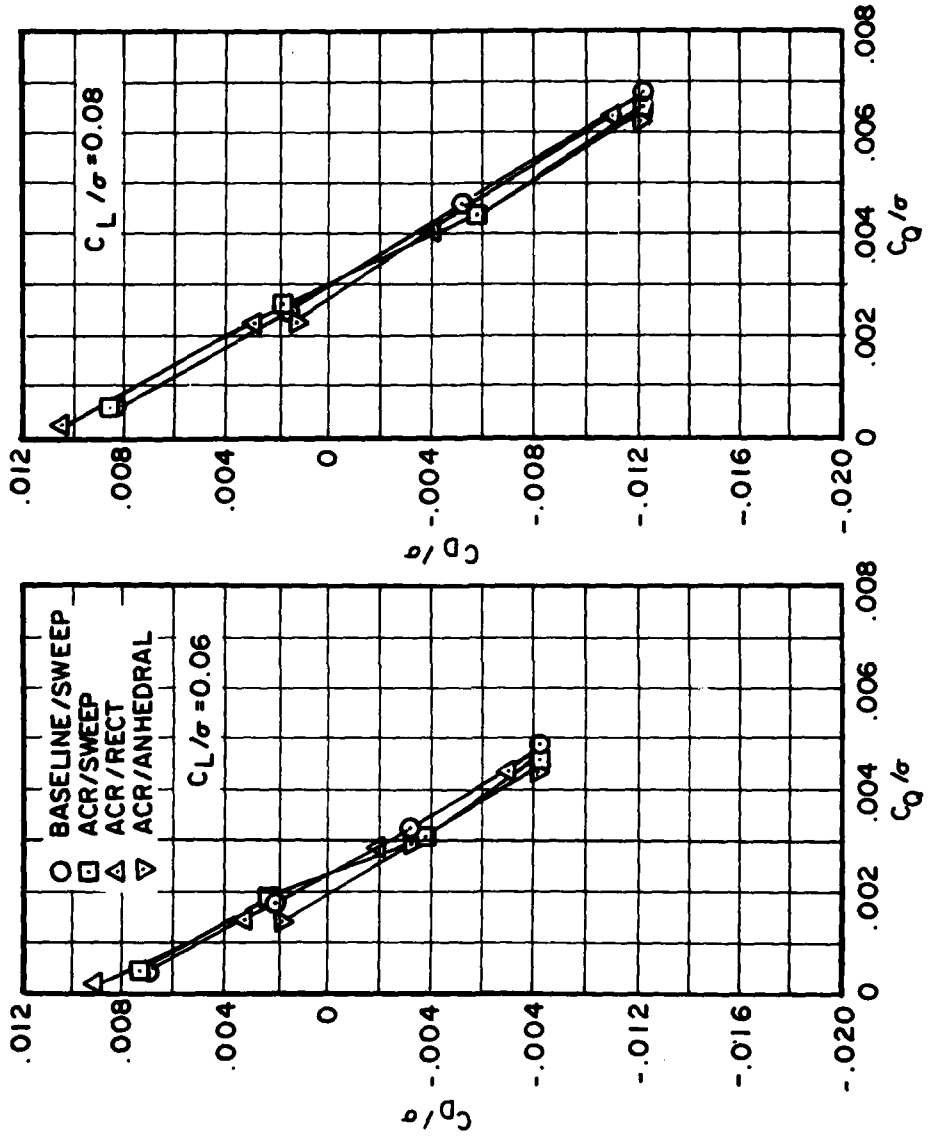

Figure 49. Model Rotor Performance at μ = 0.3, M_H = 0.65.

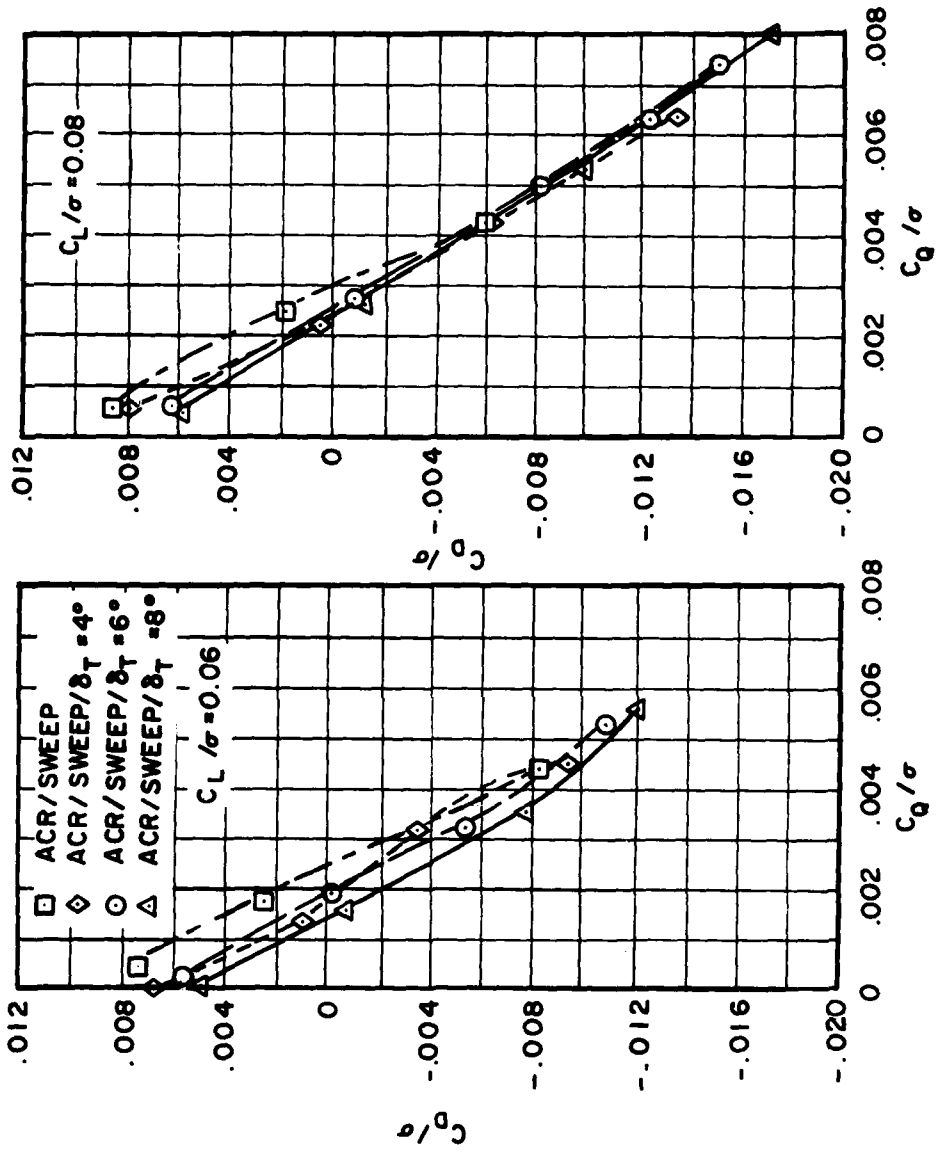

Figure 49. Concluded.

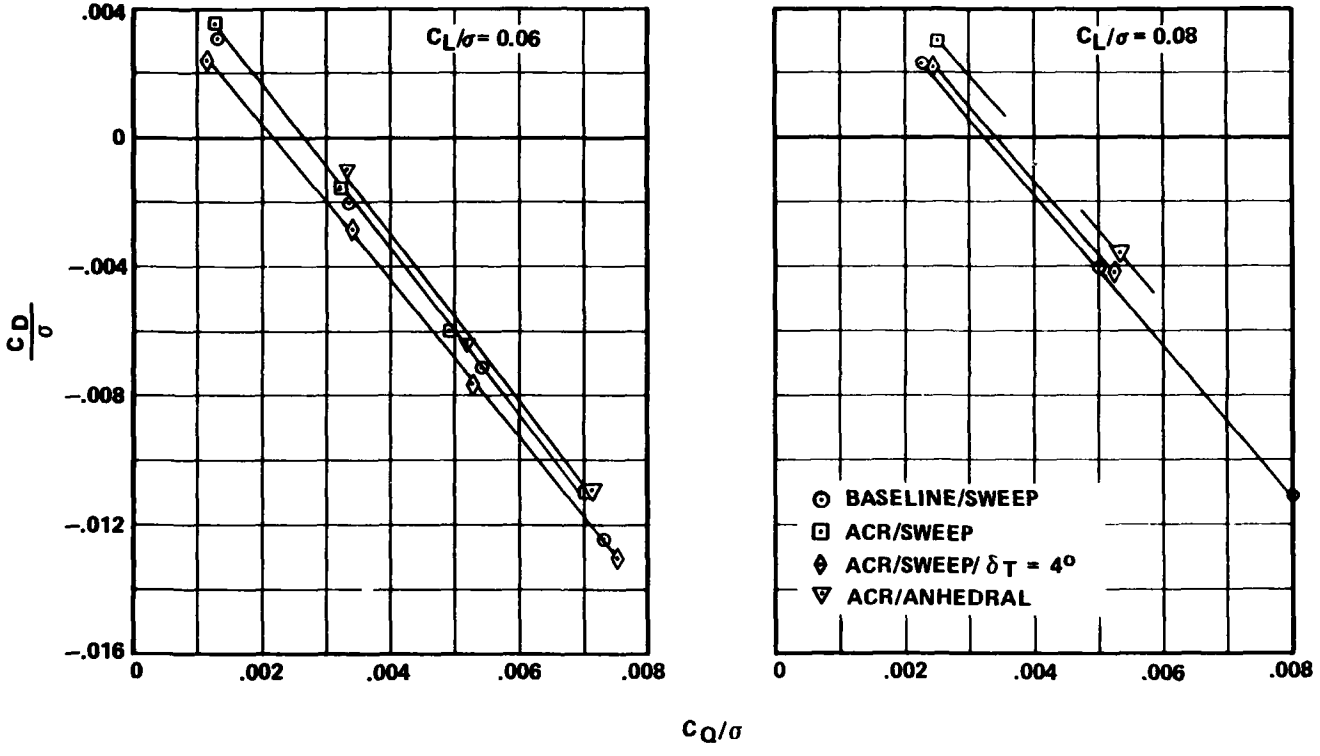

Figure 50. Model Rotor Performance at $\mu = 0.4$, $M_H = 0.65$.

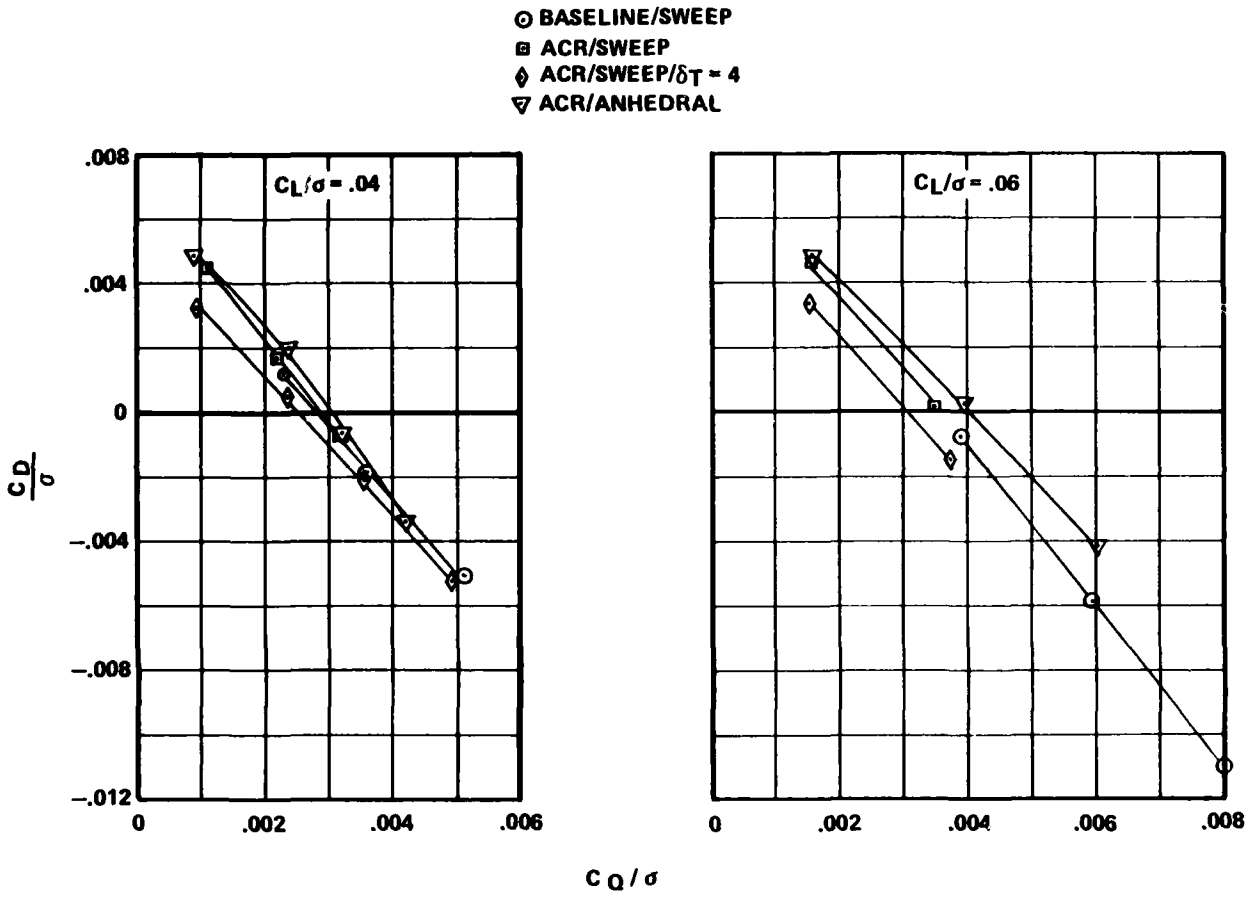

Figure 51. Model Rotor Performance at μ = 0.45, M_H = 0.65.

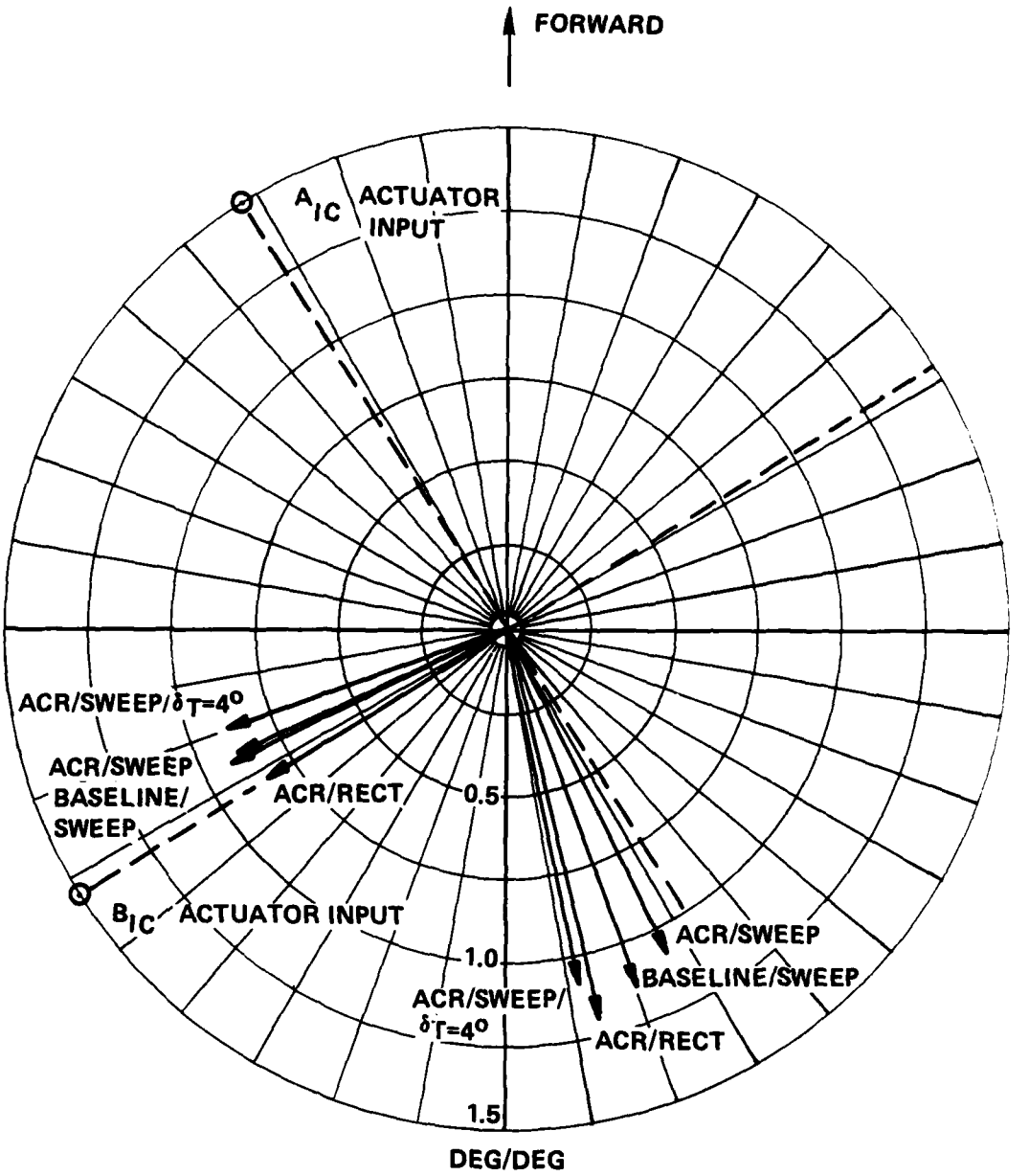

Figure 52. Model Rotor Flapping Response to Cyclic Pitch; $\mu = 0.3$, $C_L/\sigma = 0.07$, $C_{pF}/\sigma = 0.006$.

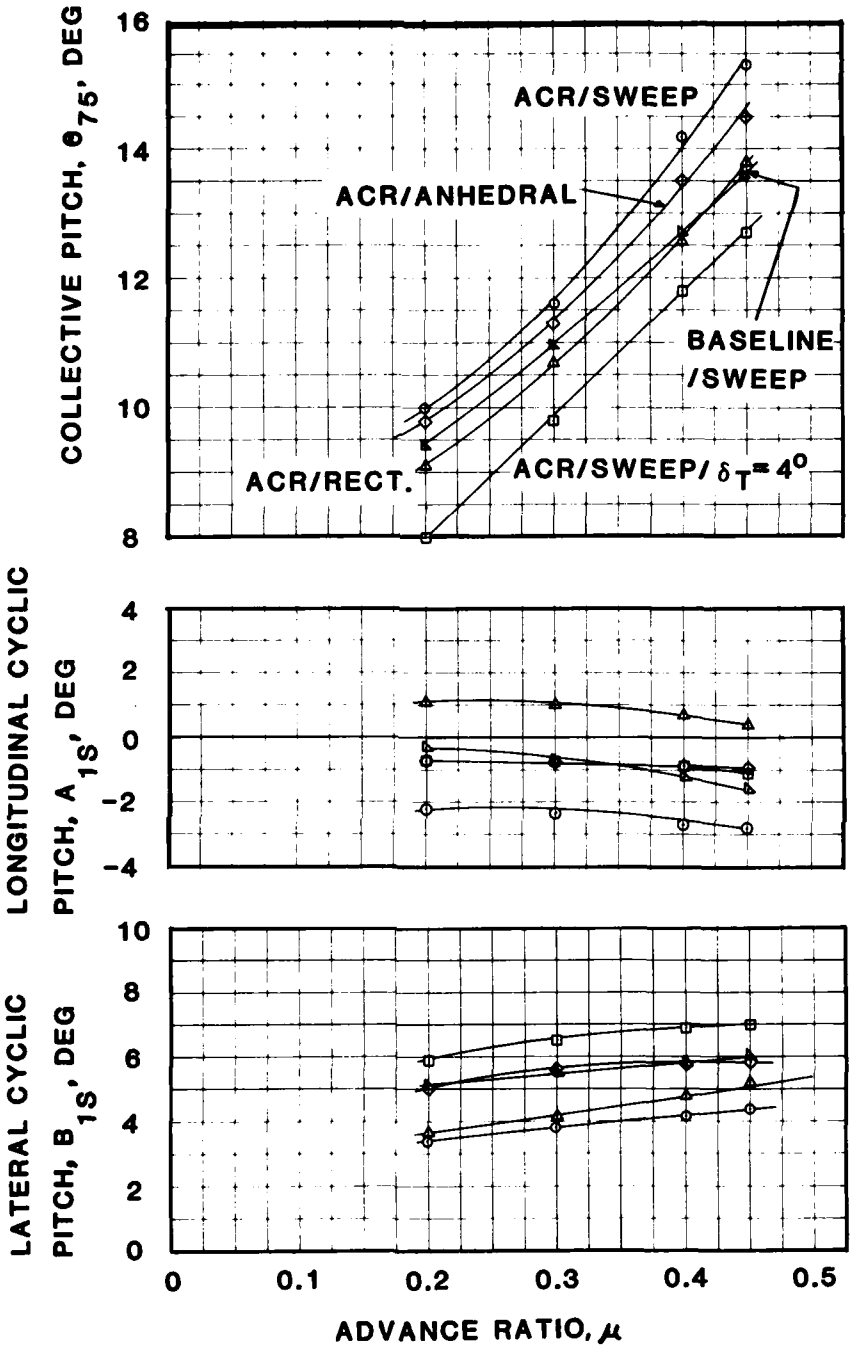

Figure 53. Comparison of Model Rotor Control Inputs Required for Trim; $C_L/\sigma = 0.07$, $f = 30$ ft^2.

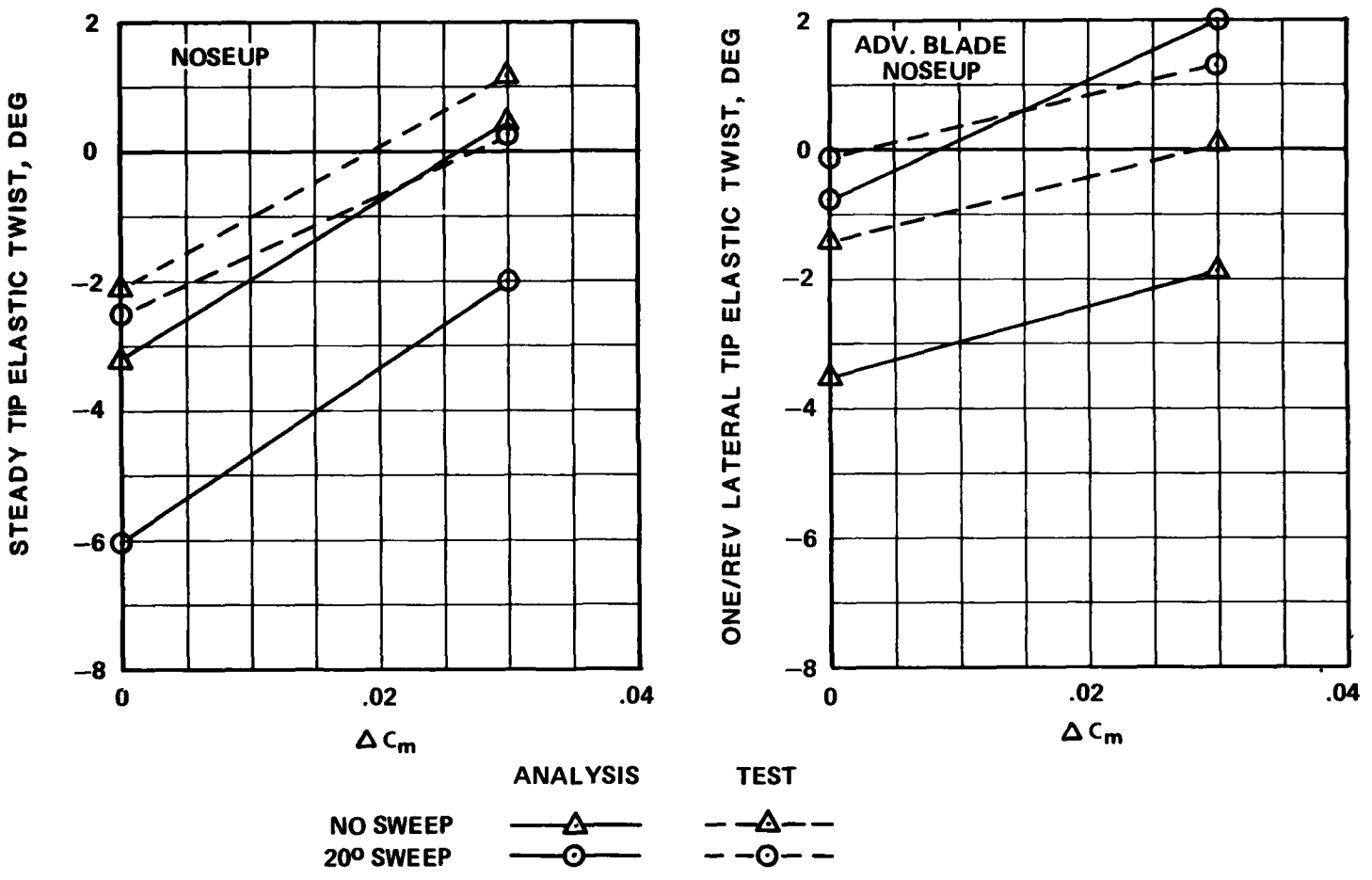

Figure 54. Correlation of Measured and Calculated Tip Elastic Twist; $\mu = 0.3$, $C_L/\sigma = 0.08$, $\alpha_s = -5^o$.

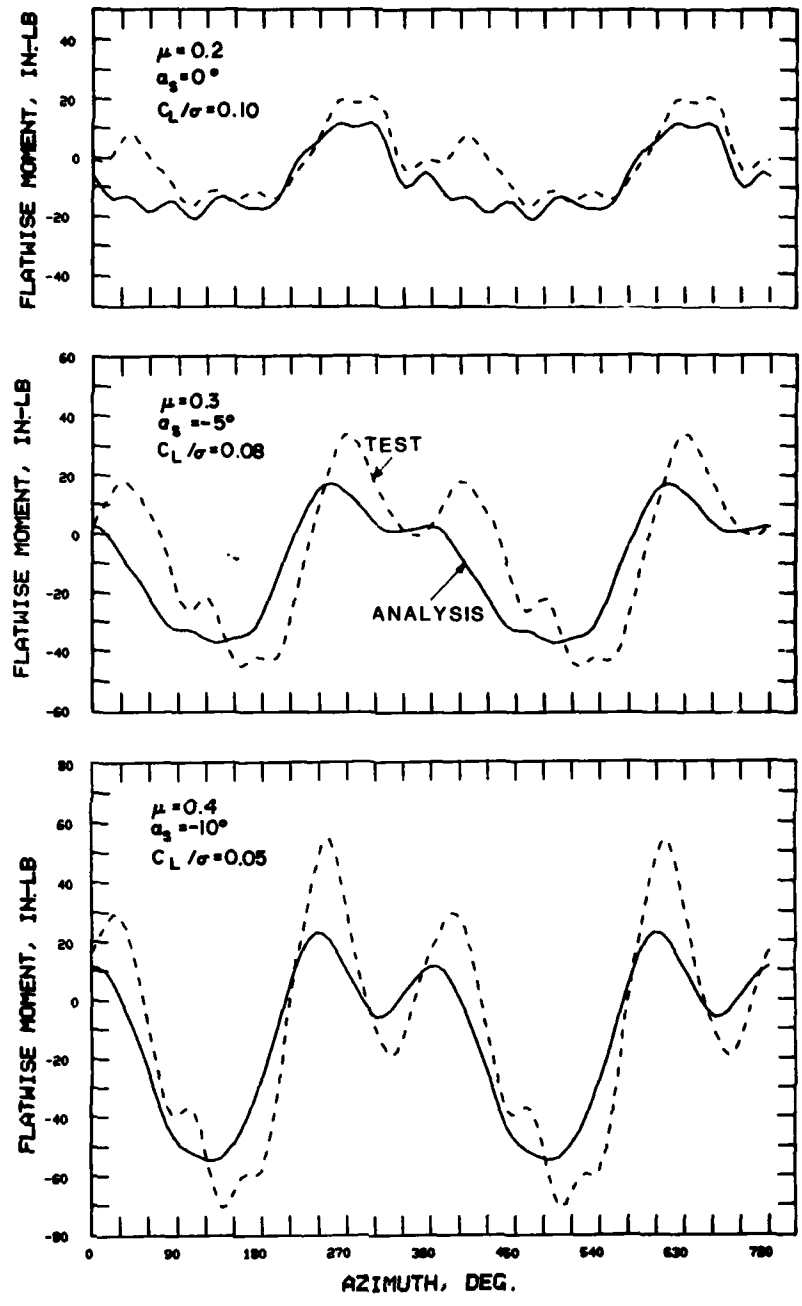

Figure 55. Correlation of Measured and Calculated Flatwise Moment Time Histories for ACR Swept Tip Blade.

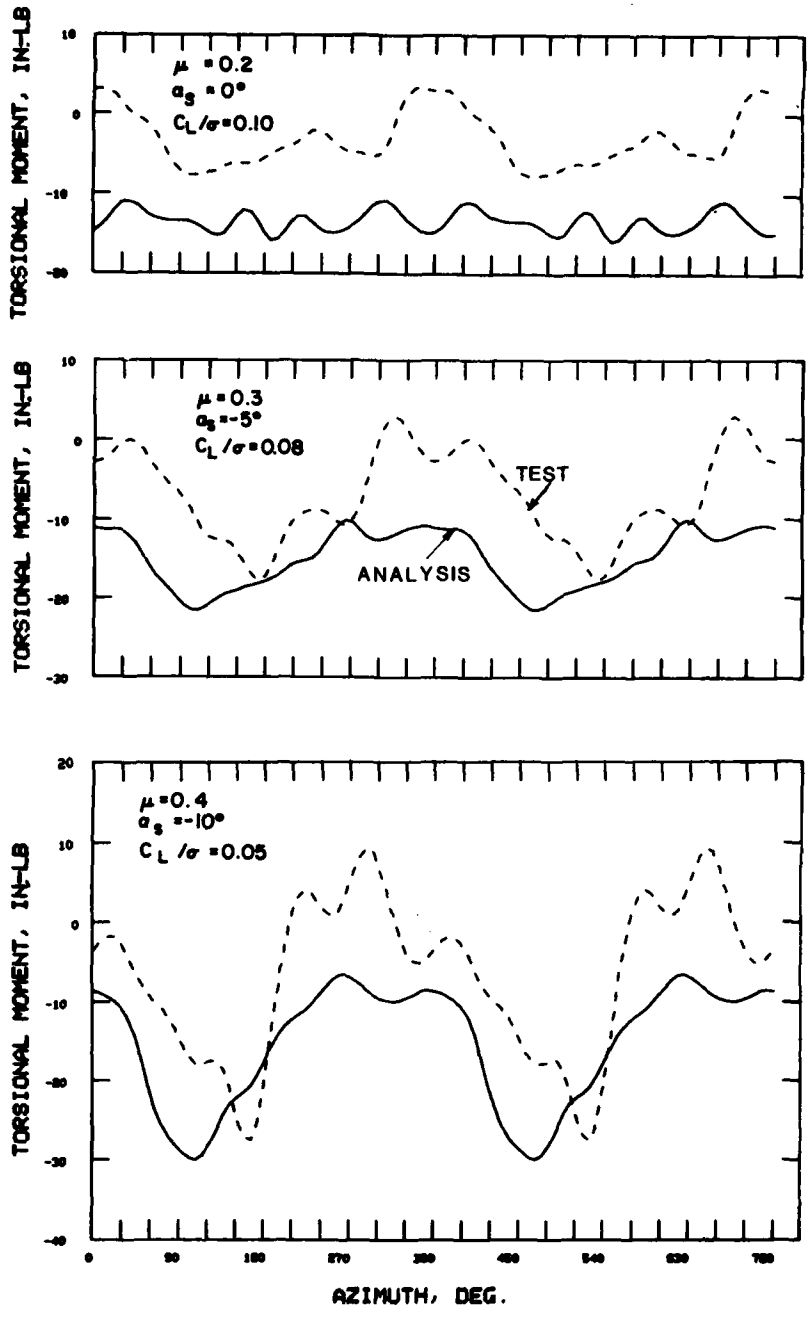

Figure 56. Correlation of Measured and Calculated Torsion Moment Time Histories for ACR Swept Tip Blade.

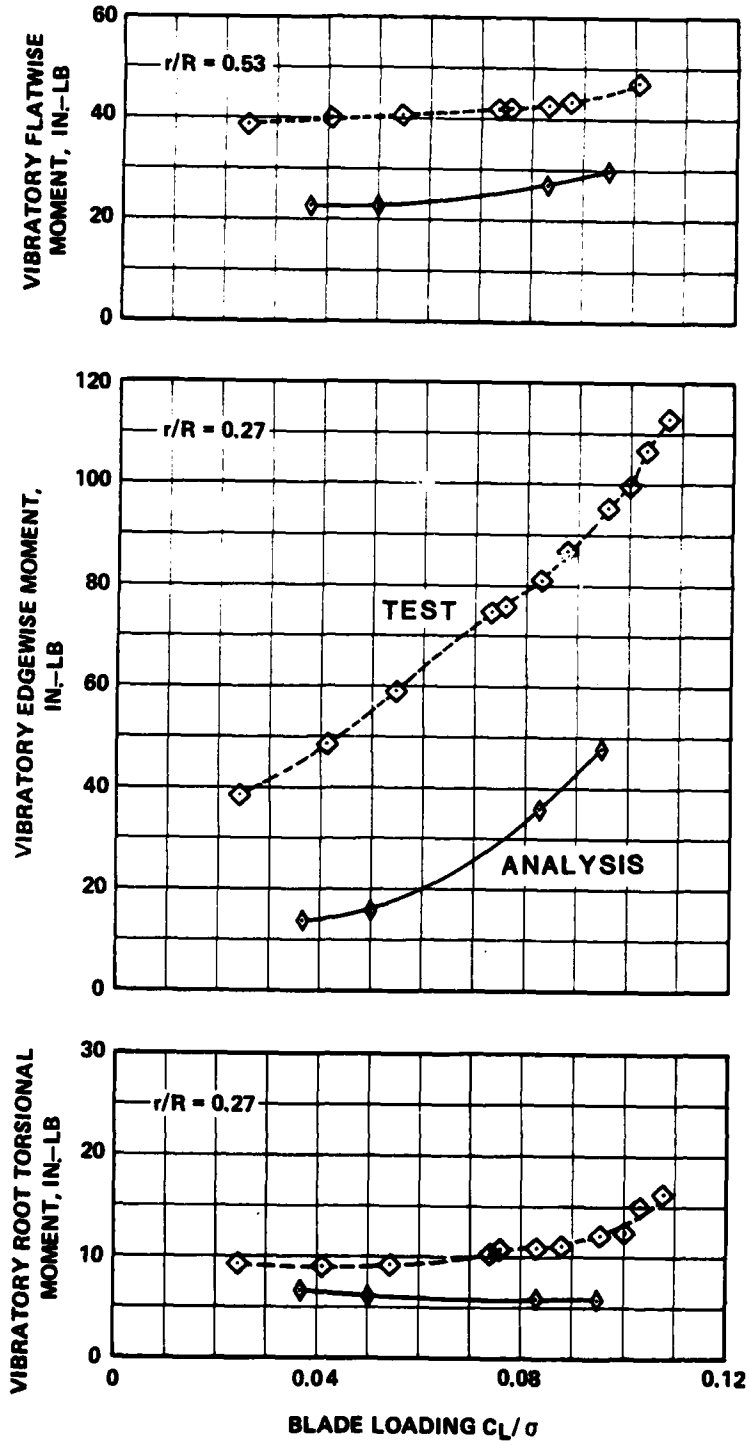

Figure 57. Correlation Between Measured and Calculated Vibratory Blade Moments for ACR Swept Tip Blade; $\mu = 0.3$, $\alpha_s = -5^0$.

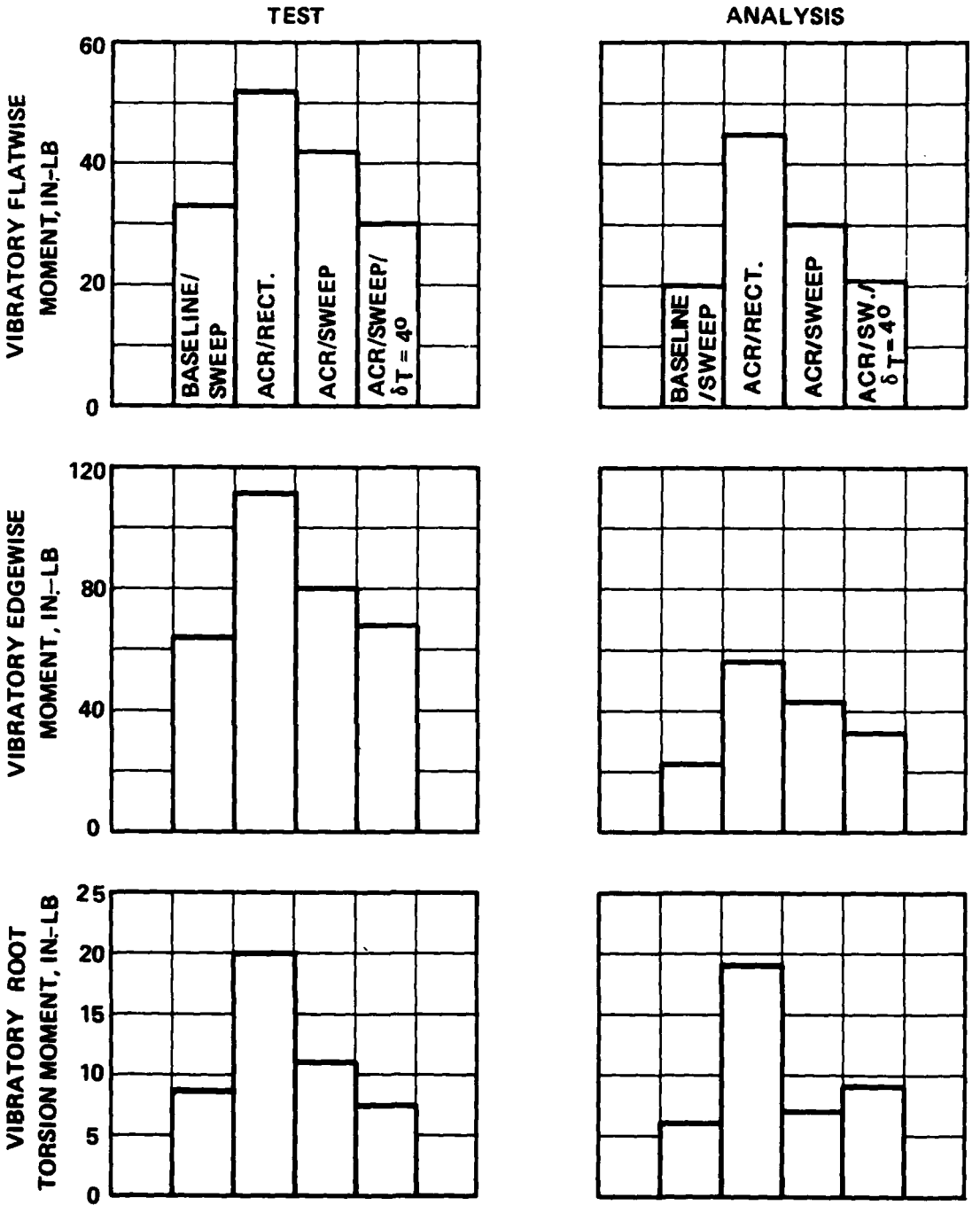

Figure 58. Correlation Between Measured Blade Moments and L/D_E for Four Model Rotors; $\mu = 0.3, C_L/\sigma = 0.08, \alpha_s = -5^0$.

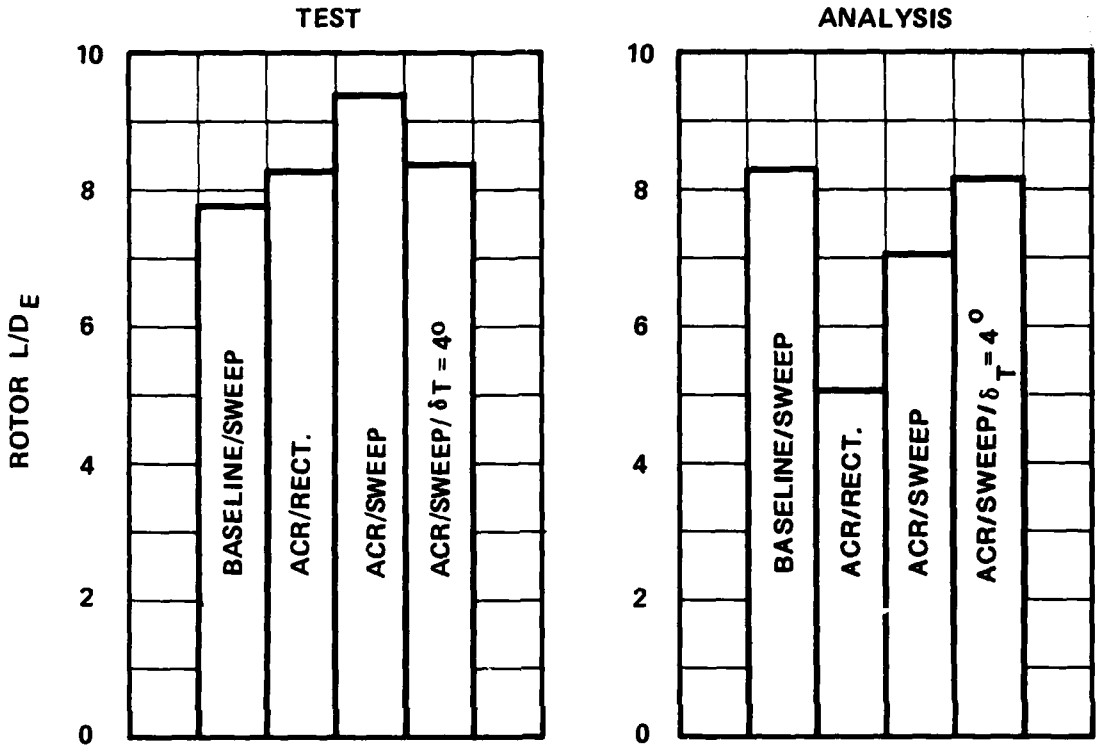

Figure 58. Concluded.

TABLE 1. MEASURED PROPERTIES OF ACR AND BASELINE MODEL ROTOR BLADES

Blade	Modal Frequency, Hz									Blade Weight, Grams
	Flatwise					Edgewise		Torsion		
	1	2	3	4	5	1	2	1	2	
Baseline										
#1	8.3	27.8	60.0	106.7	162.7	53.7	152.3	69.8	196	1197.5
#2	8.2	27.8	60.4	107.0	163.3	54.0	152.0	70.4	200.1	1193.7
#3*	8.2	27.7	59.3	106.0	161.5	53.5	151.7	69.8	199.0	1214.0
#4*	8.3	27.7	59.9	106.1	162.1	53.2	150.8	69.3	199.7	1203.0
ACR										
#1	8.3	27.5	59.9	104.0	162.0	53.0	148.8	47.0	137.0	1182.0
#2	8.3	27.1	59.8	102.9	161.2	51.9	145.9	46.4	138.3	1181.2
#3*	8.4	27.4	59.4	102.4	161.0	52.3	145.4	45.6	-	1198.0
#4*	8.3	27.1	59.2	102.6	161.2	51.7	143.9	44.8	139.0	1202.8

* Instrumented Blades

Table 2. Control Derivatives of the Conformable Model Rotor with Swept Tips; $\mu = 0.3$, $C_L/\sigma = 0.07$, $C_{pF}/\sigma = 0.005$

	N lb	A lb	P in.-lb	R in.-lb	Y in.-lb	S lb	a_o deg	a_{1s} deg	b_{1s} deg
$\frac{\partial}{\partial \theta_{75}}$ (deg)	32.0				No data available				
$\frac{\partial}{\partial A_{1S}}$ (deg)	6.04	2.01	41.18	-88.80	-3.74	3.66	0.060	0.371	0.791
$\frac{\partial}{\partial B_{1S}}$ (deg)	-15.44	-4.00	-118.80	-39.10	24.57	2.01	0.240	-0.970	0.486
$\frac{\partial}{\partial \alpha_S}$ (deg)	18.15	0.125	29.43	2.55	-20.70	-0.525	0.248	0.187	0.025

Table 3. Control Derivatives of the Conformable Model Rotor with Swept Tips and 4 Degree Tab Deflection; $\mu = 0.3$, $C_L/\sigma = 0.07$, $C_{PF}/\sigma = 0.005$

	N lb	A lb	P in.-lb	R in.-lb	Y in.-lb	S lb	a_o deg	a_{1s} deg	b_{1s} deg
$\frac{\partial}{\partial \theta_{75}}$ (deg)	34.00	2.50	81.70	17.40	79.70	2.00	0.555	0.685	0.082
$\frac{\partial}{\partial A_{1S}}$ (deg)	6.58	2.08	44.04	-88.28	-0.13	3.25	0.058	0.298	0.832
$\frac{\partial}{\partial B_{1S}}$ (deg)	-16.92	03.86	-117.96	-41.56	29.18	2.17	0.248	-1.054	0.219
$\frac{\partial}{\partial \alpha_s}$ (deg)	16.15	0.275	28.25	3.55	29.43	-0.70	0.265	0.219	0.010

Table 4. Control Derivatives of the Conformable Model Rotor with Rectangular Tips; $\mu = 0.3$, $C_L/\sigma = 0.07$, $C_{PF}/\sigma = 0.003$

	N lb	A lb	P in.-lb	R in.-lb	Y in.-lb	S lb	a_o deg	a_{1s} deg	b_{1s} deg
$\frac{\partial}{\partial \theta_{75}}$ (deg)	47.00	2.80	105.00	20.10	121.40	-2.00	0.822	1.033	0.019
$\frac{\partial}{\partial A_{1S}}$ (deg)	6.54	1.94	44.70	-90.20	-6.18	3.62	0.075	0.442	0.731
$\frac{\partial}{\partial B_{1S}}$ (deg)	-19.13	-4.21	-125.13	-29.70	23.76	1.81	0.298	-1.159	0.281
$\frac{\partial}{\partial \alpha_s}$ (deg)	18.63	0.425	32.00	-2.98	-53.17	0.325	0.328	0.285	0.046

Table 5. Control Derivatives of the Baseline Model Rotor with Swept Tips; $\mu = 0.3$, $C_L/\sigma = 0.07$, $C_{PF}/\sigma = 0.005$

	N lb	A lb	P in.-lb	R in.-lb	Y in.-lb	S lb	a_o deg	a_{1s} deg	b_{1s} deg
$\frac{\partial}{\partial\theta_{75}}$ (deg)	43.10	2.20	83.90	2.50	109.00	-1.40	0.59	0.615	0.058
$\frac{\partial}{\partial A_{1S}}$ (deg)	6.30	2.23	42.79	-93.43	-6.09	3.73	0.841	0.389	0.807
$\frac{\partial}{\partial B_{1S}}$ (deg)	-18.08	-4.24	-121.50	-35.64	25.12	2.11	0.187	-1.047	0.393
$\frac{\partial}{\partial\alpha_s}$ (deg)	18.63	0.275	23.38	0.43	-23.18	-0.48	0.273	0.195	0.072

REFERENCES

1. Doman, G. S., et al., Investigation of Aeroelastically Adaptive Rotors, Boeing Vertol Company; USAAMRDL TR 77-3, Eustis Directorate, U.S. Army Air Mobility Research and Development Laboratory, Fort Eustis, Virginia, May 1977, AD A042083.

2. Blackwell, R. H., Investigation of the Compliant Rotor Concept, Sikorsky Aircraft Division, United Technologies Corporation, U.S. Army Air Mobility Research and Development Laboratory, TR 77-7, Eustis Directorate, USAAMRDL, Fort Eustis, Virginia, June 1977, AD A042338.

3. Niebanck, C. F., Model Rotor Test Data for Verification of Blade Response and Rotor Performance Calculations, Sikorsky Aircraft Division, United Technologies Corporation; USAAMRDL Technical Report 74-29, Eustis Directorate, U. S. Army Air Mobility Research and Development Laboratory, Fort Eustis, Virginia, May 1974, AD 786562.

4. Blackwell, R. H., Investigation of the Effects of Blade Structural Design Parameters on Helicopter Stall Boundaries, Sikorsky Aircraft Division, United Technologies Corporation, USAAMRDL TR 74-25, Eustis Directorate, USAAMRDL, Fort Eustis, Virginia, May 1974, AD 748594.

5. Gabel, R., and Tarzanin, R. F., Blade Torsional Tuning to Manage Rotor Stall Flutter, AIAA Paper No 72-958, American Institute of Aeronautics and Astronautics, September 1974.

6. Paglino, V. M., The Potential Benefits of Advanced Airfoils for Helicopter Applications, NAVAIR Report prepared under Contract N00019-73-C-0225, March 1974.

7. Lemnios, A. Z., et al., Full Scale Wind Tunnel Tests of a Controllable Twist Rotor, American Helicopter Society, 32nd Annual National Forum, May 1976.

8. Prillwitz, R., Structural Evaluation of High Performance Rotor Blade Swept Tips, Engineering Report SER-651073, Sikorsky Aircraft Division, United Technologies Corporation, October 1972.

9. Weller, W., Experimental Investigation of Effects of Blade Tip Geometry on Loads and Performance for an Articulated Rotor System, NASA-TP-1303; AVRADCOM-TR-78-53, Structures Laboratory, U.S. Army Research and Technology Laboratories (AVRADCOM), Langley Research Center, Hampton, Virginia, January 1979.

10. Arcidiacono, P. J., Prediction of Rotor Instability at High Forward Speeds, Volume I, Steady Flight Differential Equations of Motion for a Flexible Helicoper Blade with Chordwise Mass Unbalance, Sikorsky Aircraft Division, United Technologies Corporation; USAAVLABS 68-18A, U. S. Army Aviation Material Laboratories, Fort Eustis, Virginia February 1969, AD 685860.

11. Landgrebe, A. J., An Analytical Method for Predicting Rotor Wake Geometry, Journal of the American Helicopter Society, Volume 14, No. 4, October 1969, pp. 20 - 32.

12. Blackwell, R. H., Aeroelastically Conformable Rotor Mission Analysis, Sikorsky Aircraft Division, United Technologies Corporation, USARTL TR-79-5, Applied Technology Laboratory, U.S. Army Research and Technology Laboratories, Fort Eustis, Virginia March 1979, AD A067338.

13. Prouty, R. W., A State-of-the-Art Survey of Two-Dimensional Airfoil Data, Journal of the AHS, Volume 20, No. 4, October 1974, pp. 14 - 25.

LIST OF SYMBOLS

a	Speed of sound, ft/sec
A	Rotor longitudinal force perpendicular to shaft, positive in upstream direction, lb
a_o	Blade coning angle, deg
A_{1c}	Lateral cyclic pitch input in actuator axis system, positive for increased pitch at 212 degrees azimuth, deg
A_{1s}	Lateral cyclic pitch, positive for increased pitch at 180 degrees azimuth, deg
a_{1s}	Longitudinal one/rev flapping, positive for flapping up at 180 degrees azimuth, deg
B_{1c}	Longitudinal cyclic pitch input in actuator axis system, positive for increased pitch at ψ = 302 degrees azimuth, deg
B_{1s}	Longitudinal cyclic pitch, positive for increased pitch at 270 degrees azimuth, deg
b_{1s}	Lateral one/rev flapping, positive for flapping up at 270 degrees, deg
C_D	Rotor drag coefficient, $D/\pi R^2 \rho(\Omega R)^2$
C_L	Rotor lift coefficient, $L/\pi R^2 \rho(\Omega R)^2$
c_m	Section pitching moment coefficient
c_{m_o}	Below-stall section pitching moment coefficient
C_{PF}	Rotor propulsive force coefficient, $PF/\pi R^2 \rho(\Omega R)^2$
C_Q	Rotor torque coefficient, $Q/\pi R^3 \rho(\Omega R)^2$
D	Rotor drag, positive for force in direction of freestream, lb
D_E	Rotor equivalent drag, $\frac{550}{V}$ (HP-HP_{PAR}), lb
f	Aircraft equivalent flat plate area, ft^2
GJ	Blade torsional stiffness, lb in^2

HP	Rotor power, hp
HP_{PAR}	Rotor parasite power, hp
K_θ	Control system stiffness, in-lb/rad
L	Rotor lift, lb
M_H	Rotational Tip Mach Number, $\Omega R/a$
N	Rotor force parallel to the shaft, positive up, lb
P	Rotor pitching moment at the hub, positive for noseup moment, in-lb
PF	Rotor propulsive force, positive for force directed opposite to freestream direction, lb
R	Blade radius, ft; rolling moment at the hub, positive for right wing up moment, in-lb
r	Blade radial coordinate, ft
S	Rotor side force, positive to the right, lb
V	Airspeed, ft/sec
Y	Rotor yawing moment, positive clockwise, in-lb
α_s	Shaft angle, positive for rotor tilted aft, deg
δ_T	Tab deflection, positive for trailing edge up, deg
Δc_m	Change in section pitching moment coefficient
σ_{75}	Collective pitch at three-quarter radius, deg
Λ	Blade tip sweep angle, deg
μ	Advance ratio, $V/\Omega R$
σ	Rotor solidity
ψ	Blade azimuth position, positive counterclockwise, referenced to downstream position, deg
Ω	Rotor speed, rad/sec